Joint Analysis of Refractions and Reflections (JARR) Method for Quantitatively Deriving Velocity Models

By

Daniel Z. Feigenbaum

Submitted to the graduate degree program in Geology and the Graduate Faculty of the University of Kansas in partial fulfillment of the requirements for the degree of Master of Geology.

Chair: Richard D. Miller

George Tsoflias

J. Douglas Walker

Date Defended: 7-12-2017

The thesis committee for Daniel Z. Feigenbaum certifies that this is the approved version of the following thesis:

Joint Analysis of Refractions and Reflections (JARR) Method for Quantitatively Deriving Velocity Models

Chair: Richard D. Miller

Date Approved: 7-23-2017

ABSTRACT:

Joint analysis of refractions and reflections (JARR) is introduced and is developed as a quantitative method for improving the accuracy of near-surface velocity model functions. These accurate near-surface velocity functions are essential in various reflection processing flows. With reflection processing, accuracy is vital to produce accurate subsurface stacked sections. To demonstrate the method, it was evaluated by calculating long-wavelength statics and post-stack depth migration on high resolution data. Seismic data were statically corrected and a migration was applied using velocities derived from the JARR method facilitated by First Arrival Tomography (FAT). One sample dataset is from the Wellington petroleum field, Wellington, Kansas and was intended to image to the basement structure (1500m). A second dataset was acquired along Highway 61, Inman, Kansas and intended to image solution features in the near-surface (upper 500m).

The JARR method utilizes a specialized processing flow designed to produce more accurate near-surface velocity functions than traditional velocity analysis methods. The method starts from raw interval normal move-out (INMO) velocity functions determined from reflections utilizing standard velocity estimation techniques (velocity panels, semblance). After a traditionally defined velocity function is selected, first arrivals are picked and saved. First arrival tomography is performed using the a-priori damped reference INMO velocity function. Synthetic first arrival rays are passed through the reference model. Time differences from calculated and observed first arrival rays are then inverted to produce a new velocity function. The process is repeated iteratively. The aforementioned method has many potential applications; however, it has the greatest impact in determining long-wavelength static corrections and high-resolution migration velocities.

Results, in challenging areas, show the JARR method to be a unique and novel way for calculating accurate near-surface velocity models when other approaches have shown marginal effectiveness. Results also support the utility of the JARR method for calculating velocities used to determine long-wavelength statics and migration of data with complex near-surface lithology and structures. These achievements were due to the JARR methods capability of producing velocity models with increased spatial and temporal accuracy.

ACKNOWLEDGMENTS:

First, I would like to thank my thesis committee, Richard D. Miller, Georgios Tsoflias, and J. Douglas Walker. Their guidance and wisdom allowed me to prosper as a student as well as a person. A special thank you to Julian Ivanov for his continual support as well as pushing me outside my comfort level to force me to grow as a geophysicist, whether through use of different seismic techniques, processing methods, or coding. Additionally, I would like to recognize the staff and graduate students at the Kansas Geological Survey for their support, including but not limited to: Shelby Peterie, Mary Brohammer, Brett Wedel, Joe Anderson, Jeremy Scobee, Joey Fontana, Sarah Morton, Amanda Livers, Yao Wang, Anthony Hoch and John Intfen.

I would like to thank Dr. Lynn Watney for allowing the use of the Wellington data for my thesis.

Finally, I would like to thank the field crews that collected both the 2005 Inman Highway 61 dataset as well as the field crew that collected the 2016 Wellington petroleum field data.

On a more personal note, I would also like to thank: Joel Feigenbaum, Kelly Feigenbaum, Jeffrey Feigenbaum, and Katherine Feigenbaum. Additionally, I would like to thank Kelsey Rook. Without their love and support throughout my academic career, this journey would not have been possible.

Contents

FIGURES & TABLES:

INTRODUCTION:

This research produced a unique method to accurately resolve near-surface velocity information from complex settings both temporally and spatially. The method requires joint analysis of refractions and reflections (JARR) to iteratively invert for velocity. This method is ideally utilized when used in conjunction with first arrival tomography (FAT). This method can be applied to many different reflection processing methods and applications. To demonstrate the value of this research, static corrections and accurate migration velocity models were derived for the near-surface emphasizing the utility of the JARR FAT method for some of the most significant challenges in reflection seismology.

Joint analysis of refractions and reflections (JARR) is a natural extension of joint analysis of refractions and surface-waves (JARS) method developed by Ivanov et al., (2006) but for the reflection method. JARS was developed to provide more accurate interval velocity functions for near-surface application of multi-channel analysis of surface-waves (MASW) method. The JARR method incorporated with FAT has been developed for incorporation into a standard processing flow in a fashion similar to that of JARS. The work flow requires several input controls and produces a velocity function proven to possess greater accuracy than the initial velocity function. The first input that the method requires are normal move-out (NMO) estimations or information pertaining to velocity of reflections. Next, first arrival picks are provided to the workflow. Additionally, other information pertaining to the tomography inversion is required as part of the input parameters. An a-priori, damped reference model, allows for convergence of the inversion to a realistic accurate velocity model of the near-surface that represents the global minimum solution.

This method was developed to reduce difficulties, correcting for geometric distortions and static variability associated with inaccurate near-surface velocity estimations. Migration as well

as long wavelength static corrections are two applications the JARR method targets and where accurate near-surface velocity information dictates the quality of reflection sections.

Traditionally, migration (mapping reflecting points to their proper location) (Claerbout, 1971; Claerbout and Doherty, 1972) is routinely not effective when applied to near-surface data (Black et al., 1993). This ineffectiveness is because the velocity function incompletely compensates for complex near-surface geometries or structures (Black et al., 1993). Most near-surface imaging applications would benefit from migration to correctly image the near-surface and fully characterize complex geology. Effectively reducing imaging distortion caused by these complex subsurface geometries is normally relegated to exploration depths where migration algorithms and analysis methods are plentiful and the velocity is much more uniform (Taner et al.; Stork, 1992; Nemeth, 1995; Clapp et al., 2004; Alaei, 2006; Min and Shin, 2006; Al-Saleh and Jiao, 2012). However, if the near surface velocity could be determined with great accuracy and resolution, dissolution features and other complex near-surface geology could benefit from migration. Migration filters have been developed for the near-surface as an attempt to improve the reflection image quality while minimizing the struggles attributed with migration in the near-surface (Ivanov et al., 1998). These migration filters should not be confused with true migration methods.

Static calculations have been derived from FAT methods (Zhu et al., 1992; Marsden, 1993; Stefani, 1993; Mayer, 2009), and are common place in processing flows for datum corrections. However, these FAT static corrections require expensive and substantial a-priori information to provide accurate solutions (check shots, vertical seismic profiles, etc.). The a-priori information is necessary to limit the non-uniqueness that is inherent in FAT (Ivanov et al., 2006). Although FAT is utilized by the JARR method to define a near-surface velocity function, the application of

the JARR method in conjunction with FAT addresses the non-uniqueness associated with FAT, without the necessity of extra a-priori information (check shots, vertical seismic profiles, etc.). Additionally, the JARR method introduces yet another method for deriving static corrections.

A near-surface dataset was collected along Highway 61, south-east of Inman, Kansas. The objective of this dataset was to image the upper 500m and look for solution features. The extremely distorted near-surface data were processed using a JARR incorporated work flow. The data pre- and post-JARR processing are strikingly different with the post-JARR processed stacked data appearing more realistic. Although this method was initially designed to define a better velocity function of near-surface, it was also tested in an exploration depth (1500m) setting. To test the application at exploration depths the Wellington petroleum field in Wellington, Kansas was processed with the JARR method integrated into the work flow. As with the Inman dataset, the final stacked sections appeared more realistic post-JARR processing.

GEOLOGIC BACKGROUND:

WELLINGTON PETROLEUM FIELD, WELLINGTON, KANSAS:

The Wellington petroleum field is located, in an agricultural area, approximately 6 km north-west of the city of Wellington in Sumner County, Kansas (Figure 1). Historically, oil production in this field has been conventional, but recently advances in enhanced oil recovery (EOR) have made this mature Mississippian reservoir a perfect test bed for CO_2 injection (Kansas Geological Survey, 2015). Wellington KGS 1-32 (# 15-191-22591) was drilled to fully sample the reservoir and monitor changes resulting from EOR using CO_2. This monitory and sample well penetrated basement and is located near receiver station 1177.

Figure 1: Google Earth image of Wellington petroleum field reflection line. Station 1001 is the northernmost station. Station 1519 is southernmost station collected. Modified from (Google Earth, September 1, 2015.).

In this area of Kansas, rocks range from Pre-Cambrian to Permian (Figure 2a-c). The surficial geology consists primarily of Quaternary Loess deposits (Walters, 1961). These deposits range in thickness from 0 to 20m (70ft) in thickness. The Sumner group outcrops along drainages where it transitions into Quaternary Alluvial deposits (Walters, 1961). The subsurface stratigraphy is dominantly alternating limestones/dolostones and shales with sandstone units interspersed (Kelly and Merriam, 1964). The main litho-stratigraphic units, of interest to this study, in the Wellington petroleum field are the Arbuckle Group, Mississippian Limestone, Lancing-Kansas City Group and the Salt Member of the Sumner Group.

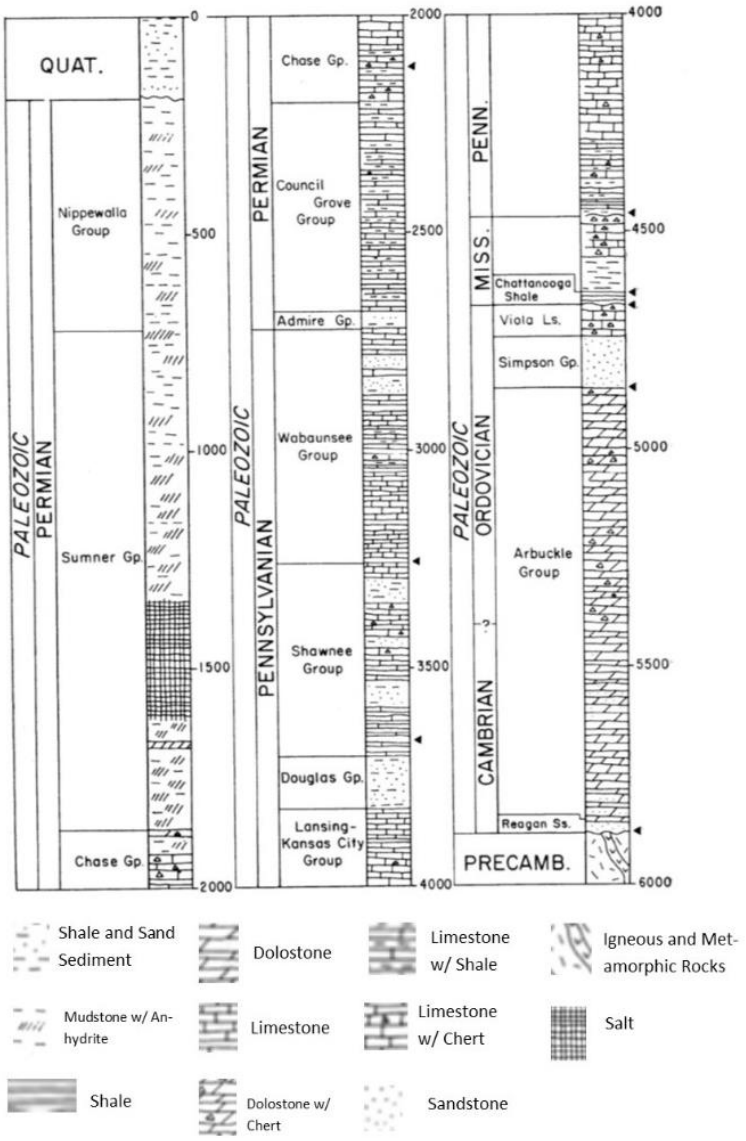

Figure 2a: A generalized stratigraphic column from Sedgwick Basin in Sumner County, Kansas. Modified from (Kelly and Merriam, 1964) to insert legend.

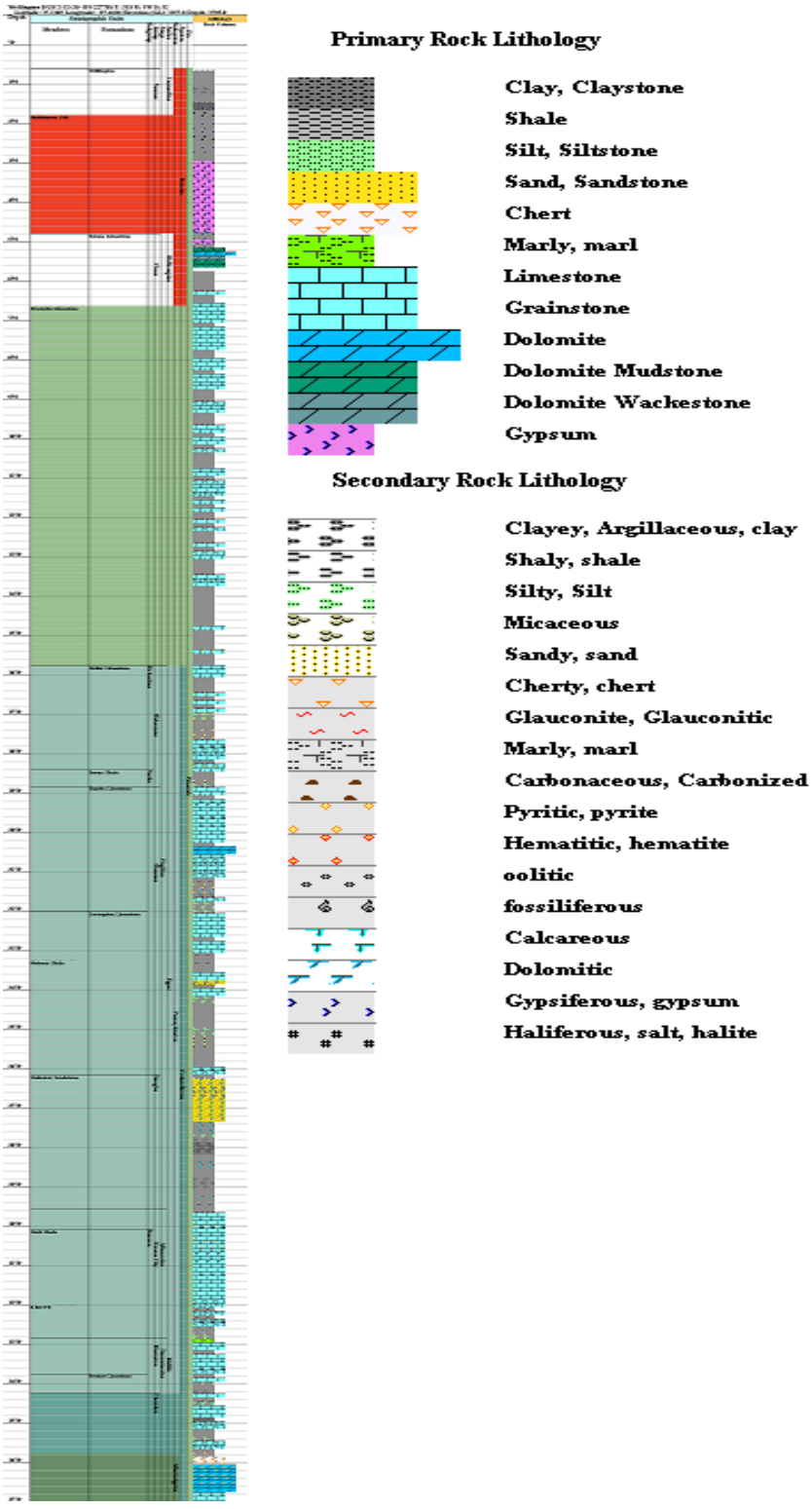

Figure 2b: Stratigraphic Column derived from Well 15-191-22770 (Survey, 2015) and is located at station 1315. This column represents from 25m to ~1190m. Each large tick on the left represents 30m. Modified from the stock output to allow the legend to be displayed at an appropriate size. This well log was generated using the KGS Gemini public software.

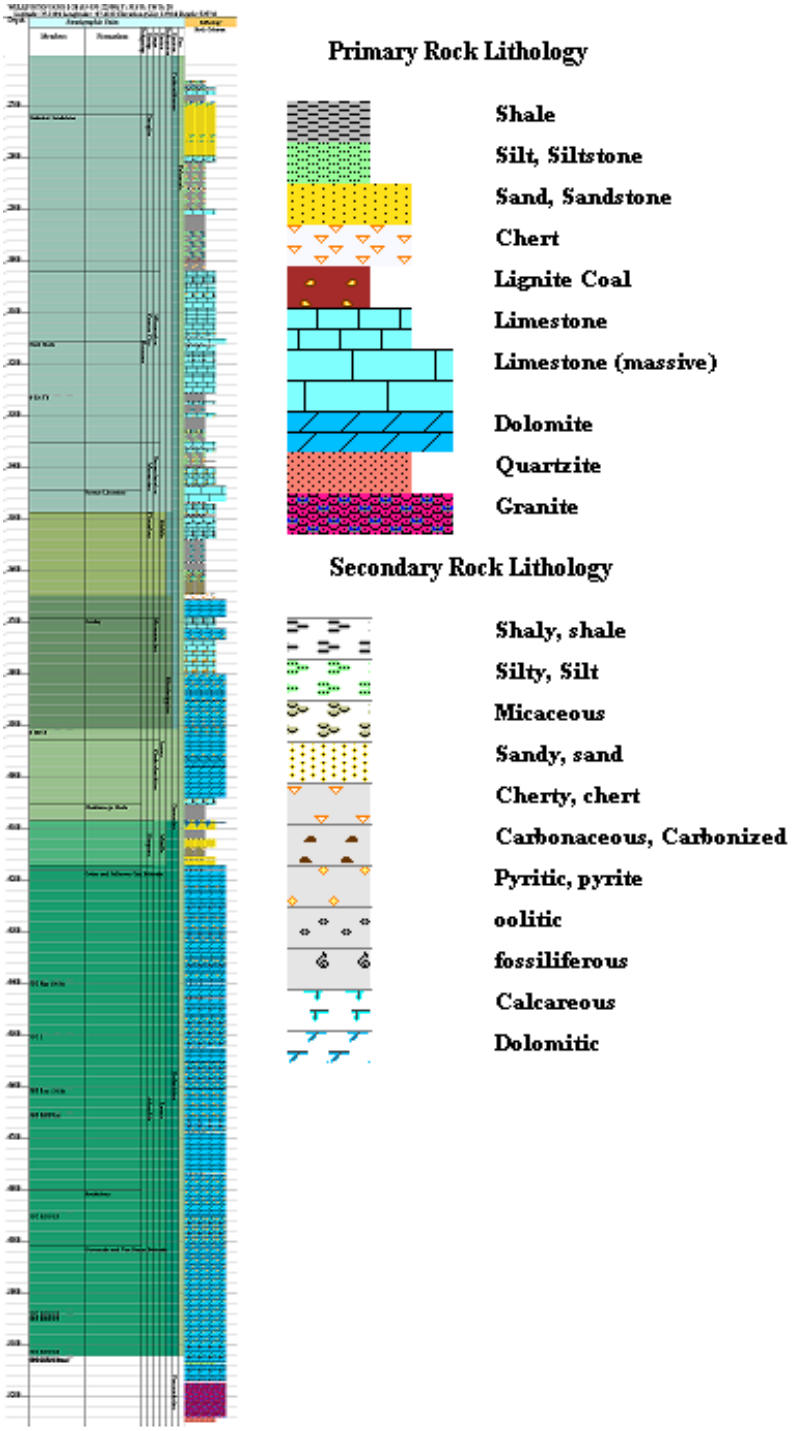

Figure 2c: Stratigraphic Column derived from Well 15-191-22591 (Survey, 2010). This column represents from ~800m to ~1600m depth. Each large tick on the left represents 30m. Modified from the stock output to allow the legend to be displayed at an appropriate size. This well log was generated using the KGS Gemini public software.

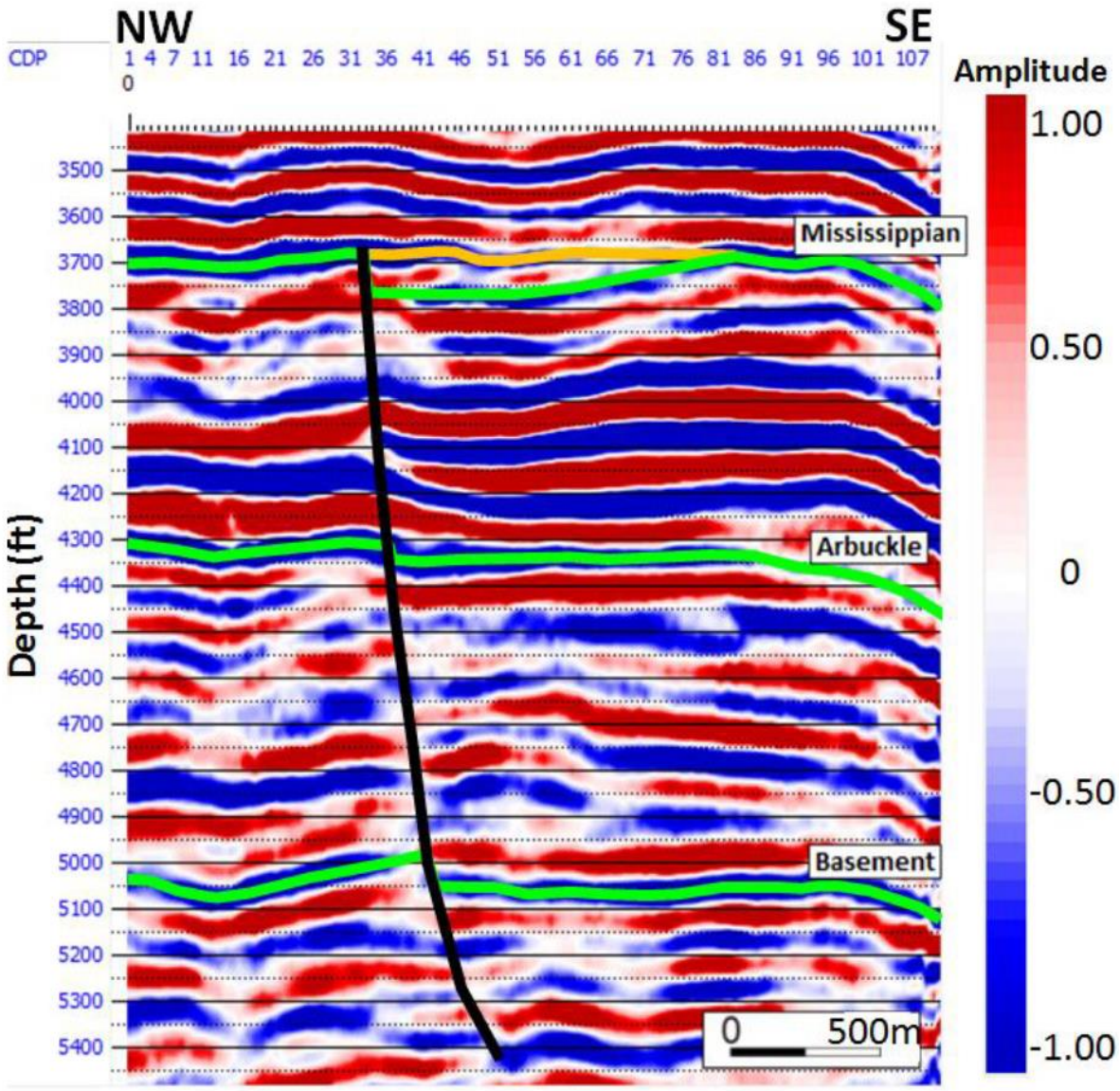

Figure 3: Normalized reflection section from a 3D Seismic Project in the Wellington petroleum field. The fault shown by black line originates in the basement and cross-cuts layers terminating in the Mississippian Limestone (Fadolalkarem, 2015).

In general, structures in Sumner County are primarily related to the Beaumont Anticline and Rainbow Graham Anticline (Merriam, 1963). Both of these features run parallel to one another, striking north-east to south-west (Kruger, 1996). Additional structures in the area include a series of north-east to south-west and north-west to south-east striking faults (Kruger, 1996).

These fault trends appear to form a crosshatch pattern in map-view. Specific to the Wellington field, is a basement fault that terminates at the base of the Mississippian Limestone that has been proposed by Fadolalkarem, (2015) (Figure 3). It appears to be a normal fault with roughly 100 feet (~30.5 meters) of displacement.

HIGHWAY 61, INMAN, KANSAS:

As the name implies, the Highway 61 Inman dataset was collected just west of the town of Inman, along Highway 61. The line is oriented southwest to northeast through McPherson County, Kansas (Figure 4). Loess, alluvial and dune deposits outcrop throughout McPherson County with the Kiowa Formation and Ninnescah Shale outcropping primarily in drainage areas (Williams and Lohman, 1949). Beneath the Ninnescah Shale lies the Wellington Formation, which consists of the upper Wellington Formation, Hutchinson Salt Member, and lower Wellington Formation (Figure 5) (Anderson et al., 1998). The Hutchinson Salt Member is primarily responsible for the generation of sinkholes in the area, as a result of natural dissolution and anthropogenic causes (Anderson et al., 1998). The Salt Member is laterally prevalent throughout South Central Kansas. The eastern dissolution front of the Salt Member is the area of concern (Anderson et al., 1998). The Salt Member beneath the seismic line is anywhere from zero to ~75 meters thick (Figure 6).

Figure 4: Highway 61, Inman Kansas Seismic Line. The seismic profile begins at shot location 1999 and extends to station 4057, ending at receiver station 4160. The line is ~5.3 km in length. A subset from stations 2500 – 3425 was used for this research. Modified from (Earth, 6-19-2015).

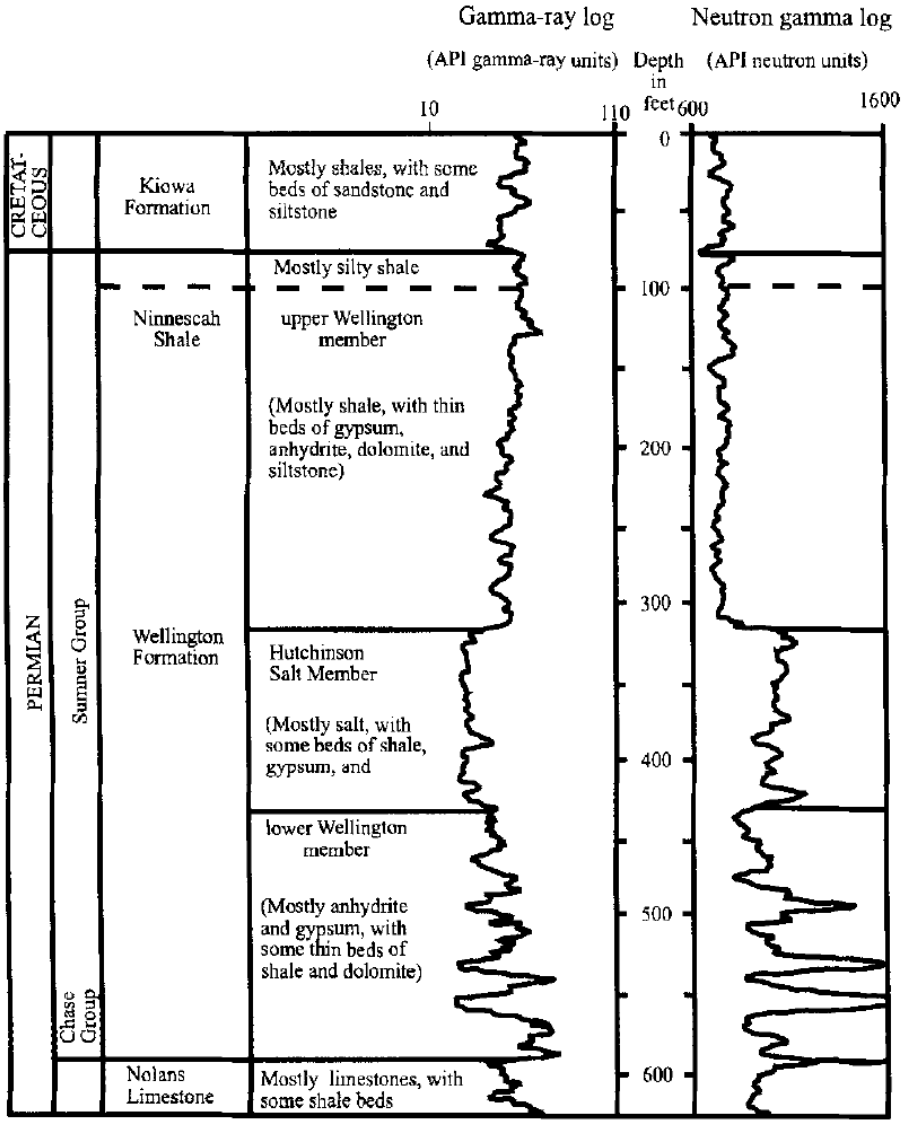

Figure 5: Stratigraphic column with gamma ray log and neutron density log (Anderson et al., 1998).

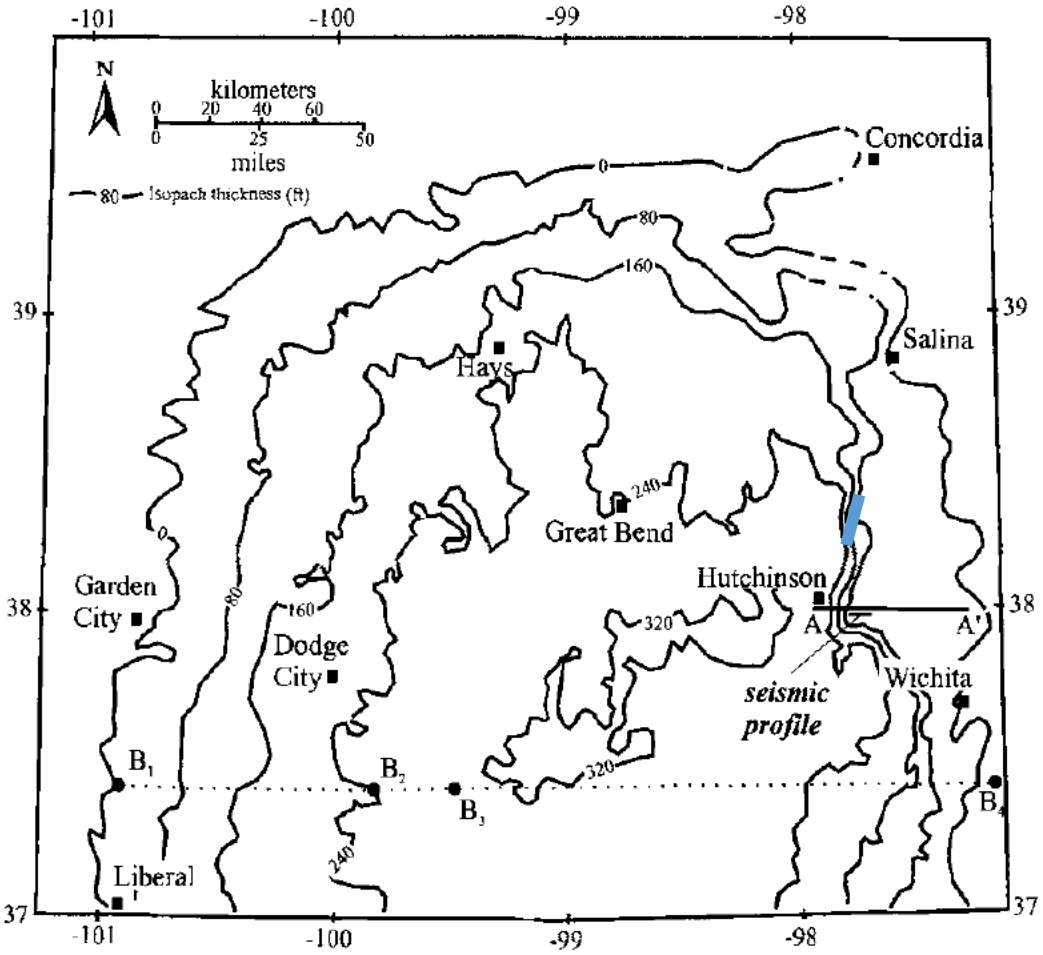

Figure 6: An isopach map of the Hutchinson Salt Member in South Central Kansas. The light blue line drawn just above Hutchinson Kansas approximates the location of the Highway 61, Inman Kansas line. Modified from (Anderson et al., 1998).

SEISMIC ACQUISITION:

WELLINGTON ACQUISITION:

The Wellington Seismic Reflection Section was collected as a preliminary study of the area before tests with CO_2 injection had begun. The section (~2.1-kilometer section) was collected, ~6 km NW of Wellington, Kansas, on August 24, 2015. The north-south trending seismic line was comprised of 530 recording channels, with 4-meter receiver station intervals.

Shot locations began at the first station location, advancing to every other station with a nominal source interval of 8 meters.

Three 28-Hz Ion geophones, spaced one meter apart, were planted at each receiver location. The receiver array was designed to cancel and reduce noise while adding and enhancing signal.

There were 22 Geometrics Geodes utilized in the collection of this fixed asymmetric split spread. The source was a 17,000 pound IVI Envirovibe, which imparted energy in a 10-second upsweep from 20-250 Hz, with a starting taper of 1 second and a final taper of 0.5 seconds.

There were three sweeps per location recorded separately over a total recording time of 12 seconds per record, and a sampling rate of one millisecond. The three sweeps were recorded uncorrelated and not vertically stacked.

Each shot gather contained 530 traces with the first two traces dedicated to the ground force trace and synthetic trace. Although there was capacity to record 528 channels, the final ten channels (519-528) were left dead due to challenges reaching the property limit.

Several petroleum pump jacks were active during data collection. This added high amplitude localized noise that was dealt with during the processing phase. Additionally, several commercial trucks were operating during some of the data collection, contributing range and severity of noise that also dealt with during the processing phase.

HWY 50, INMAN ACQUISITION:

A segment of a seismic reflection line collected in 2005 that possessed distinct structures extending to the near surface which were poorly resolved in the original processed section was used in this study. The seismic line ran from south to north along U.S. Highway 61 just south-west of Inman, Kansas. The subset is ~5 kilometers in length with two Mark 40-Hz geophones placed at each receiver station spaced every 2.4 meters (8 feet) in the highway road ditch (Figure 7). The 1/3-meter geophone array helped attenuate some of the road noise that was collected during the survey.

The seismic line was acquired with a rolling fixed split-spread that integrated ten Geometrics Geode seismographs for a collective 240 recording channels. The first channel in each record was the ground force (GF) pilot trace telemetered from the vibrator real-time. The shots were 4.8 meters (16 feet) apart, skipping every other receiver station. The subset of the 5km line studied ended at shot station 4057. The final recording channel of the subset is receiver station 4160.

An IVI Minivibe 2 (Figure 8) swept from 25 Hz to 250 Hz with a sample interval of 1 millisecond and a beginning taper of one second and an ending taper of 0.25 seconds. Three, 10-second, uncorrelated upsweeps were recorded at each shot location over a 12 second recording time. Much of the elevation data were interpolated GPS data collected during the survey.

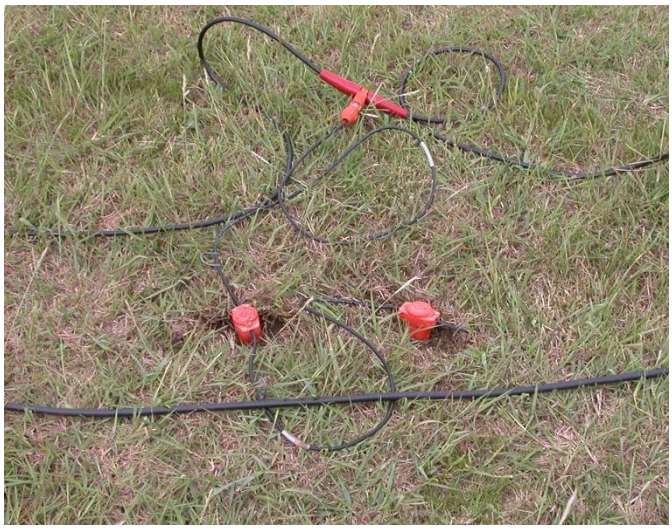

Figure 7: 40 Hz Mark geophones spaced approximately 1/3 of a meter apart. The pair was plugged into the take-out cable, which is connected to the Geometrics seismograph.

Figure 8: The IVI Minivibe 2, middle right, collected data along the side of the highway in the road ditch. The gator, middle left vehicle with yellow canopy, was responsible for firing the Minivibe and collecting the data from the seismographs.

METHODS:

VIBROSEIS METHODS:

Vibroseis sources impart energy into the ground over a specified time window and at variable, but predetermined frequency ranges (Goupillaud, 1976). Vibroseis is one of several ways to introduce energy into the subsurface for the collection of seismic data. For the two seismic sections (Hwy 61 & Wellington), it was the ideal method. All seismic energy propagating through a layered earth can be represented by the Convolutional Model (Ristow and Jurczyk, 1975). A time series describing the interaction of a seismic pulse with a layered earth model can be expressed by equation (1), where $x(t)$ is the recorded signal, $\omega(t)$ is the source signal, $\varphi(t)$ is the earth response (reflectivity), and $n(t)$ is random noise (Yilmaz, 2001).

$$x(t) = \omega(t) * \varphi(t) + n(t) \quad (1)$$

Uncorrelated signal, $x(t)$, which was recorded for each sweep, has the earth response imbedded in the data. Cross correlation with the source wavelet is required to recover the earth response. Equation (2) has been modified from Brittle et al., (2001) to maintain consistency with variable symbols defined here.

$$x'(t) = \varphi(t) * \omega(t) \otimes \omega(t) = \varphi(t) * k(t) \quad (2)$$

After the cross-correlation operation, the source signal is compressed and the embedded earth response (reflection spike sequence) is exposed as a convolved time series with a minimum phase Klauder wavelet representing each reflector in the earth response sequence. This makes analysis possible.

FIRST ARRIVAL TOMOGRAPHY:

Tomography has been utilized in the industry as a method for calculating near surface velocity and then static corrections due to an irregular lateral velocity function, as well as a method for better understanding near surface layering (Marsden, 1993; Mayer, 2009). Travel-time

tomography (reflection tomography) (RT) is utilized for developing migration velocity functions (Stork, 1992; Nemeth, 1995; Guangnan et al., 2014). Reflection tomography has become a standard practice for defining a migration velocity model. However, this method suffers from initial model reliance and threat of convergence on one of many local minima (Guangnan et al., 2014). An alternative to RT that provides greater sensitivity to inhomogeneity is first arrival tomography (FAT). All seismic waves are altered as they propagate through various velocity layer interfaces in the subsurface, but first arriving waves are unique because they are characterized by head wave energy returning to the surface following the critical refraction of downward travelling body wave energy (Zhu et al., 1992; Marsden, 1993; Lillie, 1999). Snell's law predicts the critical angle:

$$\theta_c = \sin^{-1}(\frac{V_1}{V_2}) \tag{3}$$

where θ_c is the critical angle of total refraction, V_1 is the velocity of the layer above and V_2 is the velocity of the layer below the interface (Lillie, 1999).

FAT (turning-ray tomography) exploits first arriving energy to calculate and invert for velocity variations in the near surface. It is particularly good at resolving lateral velocity variations (Zhu et al., 1992; Miller et al., 1998). Accurately resolving lateral velocity variation is helpful for seismic reflection processing because defining these irregularities can help explain and correct for non-hyperbolic reflections resulting from velocity changes with the subsurface sampling distance for a single CMP gather (Stork and Clayton, 1991). Furthermore, FAT is traditionally used to define a velocity model for the near surface used to calculate static corrections larger than the subsurface distance sampled by a given shot record (long wave statics) (Zhu et al., 1992; Marsden, 1993). This method is preferred for near-surface applications over normal refraction methods. Normal refraction methods require velocity to increase with depth. First arrival tomography can

handle conditions that are more complex (velocity inversions, strong gradients, etc.) (Zhu et al., 1992; Miller et al., 1998) and known to exist in the near surface (Steeples and Miller, 1988). Additionally, body wave first arrivals (the data used in FAT) are inherent in all reflection shot locations. Body wave first arrivals occur more regularly when compared to traditional refraction methods, thereby making it a more useful tool (Miller et al., 1998).

Unfortunately, as robust as FAT is, there are some shortfalls; non-uniqueness of the tomography, errors inherent in the picking of the data, and error in the initial model (Ivanov et al., 2006) are a few issues that FAT must contend with. An additional pitfall of FAT is that the maximum depth of investigation is generally limited to approximately one fifth to a quarter of the maximum shot offset (Zhu et al., 1992; Stefani, 1993). This inevitably leads to reduction in confidence with depth of the final model due to ray coverage (Stefani, 1993).

Joint analysis of refractions and surface waves (JARS) method was developed partly to address the initial model problem as well as non-uniqueness inherent in FAT. JARS relies on an a-priori pseudo Vp model to address these issues. The Vp model is derived from a Vs model estimated using multi-channel analysis of surface-waves (MASW) (Park et al., 1998; Xia et al., 1999; Ivanov et al., 2006). JARS has proven to be a successful stabilizing solutions and providing better tomographic results (Ivanov et al., 2007; Ivanov et al., 2010; Ivanov et al., 2013). Solutions produced using a-priori reference models allow interpretation with greater confidence, in that the solution is the universal minima rather than the local minima (Ivanov et al., 2006)

The conventional FAT equation:

$$\begin{bmatrix} L \\ \beta D_d \\ \lambda D_s \end{bmatrix} [s^{est}] = \begin{bmatrix} t^{obs} \\ \dots \\ \beta s^a \\ \lambda h \end{bmatrix} \quad (4)$$

provides the least-squared solution. L is the length the ray traveled through the velocity model, D_d is the weighted matrix for a reference model, D_s is the smoothing matrix, s^{est} is the model vector from the velocity model, t^{obs} is the vector of picks of the first arrival data, s^a is the stabilizing vector such that the solution remains close to the initial model, h is another smoothing vector, β is a damping constraint and λ is a smoothing constraint (Ivanov et al., 2006).

The JARS method utilizes an updated inversion equation that takes advantage of a reference model located within the neighborhood of the true solution:

$$\begin{bmatrix} L \\ \beta D_d \\ \beta_2 D_d \\ \lambda D_s \end{bmatrix} [s^{est}] = \begin{bmatrix} t^{obs} \\ \beta s^a \\ \beta_2 s^{aa} \\ \lambda h \end{bmatrix} \quad (5)$$

where L is the length the ray traveled through the velocity model, D_d is the weighted matrix for a reference model, D_s is the smoothing matrix, s^{est} is the model vector from the velocity model, t^{obs} is the vector of picks of the first arrival data, s^a is the stabilizing vector such that the solution remains close to the initial model, s^{aa} is the reference model, h is another smoothing vector, β and β_2 are damping constraints and λ is a smoothing constraint (Ivanov et al., 2006).

Miller et al., (1998) analyzed FAT velocity solutions to better understand the near surface. The velocity solutions were compared to the stacked reflection image produced over the same location. Their results were promising with regard to correlating near surface structures and subsurface geologic layers. The initial velocity models acquired and utilized by Miller et al., (1998) were derived from first breaks. Miller et al., (1998) note the benefits of interpreting the reflection images jointly with the FAT velocity solutions; however, they do not analyze or process the reflection information with the refraction information jointly.

JOINT ANALYSIS OF REFRACTIONS AND REFLECTIONS (JARR)

JARR is being introduced as a natural extension of the JARS method, (Ivanov et al., 2006) and as an alternative method to what was introduced in the previous section (Miller et al., 1998). Unlike with Miller et al., (1998), NMO velocity corrections were analyzed to develop an initial velocity model of the near surface.

The JARR method utilizes an initial a-priori damped reference interval normal move-out (INMO) velocity model based on observed reflection hyperbola. The standard inversion requires smoothing parameters established in Equation (4) to constrain the non-uniqueness of tomography as well as stabilize the final tomographic velocity solution. These parameters are arbitrary at worst and are tuned based on experience with the dataset at best.

JARR uses Equation (5) which replaces the smoothing parameters by constraining the inverted velocity function to the initial model. Damping the reference model allows for JARR to take advantage of the spatial and temporal velocity estimations and resolution of reflection information while inverting for a velocity function that represents the global minimum. While utilizing the advantages of FAT, the JARR method also addresses the shortfalls of the FAT method. As introduced earlier, FAT struggles from an inherent lack of uniqueness in the final solution. The JARR method's damped initial reflection NMO correction velocity model constrains the solution and forces the inversion to converge on the global minimum, reducing the non-uniqueness associated with FAT. Forcing the final FAT solution when used in conjunction with JARR provides greater confidence in the final solution.

The JARR method can be used in conjunction with other techniques such as standard refraction tomography or other methods that calculate or invert for velocity functions. Whichever method is employed the main purpose of JARR is to provide a-priori information to constrain the calculations and jointly solve for more accurate results consistent with the subsurface geology.

JARR METHOD WALK-THROUGH:

This section provides an explanation of each parameter required to operate the JARR method. Furthermore, the explanation only describes how to utilize the JARR method with regard to R-Tomo, the software utilized for this research.

First, provide an a-priori reference INMO velocity model. Next provide the first arrival picks as well as the source file. The source file allows for fluid movement from the station number coordinate system to the true physical lengths of the reflection survey. Once these information sources are provided, the JARR parameters need to be specified.

The first parameters that must be defined in the JARR method are the velocity boundaries. The velocity boundary values limit the range of possible velocity values for the inversion process. They can be derived from either the velocity model or from other a-priori information collected or known. This research utilized the data maximum and minimum velocity values because the JARR method argues that the velocity model provided is the only a-priori information. Furthermore, the interval INMO velocity model was generated from physical reflection NMO measurements. This allows the search window to be tied to the physical data rather than arbitrary velocity model values.

The second parameter which needs to be defined is the amount that the inverted model can be changed in one step. The inversion takes a minimum of one iteration. This parameter defines the maximum change from iteration to iteration. It helps stabilize the inversion process.

The next and arguably most important parameter which needs specification is the damping of the a-priori model. This parameter allows the JARR method to address the non-uniqueness associated with first arrival tomography as well as push the solution to the global minimum (Ivanov et al., 2006). The damping value is what makes the JARR method unique. It is a measure of how much the inversion can adjust the values of the a-priori model. A damping factor of zero indicates that there is no damping and the inversion is free to adjust the model as if damping was not applied.

The damping value can be any positive integer. Testing is required to find the damping value that provides the lowest RMS value as well as the most realistic solution.

An optional parameter that can be used in the JARR method is the emphasis on the near-offset data. It weights the fitting of near-offset first arrival values. It was used in this research to address the complexities of the near-surface by emphasizing the solving of near-offset values. Testing was necessary to find the ideal near-offset emphasis.

Next, the horizontal smoothing factor "lambda" must be selected. This value can be any positive integer. This value forces mathematical smoothing in the horizontal direction. It helps address instability in the horizontal direction. The larger the value, the more horizontal homogeneity is assumed in the subsurface. Testing is required to achieve the optimal value to achieve the lowest RMS value and most realistic results.

Smoothing order is the next parameter that needs to be defined. This dictates whether the inversion uses first order or second order smoothing. This value requires testing to determine if the result is more realistic with first or second order smoothing.

Finally, the number of iterations for each pass needs to be selected. Depending on how a model is structured, inverting more than three iterations begins to introduce instability into the inversion process, producing increasing error.

Once the parameters have been specified, the first arrival tomography aspect of the JARR method can be completed. The final solution can be iterated to achieve a more accurate solution. This is described later on as the "leap-frog" method. The "leap-frog" method allows for supplying a realistic and accurate solution back into the first arrival tomography, while also changing the parameters described above. This can be achieved many times, slowly moving towards a solution that has both low RMS error and appears qualitatively accurate.

MIGRATION METHODS:

MIGRATION PROCESSING:

Migration is a term used to describe the process of calculating the true dip of a reflection event, and re-mapping that point back to the correct location in the subsurface (Chun and Jacewitz, 1981). Migration is important to reflection data processing and the production of an accurate stacked image because processing routines assume all reflections on NMO corrected CMP gathers are flat and zero-offset between the source and receivers. Any reflector in the subsurface that has dip produces reflections that violates these assumptions, distorting the location of reflection events in the subsurface away from true (Yilmaz and Claerbout, 1980). These distortions are the target of migration methods. Restoring the true subsurface geometries and locations is the goal of migration.

There are three types of migration used in reflection data: Diffraction (Kirchhoff), Finite-Difference (Wave Equation) and Frequency-Wavenumber (FK, Stolt). Both Kirchhoff and FK migrations handle steeply dipping layers well. FK is robust in low S/N (signal to noise) data, while Kirchhoff is less effective on noisy data. Finite difference methods work well in low S/N, but struggle with steeply dipping reflections, and take a lot of computing time (less of an issue with today's computers). The FK method is less effective with highly variable velocity functions (Chun and Jacewitz, 1981). All things equal, an accurate velocity model is the most important component to the effectiveness of any migration method.

For this research, the focus was on the Kirchhoff post-stack depth migration, as well as the Stolt post-stack depth migration. Stolt migration was first published by Stolt, (1978). Utilizing the relationship between the Fourier Domain (FD) and the space-time domain data is transformed between domains using the 2-D Fourier transform. In the Fourier domain the data are corrected and true dip is restored based on the supplied migration velocity function:

$$\bar{F}(k_x, k_z) = \frac{k_z}{\sqrt{k_x^2 + k_z^2}} F(k_x, \sqrt{k_x^2 + k_z^2}) \quad (6)$$

where $\bar{F}$ is the Fourier transform of the migrated section, F is the 2-D Fourier transform of the unmigrated section, k_x is the wavenumber in the x-direction, and k_z is the wavenumber in the z direction (Chun and Jacewitz, 1981). Remapping of the data in the FK domain from k_z = 1 to the true location on the pink fan can be visualized for a full FK migration (Figure 9). Detailed derivations have been published and are readily available (Berkhout, 1981).

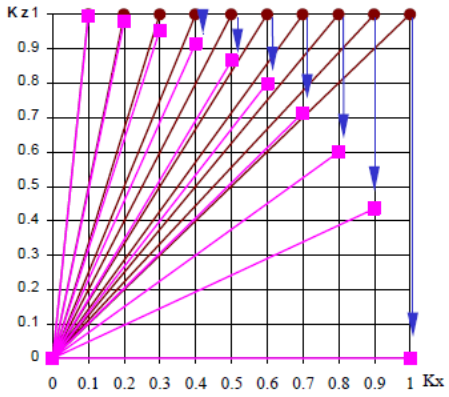

Figure 9: Depiction of the FK migration and how values are re-mapped in the Fourier domain (Ivanov et al., 1998).

Kirchhoff migration is based in Huygen's second principle where every point in the subsurface is a diffracting point (Zhu et al., 1998; Yilmaz, 2001). This principle defines reflections as a summation of many closely spaced diffracting points. If a reflection is interrupted due to subsurface geology or structures, diffraction tails can become visible on the seismic reflection data. Kirchhoff migration aims to correct these diffractions by means of Kirchhoff summation in a migration algorithm such as seen in Equation (7):

$$P_{out} = \frac{\Delta x}{2\pi} \sum_x \frac{\cos\theta}{\sqrt{v_{rms} \cdot r}} \rho(t) * P_{in} \quad (7)$$

where P_{out} is the migrated image, v_{rms} is the input velocity values (from a model), $r = \sqrt{(x - x_0)^2 + z^2}$ where x and z are the input coordinates, $\rho(t)$ is the time derivative wave field

filter which accounts for phase-shifts and amplitude changes, and P_{in} is the input seismic image (Yilmaz, 2001). Detailed derivations of the Kirchhoff method are illustrated in Schneider, (1978) and Berkhout, (1981).

Kirchhoff migration can be performed on both pre-stack and post-stack reflection seismic data. Pre-stack Kirchhoff migration performs the migration calculations on the shot records while the post-stack version of the Kirchhoff migration restores the waveforms on NMO corrected and stacked data.

Migration of reflections from near surface reflectors is not always utilized due to very slow velocities and a lack of velocity control (Black et al., 1993). Using the noise suppression characteristic of migration while minimizing the spectral degradation Ivanov et al., (1998) proposed using the Stolt migration as a filter by over estimating the station spacing changing the k_x. This approach compresses all of the data in the FK space down towards the k_z axis (Figure 10). A full migration is applied but because the data occupies the smaller region in the FK domain, it is only partially migrated. This essentially results in a severe under-migration of the data, which only partially restores the reflections to their true location. Generally, an improved signal to noise ratio stacked section results from this method, but it does not fix (or claim to fix) miss located reflecting points due to complex geometries by restoring them completely to their true location.

The approach introduced by Ivanov et al., (1998) is a migration filter approach and should not be considered migration. This is a smoothing technique that provides minimal changes in reflection points where the change is extremely minimal. This is an approach utilized in the near-surface for enhancing reflection quality. JARR can be utilized as a full migration technique that can be utilized as an alternative to the approach provided by Ivanov et al., (1998) or in concert.

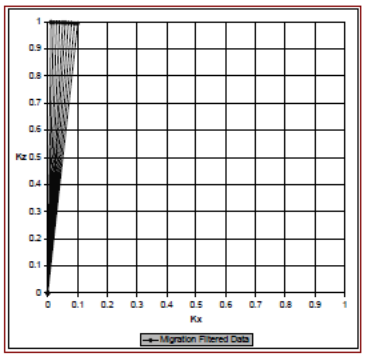

Figure 10: All the data has been compressed to between 0 and 0.1 by way of altering station distances. A full migration is applied but no data is represented in the far offset of the migration. Therefore, all of the data is migrated slightly (Ivanov et al., 1998).

MIGRATION VELOCITY ANALYSIS:

Migration velocity analysis (MVA) is the process by which the velocity model used to calculate the migration is updated and refined to produce a more realistic solution (Sheriff, 2002). Various methods have been proposed to achieve better velocity models as a way to address the difficulties associate with migration velocities. Some examples of MVA methods include Reflection tomography (traditionally or with incorporation of a-priori information) (Stork, 1992; Clapp et al., 2004), tomography of migrated gathers (Alaei, 2006), tomography on common image gathers (Nemeth, 1995; Al-Saleh and Jiao, 2012), damped wave-equation tomography for Kirchhoff migration velocities (Min and Shin, 2006), and depth migration velocity analysis using NMO like depth panels (Taner et al.). Regardless of the method, they all aim to provide accurate velocity information, which is vital for producing appropriate migration results (Zhu et al., 1998). All these methods were designed for exploration depths targets. To address the unique issues of the near surface I will introduce the JARR method, which is a novel method for deriving migration velocities based on refining near-surface velocities.

The concept for the JARR method was introduced earlier to minimize static issues. Like the static application of JARR, the migration use requires three important pieces of information are needed. Foremost, first-arrivals must be selected from the dataset. For the case presented here,

first arrivals have already been selected and corrected using the JARR method applied to static corrections. Second, an initial velocity model must be defined, which for most cases would simply be the interval velocity function generated from NMO velocity analysis. Finally, a source file is generated that allows for the transformation between reference frames. Unique to the JARR method is calculated INMO velocities that are close to the true velocity solution and therefore damped. This addresses the non-uniqueness issues common with the FAT method by forcing the search for the solution to be constrained to the provided model, allowing for the solution to represent the global minimum.

As stated earlier, FAT has limited ability to produce results at depth. Fortunately, velocities at depth tend to be fairly consistent with the exception to extreme structural cases. With this in mind, the damped JARR FAT velocity solution has the interval NMO velocities appended to generate a full velocity model of the subsurface. This produces a velocity model that addresses complexities of the near-surface, and the relatively simple and smooth nature of deeper velocities. This is not to say that the deeper, exploration depth velocities are not complex but when compared directly to the near-surface they are substantially more uniform. For example, an unconsolidated sediment in contact with a lithified limestone, which is common in the near-surface, will have an extreme velocity contrast and therefore a drastically different acoustic impedance. Compare the extreme velocity variation in the near-surface to complex exploration depth velocity variation such as salt in contact with limestone or saturated shale, the velocity contrast is large however it is not as large as the near surface example.

The migrated image provides useful information for testing if a particular method has achieved its intended outcome. If an incorrect velocity function is applied, the corrected reflections tend to “smile” or “frown” depending on whether they are over or under migrated (Figure 11) (Zhu

et al., 1998). It is common for near-surface depths and to a lesser degree for exploration depths that conventionally generated velocities with results in either over or under migrated sections (smiles and frowns). Therefore, it is customary to "tweak" the velocity model as necessary to flatten the final migrated image. This is done through qualitative means for near-surface data. Or, as noted by Black et al., (1993), migration is often simply neglected for near-surface data due to its complexity and lack of an acceptable cost to benefit ratio.

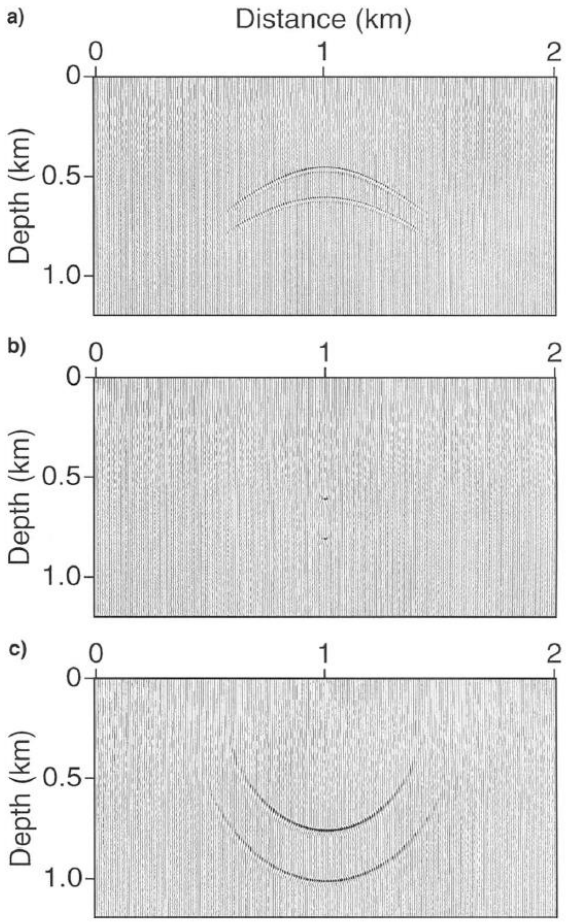

Figure 11: a) over migration (too high velocity, "frown"), b) perfect migration (correct velocity), c) under migration (too low a velocity, "smile") (Zhu et al., 1998).

DATA PROCESSING METHODS:

All data within this thesis were processed using software developed at the Kansas Geological Survey, in Lawrence, Kansas. That software includes, *WinSeis, SeisUtilites, R-Tomo,* and *LW Seis*.

The Highway 61, Inman, Kansas dataset was collected using English units, (feet, miles, etc.), but was converted to metric so that both datasets shared the same units. For clarity, to address unusual increments or numbers due to the conversion, the Inman set will have the English units in parenthesis.

WELLINGTON PROCESSING METHODS:

The Wellington Field 2-D seismic profile underwent an extensive processing flow (Figure 12). Specific steps were critical to the quality of the final section. A highly used and effective spectral conditioning tool that enhances signal and attenuates noise is referred to as vibroseis whitening (Coruh and Costain, 1983; Lambrecht et al., 2004). After vibroseis whitening, the data were correlated with a synthetic sweep used to drive the mass, also referred to as the pilot. SeisUtilities correlation and decoding was used for the cross-correlation. After cross-correlation the source and receiver geometry was assigned to the dataset from the field notes.

Each of the three sweeps delivered by the vibrator at each station were recorded separately and uncorrelated. Although the field seismograph has the ability to stack in the field, these data were not. Stacking in the computer rather than the field seismograph allows for greater control over the quality. Records that are extremely noisy can be avoided completely where in field stacking this is not possible and a complete reshoot of the record is necessary. In most cases, only the second and third records were stacked. The first shot records were not used because they lacked comparable amplitude and frequency content when compared to the second and third record (Figure 13). Incomplete source plate coupling of the first shot at each location accounts for the

discrepancy in the quality when comparing the first to the second and third shot. However, extreme noise levels prohibited including certain records altogether. The extreme noise levels were attributed to cultural noise (airplane, commercial truck, etc.) at Wellington. For some cases with extreme noise, the entire station was removed from the dataset.

Spherical divergence was applied to ensure trace amplitude uniformity and consistency with energy propagation. This process accounts for spatial attenuation of the wave-front amplitude as it propagated away from the source (Newman, 1973). After testing, a spherical divergence value of three decibels per second (dB/s) visually normalized the traces consistent with the amplitude character of the dataset overall.

A spectral balance was applied over the envelope of frequencies imparted by the source (Figure 14). This process was done to balance high frequencies to help differentiate the high frequency reflections from narrow band source and background noise. Tests showed that spectral balancing was a necessary step to bring out the high frequency reflections of the near-surface in the stacked shot records.

Killing (muting) of noisy/bad traces was the next pre-processing step carried out. Killing traces was a vital step in removing irrecoverable noisy traces. Removing these traces dramatically increased the quality of the dataset. Traces associated with pump-jack noise, bad traces, aircraft and commercial trucks were removed.

Initially, a trapezoid band-pass filter was applied with corner frequencies 25, 50, 200, 250. A high cut filter with corner frequencies of 90 and 180 Hz was used to dramatically reduce the high frequency noise, and partially attenuated the surface wave energy (Figure 14). Testing performed using low cut filtering yielded no positive results.

Frequency Wave-number (FK) Filtering was performed to attenuate/remove high velocity surface waves. This processing step was successful in filtering linear velocities that ranged from 1000 m/s to 2300 m/s (Figure 15). When velocities not inside this range were removed noise was introduced in the final stacked section that aliased at 45-degrees relative to the time zero line. A higher velocity surgical mute was used to remove energy remaining after FK filtering (Figure 16).

Surgical muting zeroed values below a linear velocity of 700 meters per second. This reduced slower surface waves and the air-coupled-wave. Zeroing this portion of the data dramatically enhanced the image quality (Figure 17) (Baker et al., 1998). Additionally, first arrival muting removed first arrival, direct arrival, and refractions (Figure 18). This was essential to ensure that coherent reflection energy on CMP stacks were solely reflections (Steeples and Miller, 1988).

The data were sorted into Common Mid-Point (CMP) gathers (Figure 19). For velocity analysis in conjunction with surface consistent statics. Using CMP constant velocity panels, in conjunction with velocity semblance panels allowed the creation of an in-depth velocity model (Figure 20). The constant velocity panels were gathered into 15 stacked CMP traces with velocities ranging from 2000 m/s to 4000 m/s. Semblance panels were created using the same CMP traces and analyzed to ensure the maximum semblance amplitudes correlated to the strongest reflections on the constant velocity panels.

A brute stack was generated after the application of NMO velocities to the traces to inspect the accuracy of these velocity values. Additionally, the stacking and interval velocities were scrutinized manually for unrealistic velocity inversions or sharp unexplainable lateral velocity changes. These steps were repeated multiple times, ensuring the most accurate and representative velocity model. Once an appropriate velocity model was achieved, surface consistent statics were

applied to the dataset. A correlation coefficient of 0.2 was used in the surface consistent static correction processing as the bound for acceptable correlation between CMP traces. This fixed small wavelength time variations of reflections due to surface elevations and the source and receiver static errors (Figure 19). These elevation based static shifts were applied to the original CMP without NMO corrections. With the hyperbolic shape of the reflection corrected for source to receiver offset and subtle short wavelength velocity variability, the improved analysis resulted in more accurate NMO velocities. Velocity analysis and surface consistent statics were performed one last time to produce a twice static corrected dataset with three velocity analysis runs. The final NMO corrected CMP gathers were stacked to generate a final time (Figure 21), and depth section (Figure 22).

In spite of the extensive processing, concerns remained with the reflection quality on the stacked sections (Figure 21, 22). A quick check of the data confirmed long wavelength statics and surface elevations were still responsible for artifacts. Therefore, more extensive and accurate static corrections were required and the JARR method was utilized to address that need.

In this instance, a migrated section was generated. The resulting 2-D reflection image was so poorly migrated it was not possible to garner any useful information. The poor migration of the data was partly due to the static problems, and partly to do with incomplete and inaccurate velocity information. Without a-priori information from wells a proper velocity model could not be synthesized and therefore only the NMO velocities were available for migration velocity information. This method was designed to handle data with no a-priori information. Therefore, deriving velocity information from wells in the area would not only preferentially skew the efforts to calculate a proper velocity model but would render the method virtually useless. Therefore, this

research highlights the contrasts between data that has not undergone the JARR method and data that has regardless of what the well information would indicate.

Static corrections derived from FAT were utilized to define the most accurate starting model for JARR. As previously stated FAT required first arrival picks, a source file, and a velocity model. The first arrivals were picked along the peak positive amplitude of the first arriving energy at 10 dB display gain. These parameters were chosen to account for correlation side lobes from vibroseis correlation (Figure 23), a natural artifact, and to ensure uniformity in picks across the dataset. Correlation side lobes arise when the correlation pilot trace approaches returned energy from the subsurface. When the correlation pilot trace matches the subsurface energy the largest amplitude value is returned. Finally, the velocity model was constructed from the NMO velocities using Dix equation to formulate the INMO (Figure 20) (Dix, 1955).

The INMO velocity model is treated as an a-priori reference model, and damped in a similar fashion as is practice with the JARS method. Instead of using velocities derived from surface-waves as the initial model, velocities are derived from reflection NMO corrections (Figure 20). The novel nature of the JARR method allowed for a much more refined and accurate near surface velocity model for inclusion in migration and static applications.

A "leap-frog" method of iterative analysis was employed to obtain the most accurate solution with the lowest RMS velocity. The preliminary solution derived from the initial model was used as a new model, and the process was repeated until the final solution converged to a low RMS error and appeared qualitatively reasonable (Figure 24a). A datum of 16 meters' depth was used. Since below this depth, the velocity values were laterally consistent, interpreted to mean the velocity variability in the near-surface (weathering zone, elevation changes, etc.) had been accounted for by the velocity function. These tomostatic corrections were applied to (Figure 25)

correct the long wavelength statics of the dataset. These long-wavelength static corrections produced time shifts from 0 to 10ms on each trace of the shot record. As previously discussed in the FAT section, long-wavelength static calculations are meant to reconcile lateral inconsistencies in the subsurface on the order of half a spread size or larger. Changes to the final stacked sections using the JARR method are illustrated (Figure 26, and Figure 27a) by a stacked time section and stacked depth section. The parameters chosen to achieve the final velocity solution are provided in Table 1.

Synthetic seismic traces (Figure 27b) and lithologic logs alongside synthetic seismic traces (Figure 27c) have been placed at the appropriate location along the 2-D seismic profile. The synthetic seismic traces as well as the lithologic log were generated from well information located along the 2-D seismic profile. The synthetic seismic traces that were generated are a single frequency at 80Hz. This frequency was chosen because it matches the peak frequency of the dataset.

Large velocity inversions such as those present in Figure 28a and Figure 30 are usually concerning, because it signifies poor velocity estimations. The Dix equation does not provide perfect results and relies on assumptions that if broken can produce artifacts (Dix, 1955). This is true unless the velocity inversion can be explained by geology.

Well 15-191-22770 (Figure 2b) (Survey, 2015) indicates the Hutchinson Salt is present in Wellington between ~80m and ~180m depth. Beneath the Hutchinson Salt there is a large package of interbedded limestones and shales indicated by the same well (Survey, 2015). Seismic velocities of salt regardless of depth tends to be approximately 5,000 m/s. In shallow depths the velocity of shales and limestones can vary from as low as approximately 1,500 m/s up to 3,000 m/s (Sheriff, 1976). The high velocity layer in Figure 28a begins at approximately 125m and

extends to approximately 400m depth. This follows the picks through NMO analysis. The high velocity layer in Figure 30 follows the same pattern as Figure 28a with more accuracy in the upper 250m. This is indicative of the suture zone between the JARR velocity function and the NMO velocity function. Regardless, both functions are in agreement at the suture zone of 240m and follow the geology represented in the near-surface indicated by Well 15-191-22770 (Survey, 2015).

Although the velocity inversion can be explained by the Hutchinson Salt Member, other concerning velocity variation is present when the velocity model is compared to Well 15-191-22591. Sonic log information (Sirazheiv, 2012) has been inserted into the INMO velocity model to check the accuracy of the velocity model (Figure 28b). The variation and the velocity increase at approximately 550m depth associated with the Topeka limestone are not represented in the INMO velocity model. Below this horizon, the general trend has been sampled by the velocity model. However, the velocity model shown in Figure 28a and Figure 28b has continually been under sampled when compared to the interval velocity shown in the well.

There are two different explanations that can account for the discrepancies between the sonic log and the velocity model. The first explanation is related to sampling interval. The INMO velocity model for this research was generated on a limited number of velocity picks, derived from a combination of velocity panels and velocity semblance panels. The sonic log is sampling the interval velocity at a much finer scale. This discrepancy in sampling interval can explain certain aspects of failing to identify the velocity variation in the subsurface. This second discrepancy in velocity model characteristics can be explained by the non-uniqueness attributed to velocity analysis with little to no a-priori information. Without any a-priori information, reflection picking was based on the coherency of the reflection events on the velocity panel. Within each velocity

panel, multiple velocities at very small depth changes provide just as coherent and possibly correct NMO velocity solutions (Figure 28c; Figure 28d). These slight changes in picking can dramatically change the velocity profile when using Dix equation to calculate the INMO velocities (Dix, 1955). Slowing a near-surface velocity pick (Figure 28c) or failing to pick a velocity (Figure 28d) removes a velocity inversion in the near-surface that was associated with the Hutchinson Salt Member. Additionally, increasing the deeper velocity by as little as 300m/s is enough to push the deeper velocities into the range expected by the sonic log (Figure 28d).

These small variations dramatically change the overall character of the velocity profile (Figure 28c; Figure 28d) while not drastically adjusting the overall final image (Figure 28e, Figure 28f). The major difference between the final image with the original velocity model and the new models that better resemble the sonic log are the fine scale features (reflection continuity of small reflections) and slight reflection amplitude variations (amplitude drop out). Reflection depth positioning and lateral horizontality of the reflections appears to be barely affected by these changes in velocity models.

Cross-correlation of the average response from CMP 2520 – CMP 2525 of the original stacked CMP solution with the adjusted velocity model solution indicated good correlation. Cross correlating the CMP's derived from the velocity model shown in Figure 28c with the CMP's of the original stacked section the cross correlation coefficient is 0.6729. Cross correlating the CMP's derived from the velocity model shown in Figure 28d with the original stacked section the resulting cross correlation coefficient was 0.5309. These values are not approaching a cross correlation coefficient of 1, which would indicate perfect correlation, but are still significant. This significance is shown by comparing the cross correlation coefficient threshold of surface consistent statics and these values. For surface consistent statics, it was considered a success when using a

cross correlation threshold of 0.2. The cross correlation coefficients compared above are twice to three times larger, which indicates substantial cross correlation between CMP traces. For these reasons, it is safe to assume that the velocity model initially used in this research was justifiable, due to the non-uniqueness of velocity estimations as well as the error produced by the use of the Dix equation to derive INMO velocities (Dix, 1955).

It is important to note that the well information was not used in the JARR method. It was only used as a check to identify the accuracy of the method. Additionally, the velocity model was not adjusted to more closely resemble the velocities shown in the sonic log. This was not done because the goal of this research is to illustrate the ability of the JARR method to achieve results with no a-priori information.

Once the dataset had static corrections applied using JARR the data were re-processed. First arrivals were re-selected. NMO velocity analysis was re-conducted on the corrected dataset to achieve a new INMO velocity function (Figure 28a). The new NMO velocity shown in Figure 28a was utilized as the initial a-priori reference model for the JARR method. A final JARR FAT velocity model with minimized RMS error (Figure 29) was calculated. The parameters that were used to achieve the JARR method INMO velocity model are provided in Table 1. The velocities provided by the JARR method had limited depth. The INMO velocity function was appended to the JARR method velocity function to achieve a complete INMO velocity function (Figure 30). The combination velocity function model is defined to depths of 3,500 meters depth. This allows for the complete migration of the data. The data was migrated using both post-stack Stolt (FK) (Figure 31 and 32) and post-stack Kirchhoff migration (Figure 33).

Parameter	**JARR – Static Parameters**	**JARR – Migration Parameters**
Damping Value:	(First Pass) 50 (Second Pass) 200	50
Near – Offset Emphasis:	51 Times	51 Times
Horizontal Smoothing:	(First Pass) 6400 (Second Pass) 800	3200
Number of Inversion Iterations:	(First Pass) 4 (Second Pass) 2	4
"Leap-Frog" Iterations:	1	0
Initial RMS Error (ms):	90.5	65.1
Final RMS Error (ms):	9.01	5.81
Number of Tests:	12	1

Table 1: This table indicates all the values used for the JARR method for both statics and migration for the Wellington, Kansas dataset. For the second pass, the solution from the first inversion is supplied as the a-priori reference model.

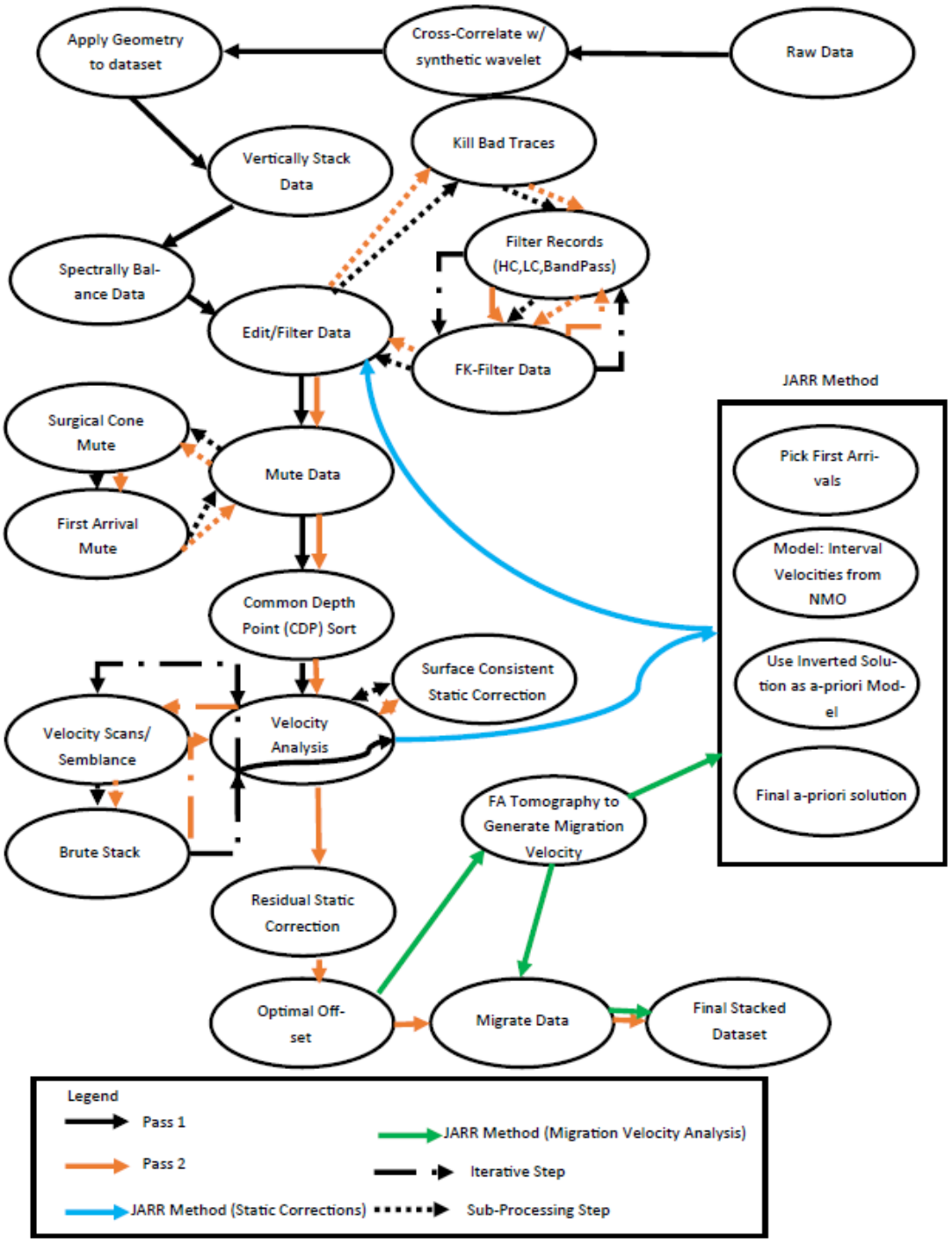

Figure 12: Processing flow for data processing both Wellington Kansas and Highway 61 datasets.

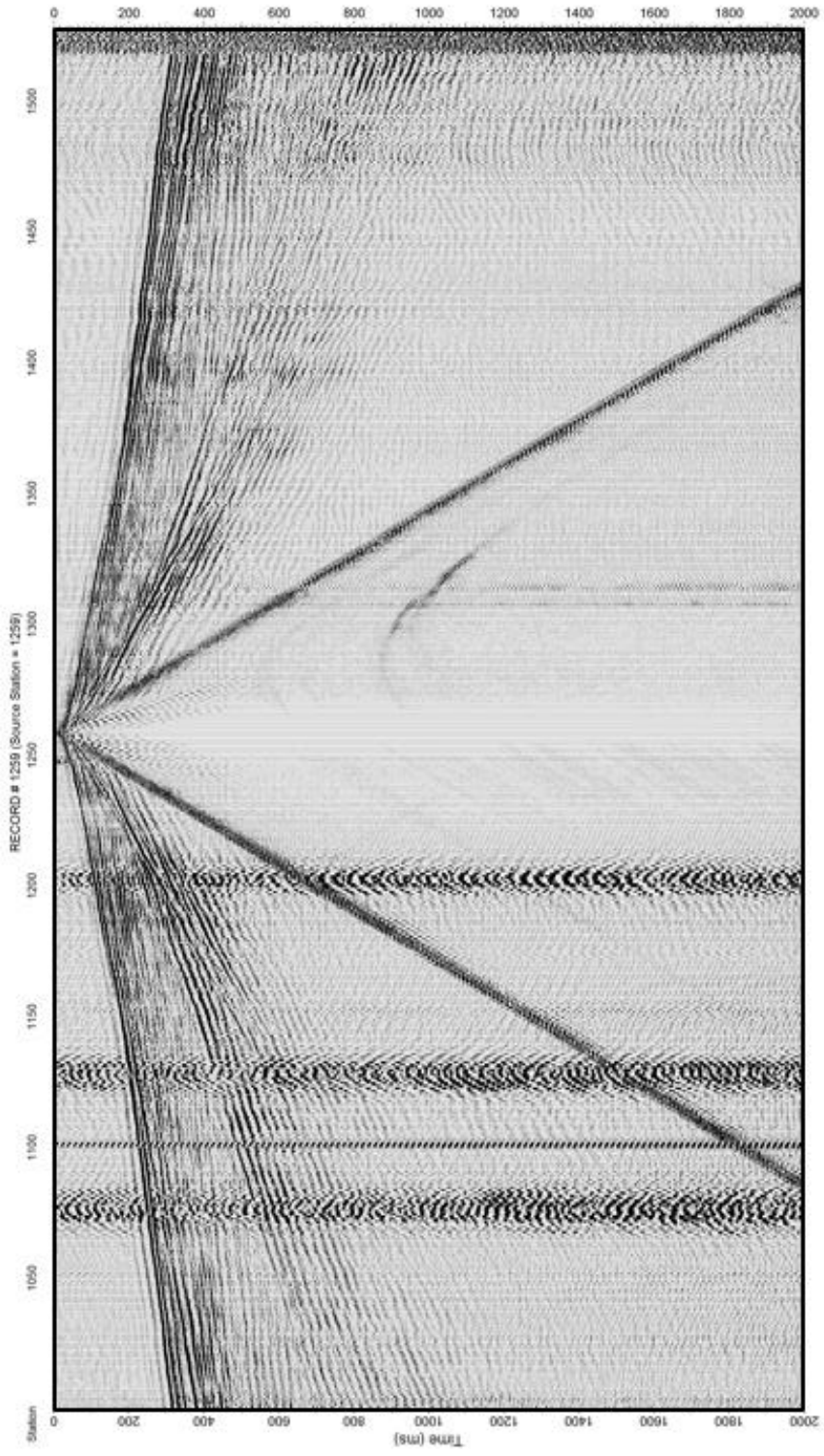

Figure 13: This is a representative post-correlation vertically stacked shot record.

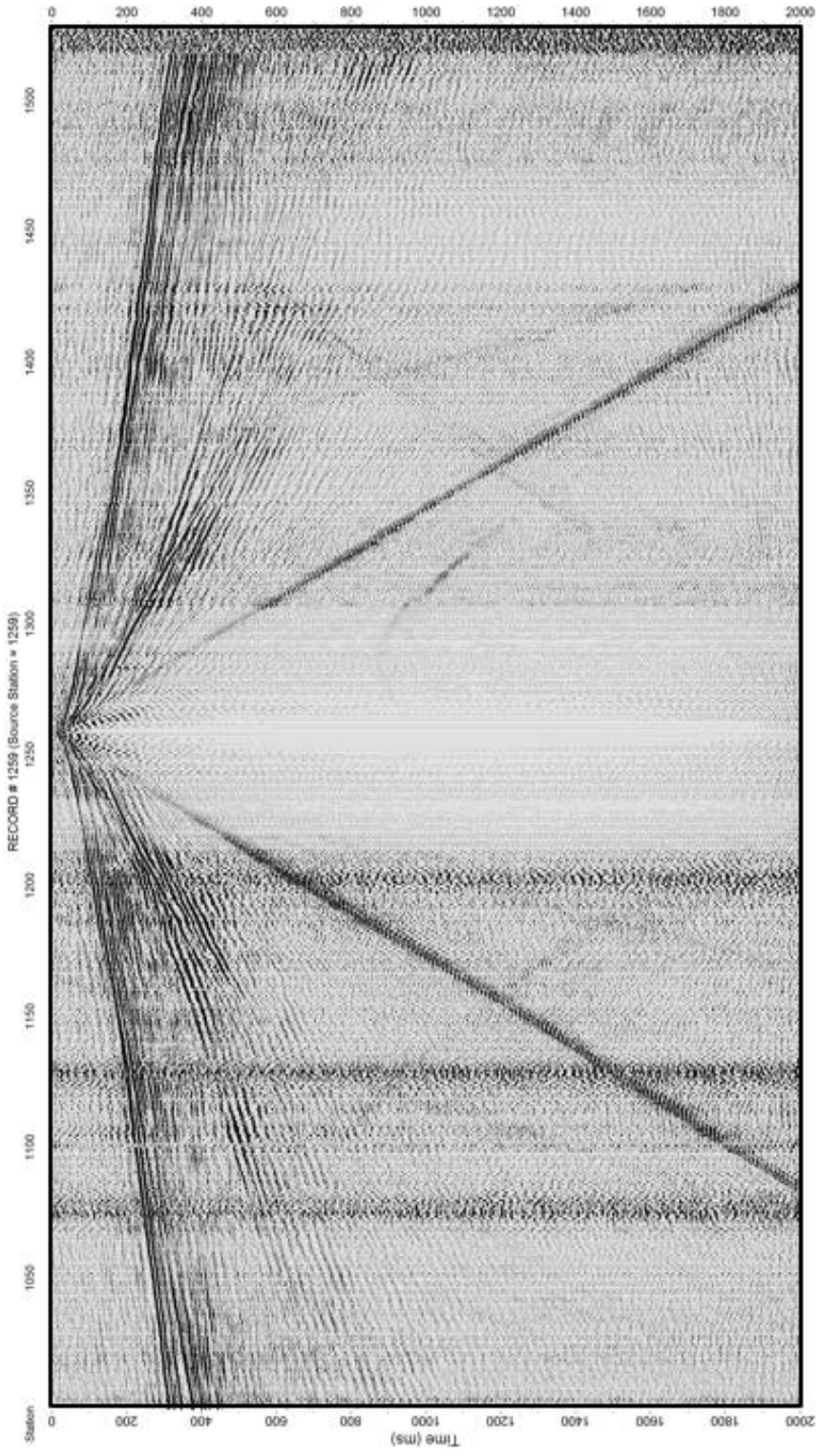

Figure 14: Representative shot record post-spectral balancing, spherical divergence and frequency filtering. A band-pass filter with corner frequencies of 20-50-200-250 was applied.

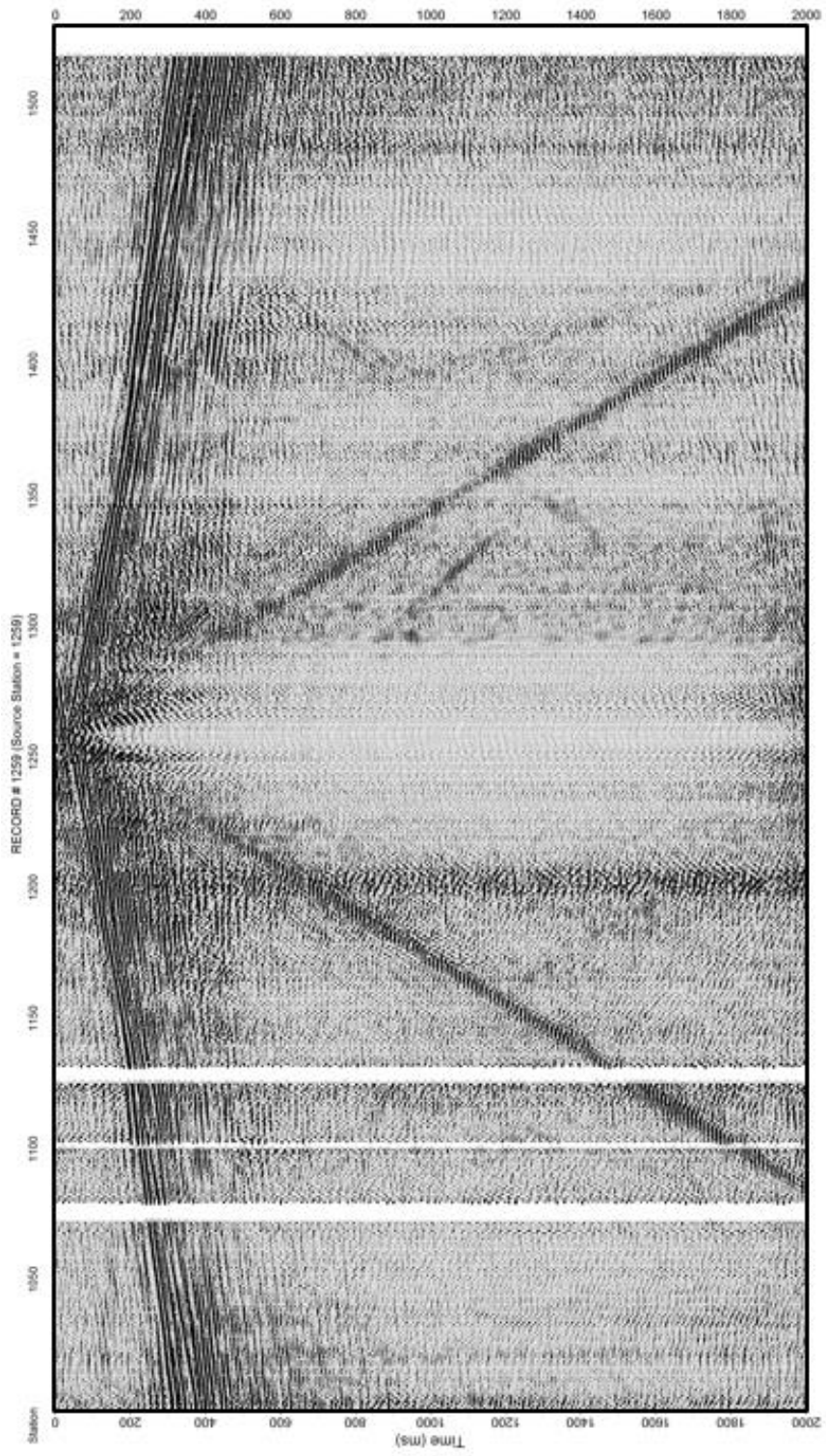

Figure 15: This is a representative shot record after FK filtering. This FK-filtering drastically reduced the energy of the surface-waves.

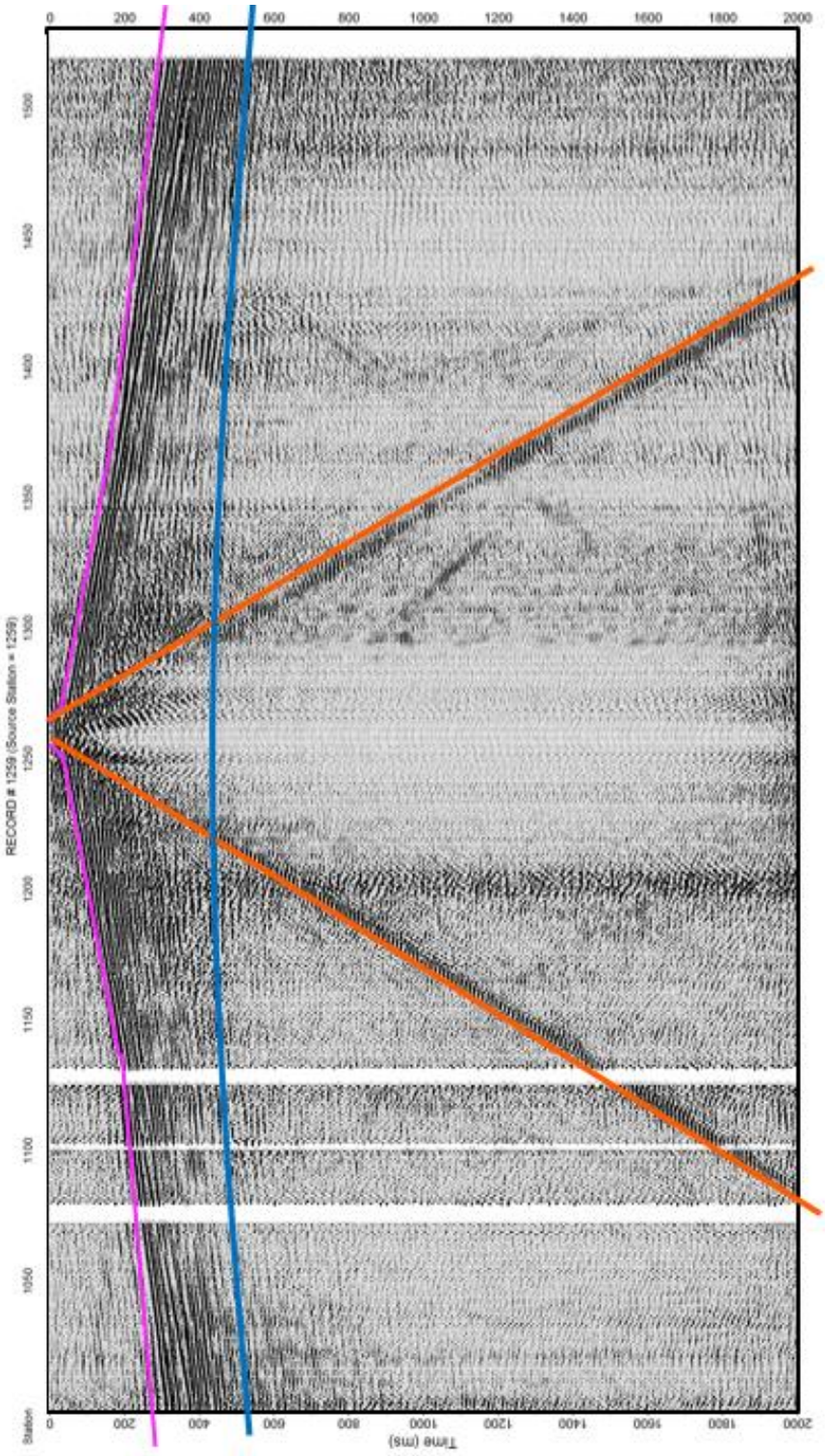

Figure 16: This is the representative FK-Filter from figure 15. The orange lines run atop the air-couple wave. The pink lines run atop the first arrival refractions. The blue hyperbola indicates a reflection.

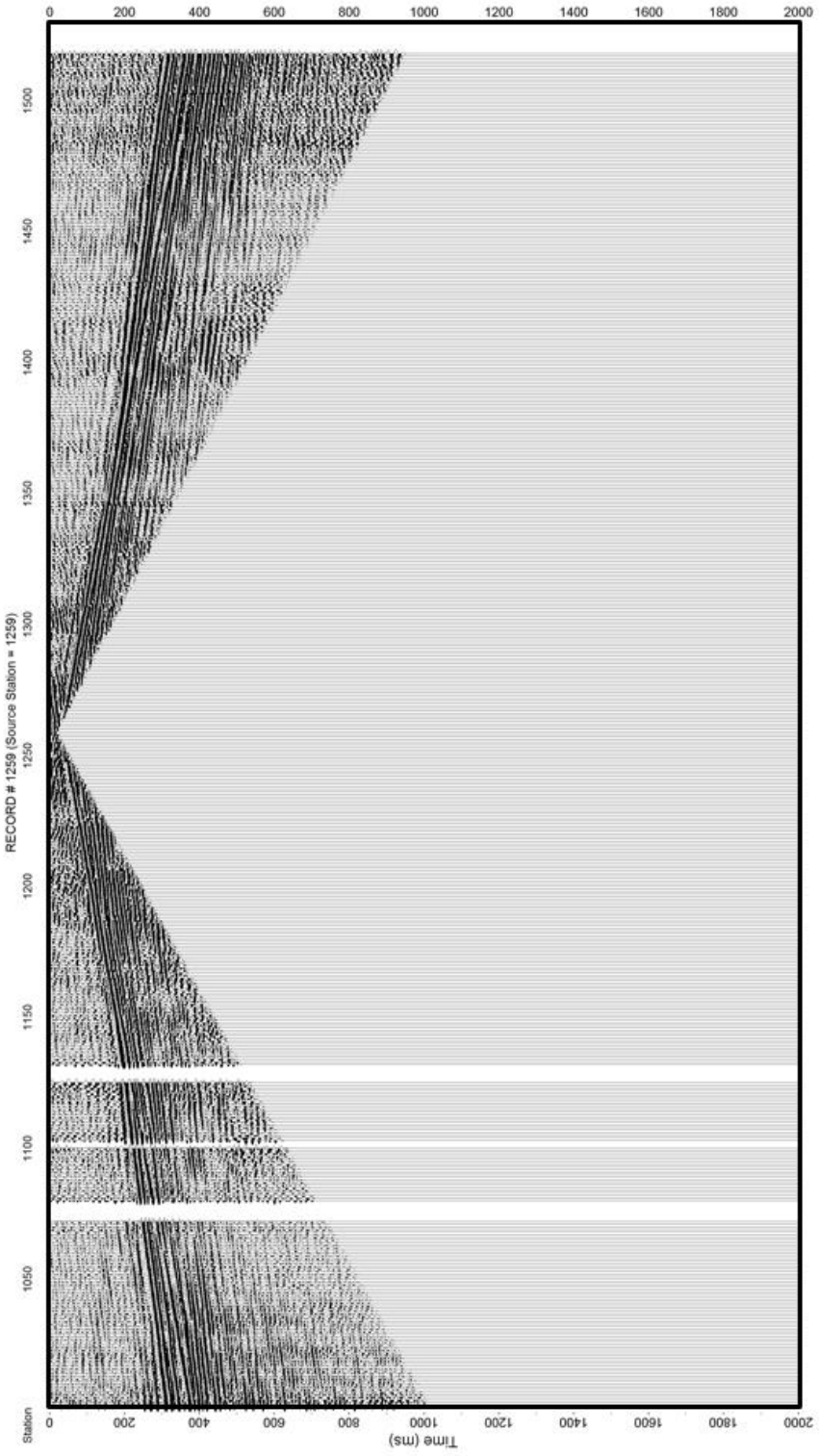

Figure 17: Representative shot record of an applied surgical cone mute to remove direct wave energy.

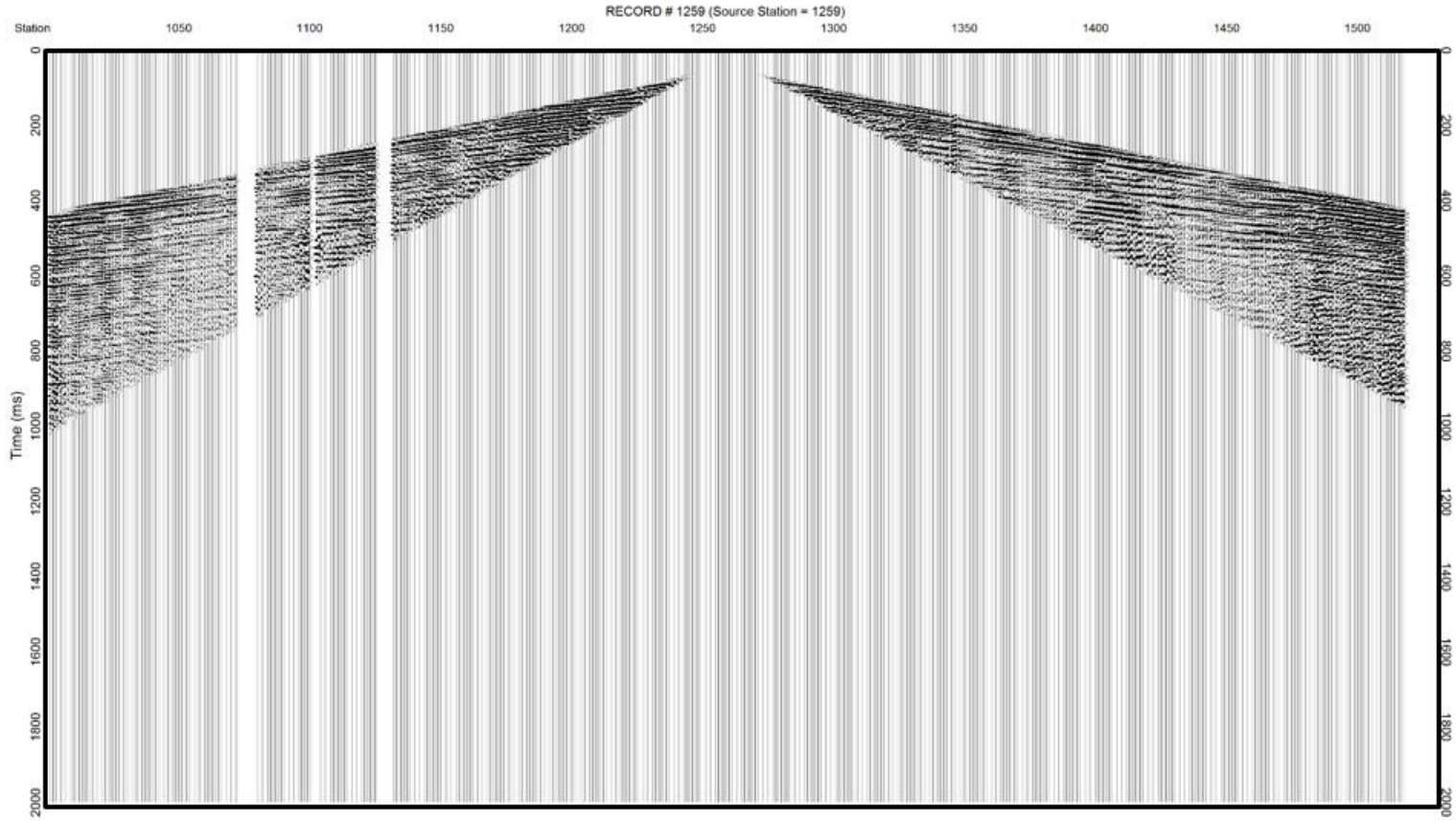

Figure 18: A representative shot record after first arrival muting was applied. This step was done to remove first arriving energy and refractions which can constructively stack and appear as reflections.

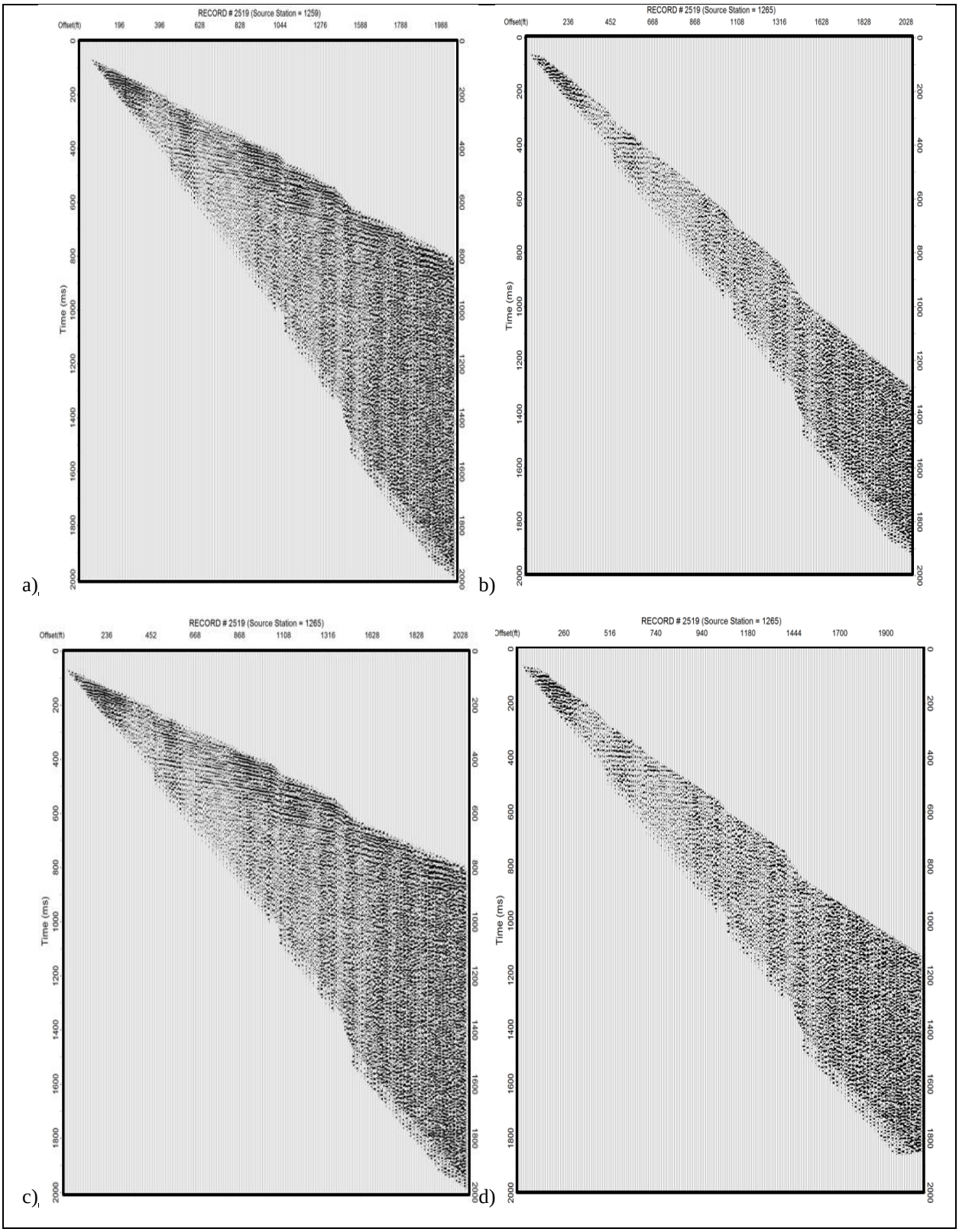

Figure 19: a) is a CMP gather pre-NMO velocity correction. b) is a the NMO velocity corrected CMP. c) is the surface static corrected CMP gather before NMO velocity correction. d) is the surface static corrected CMP after NMO velocity correction.

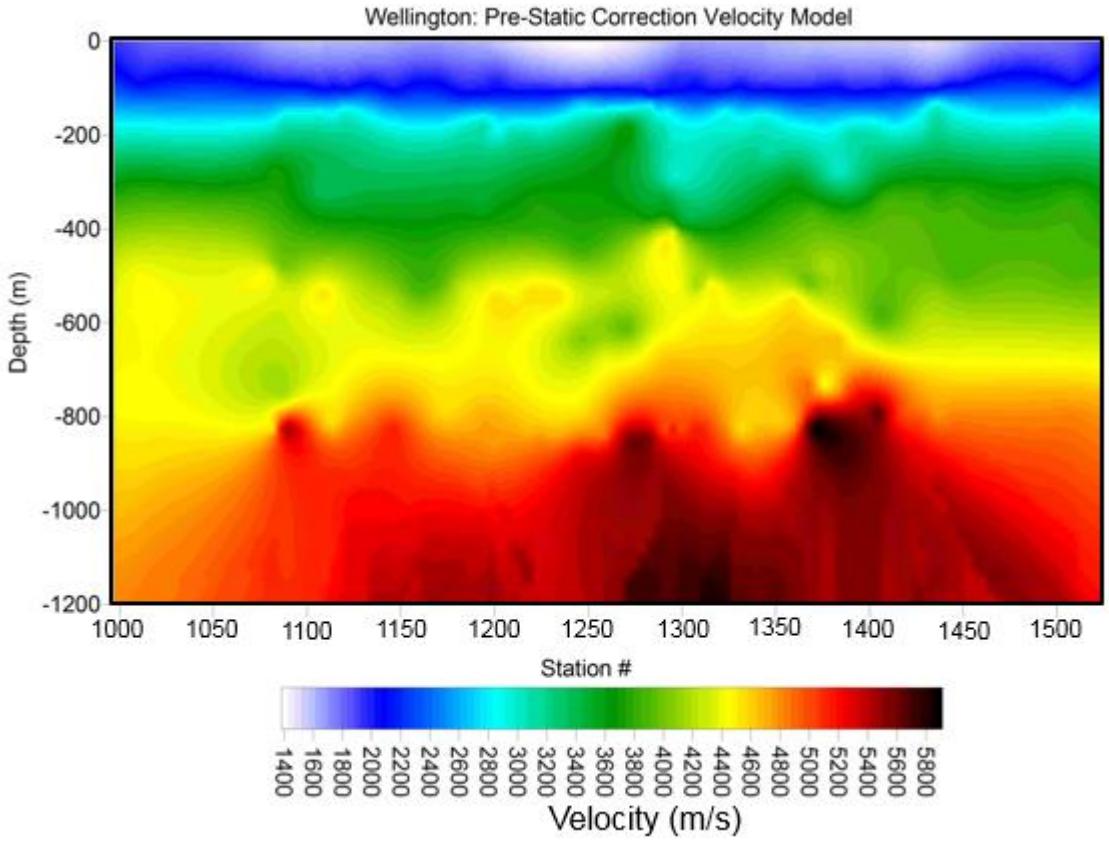

Figure 20: Initial interval velocity model derived from NMO corrections.

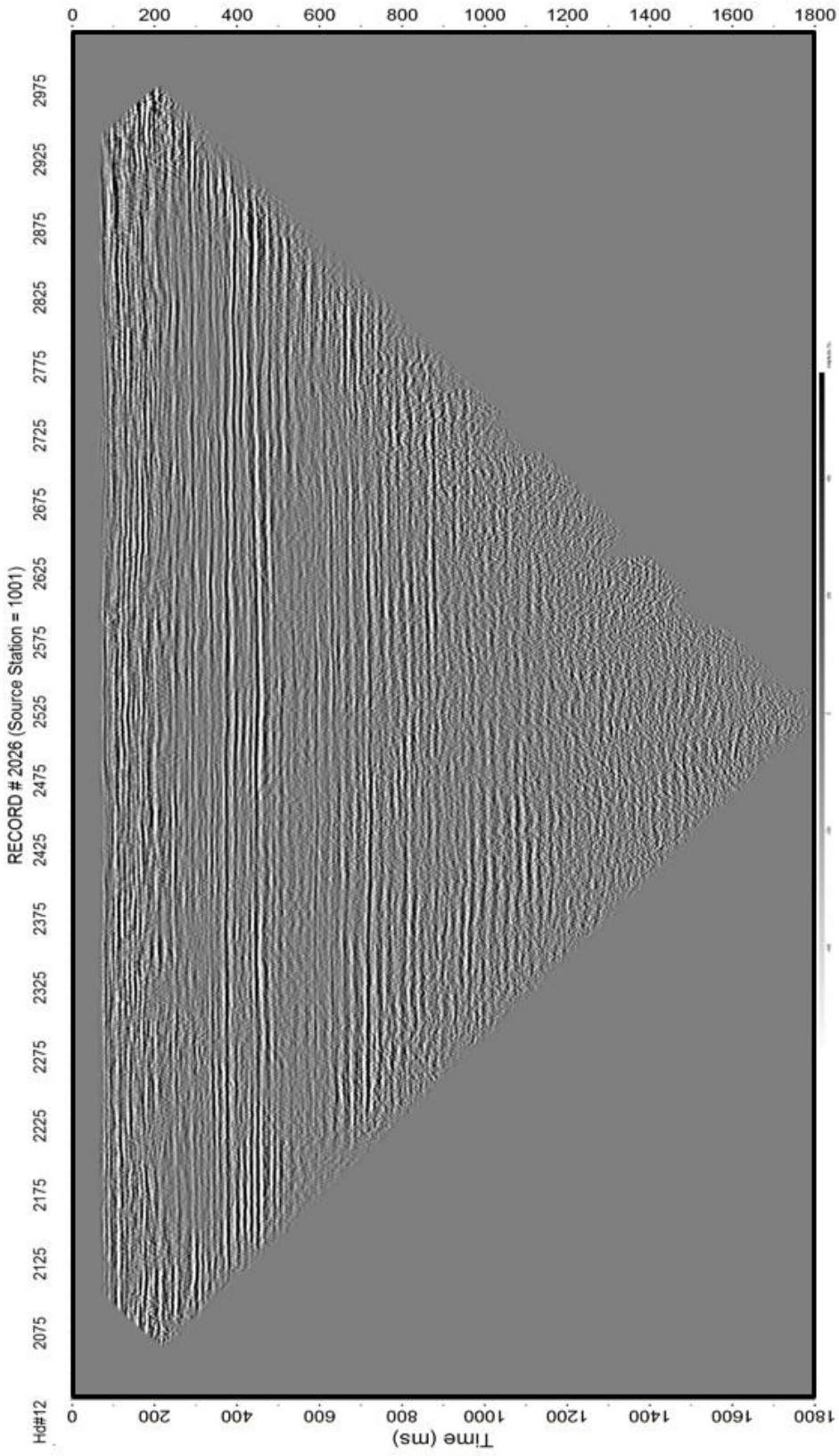

Figure 21: Pre-migrated, pre-JARR Static corrected stacked time section of Wellington.

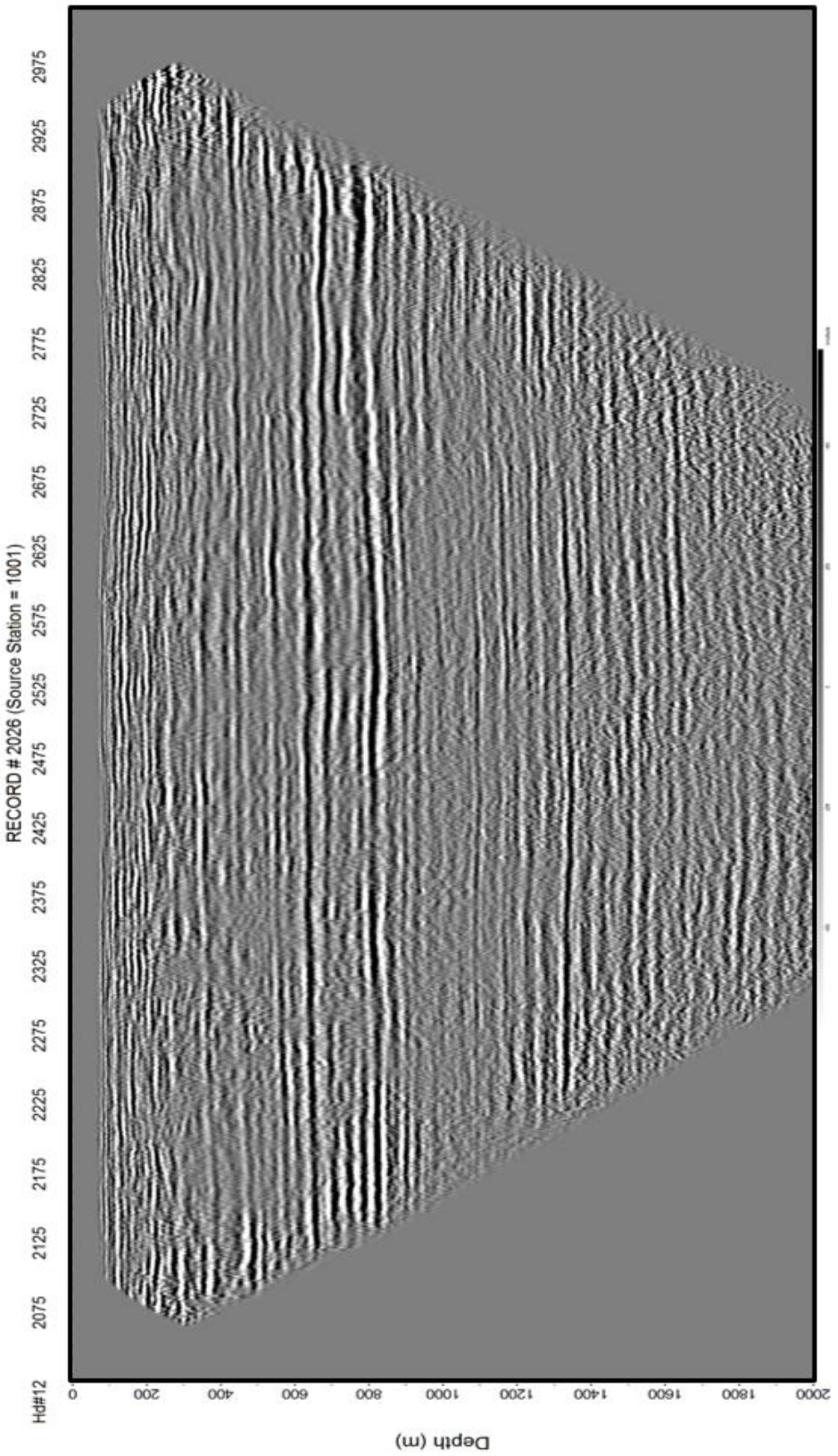

Figure 22: Pre-migrated, pre-JARR Static corrected stacked depth section of Wellington.

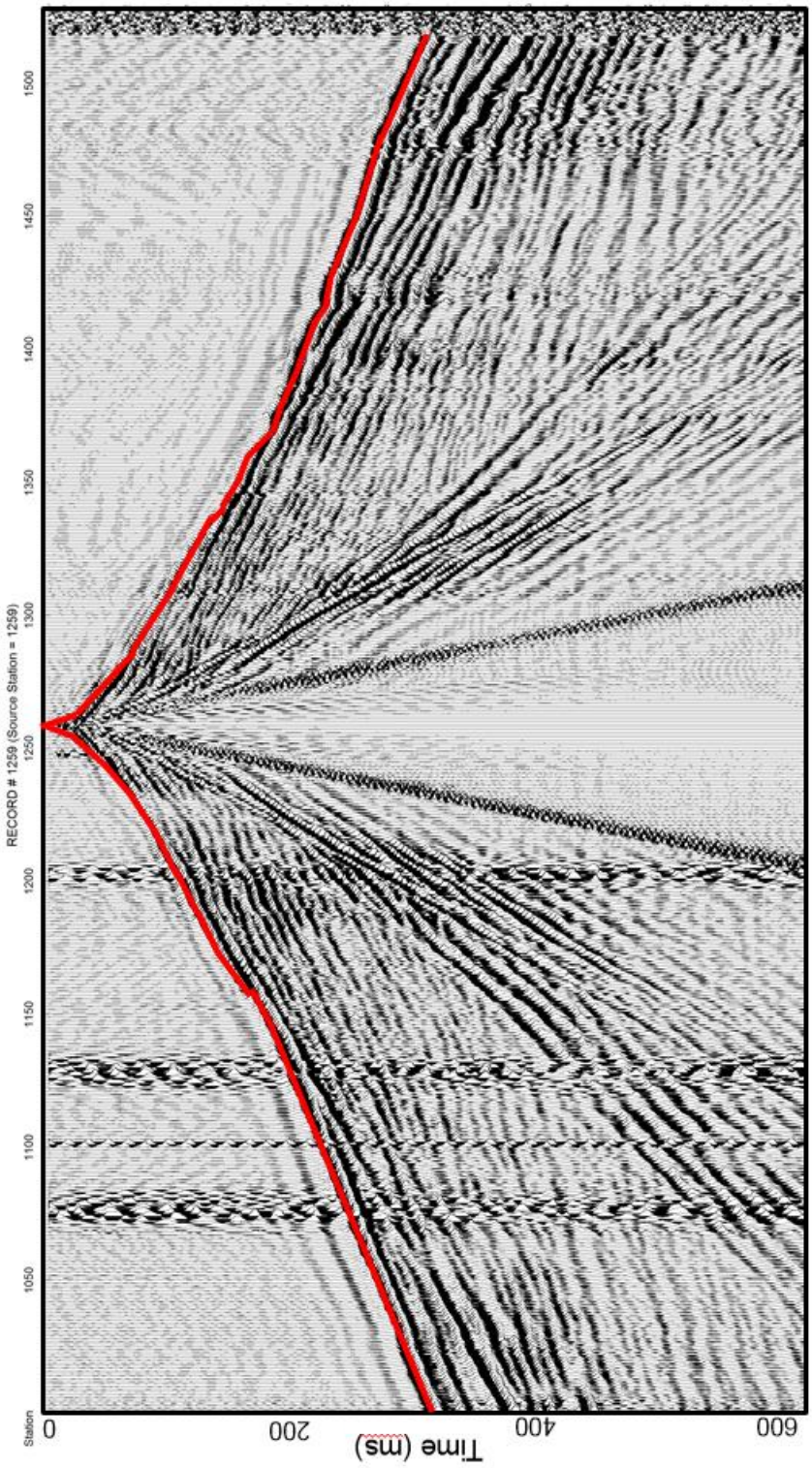

Figure 23: Representative shot record of first arrival picks. The first arrival picks are designated with red lines.

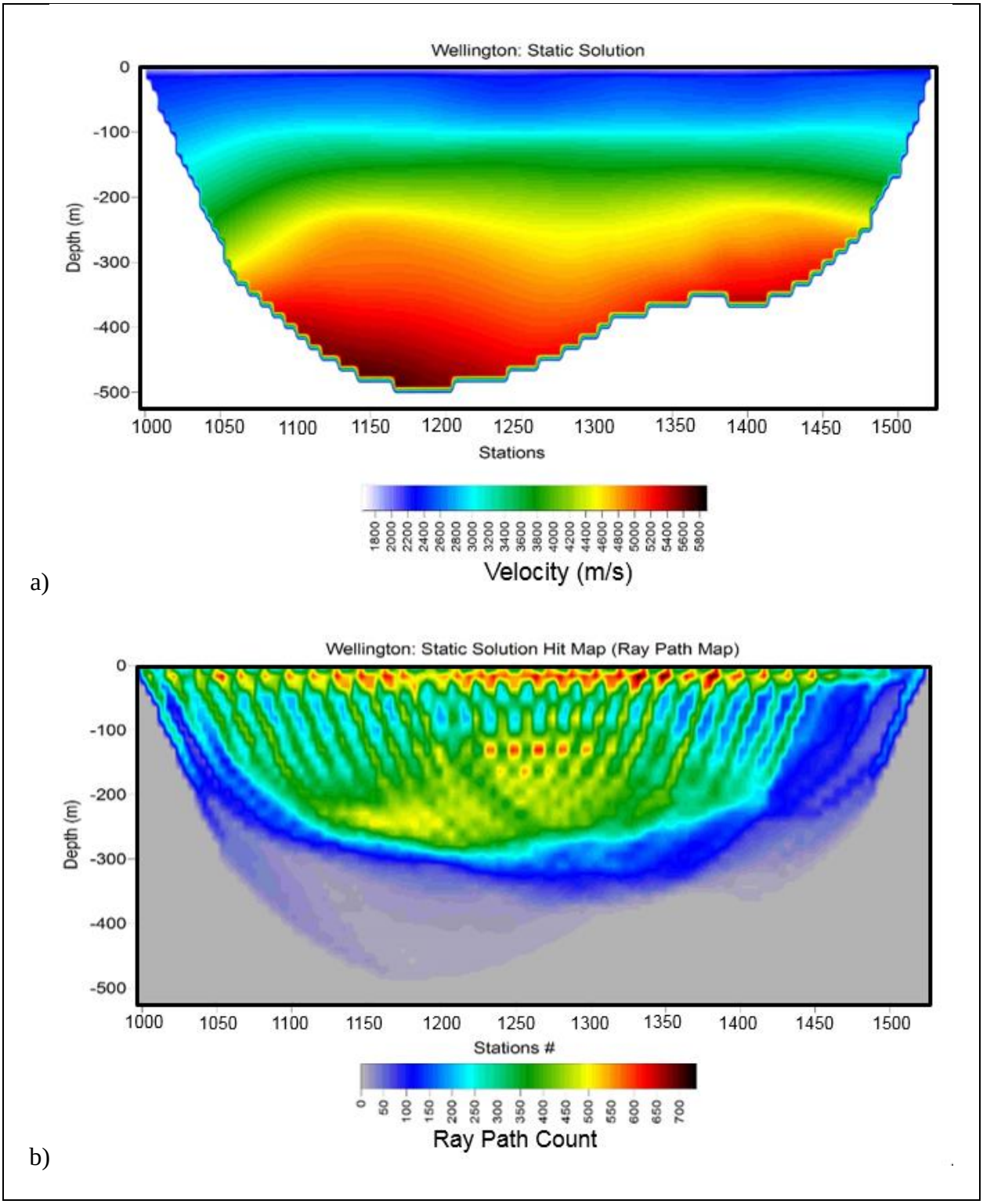

Figure 24: a) Interval velocity solution from JARR method. b) a ray-path map, illustrating the density of the regions where FAT rays traveled. A static datum was applied at 16 meters.

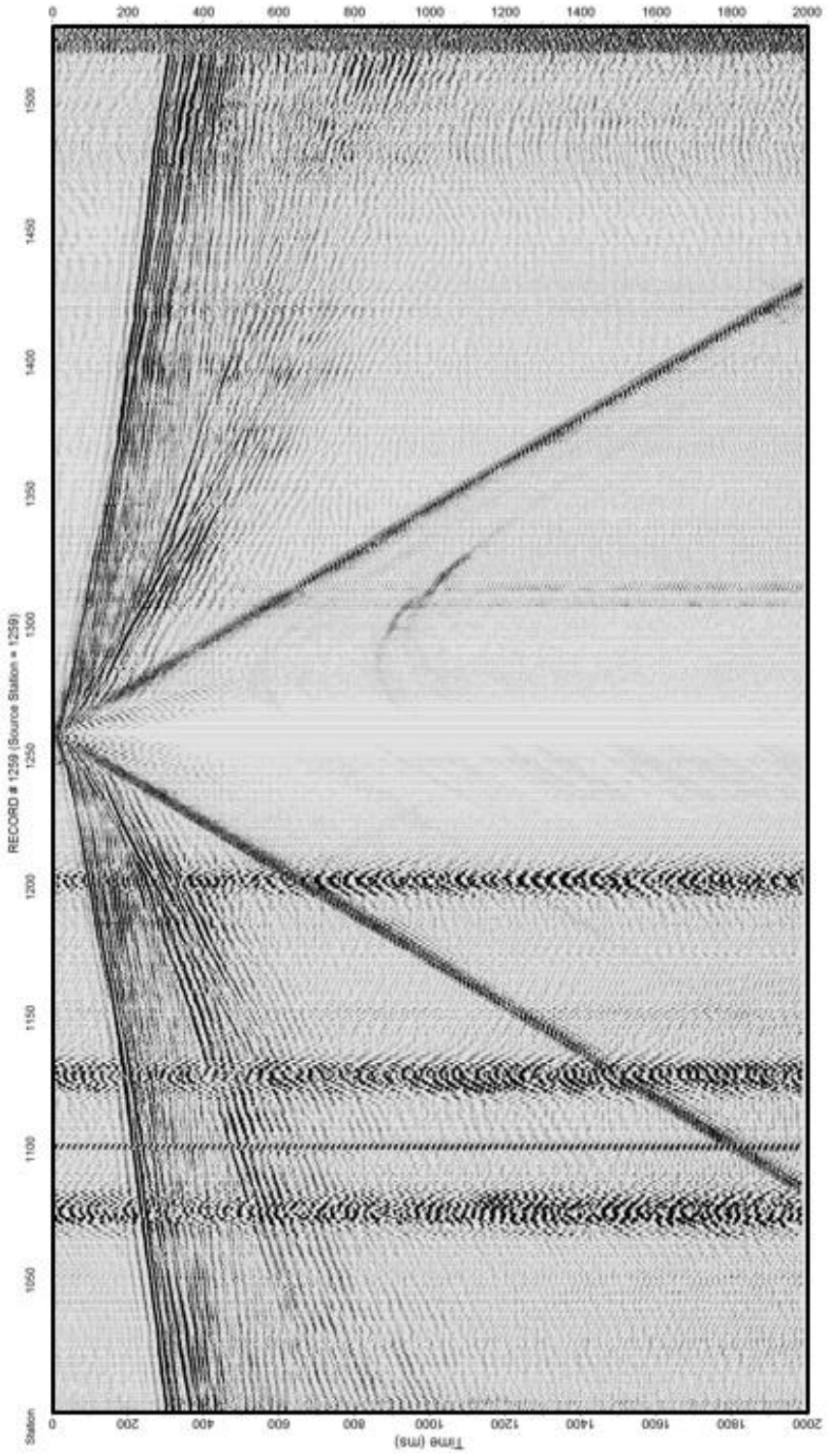

Figure 25: Representative shot record, post JARR static corrections.

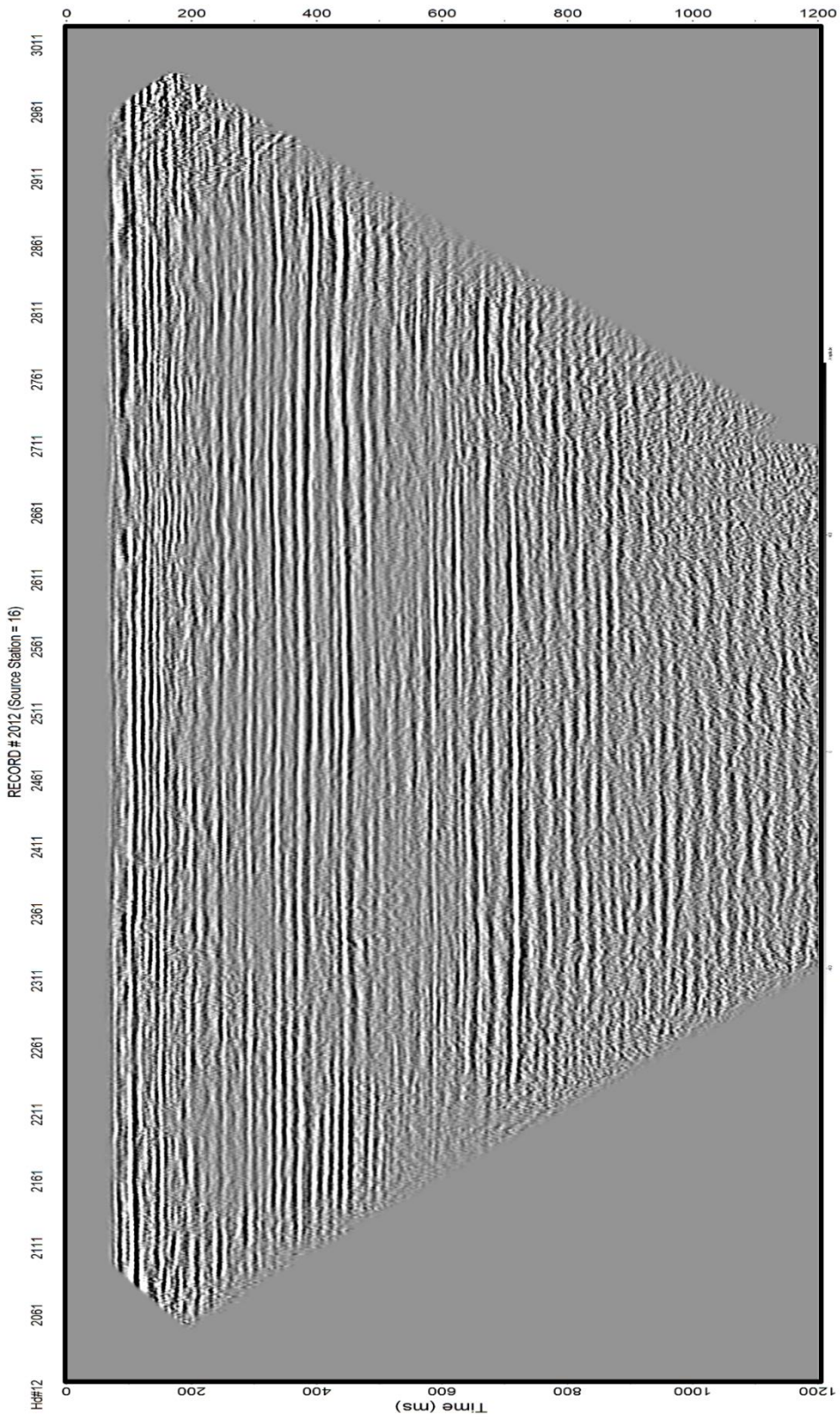

Figure 26: Pre-migrated, post-statically corrected stacked time section of Wellington.

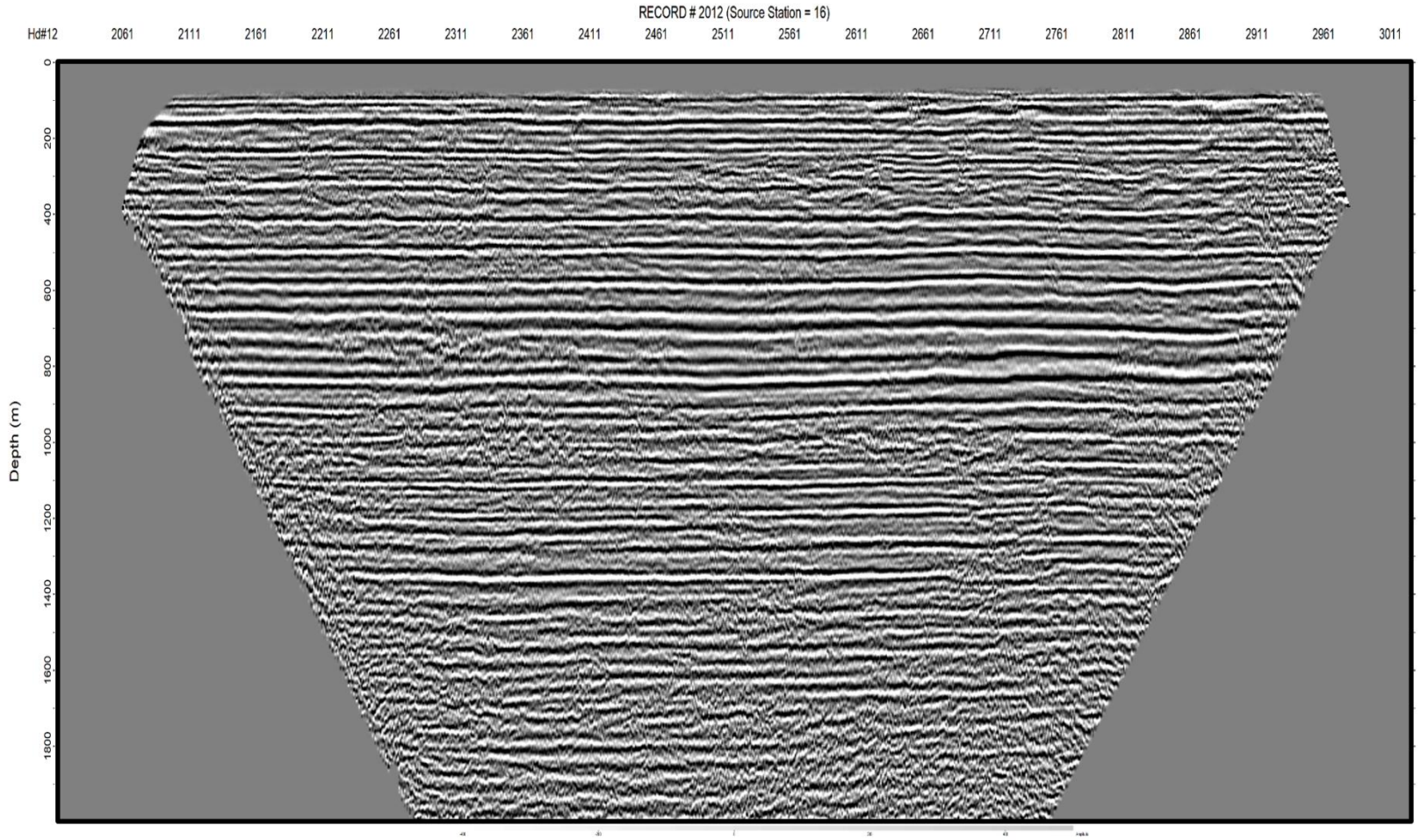

Figure 27a: Pre-Migrated, post-statically corrected stacked depth section of Wellington Kansas.

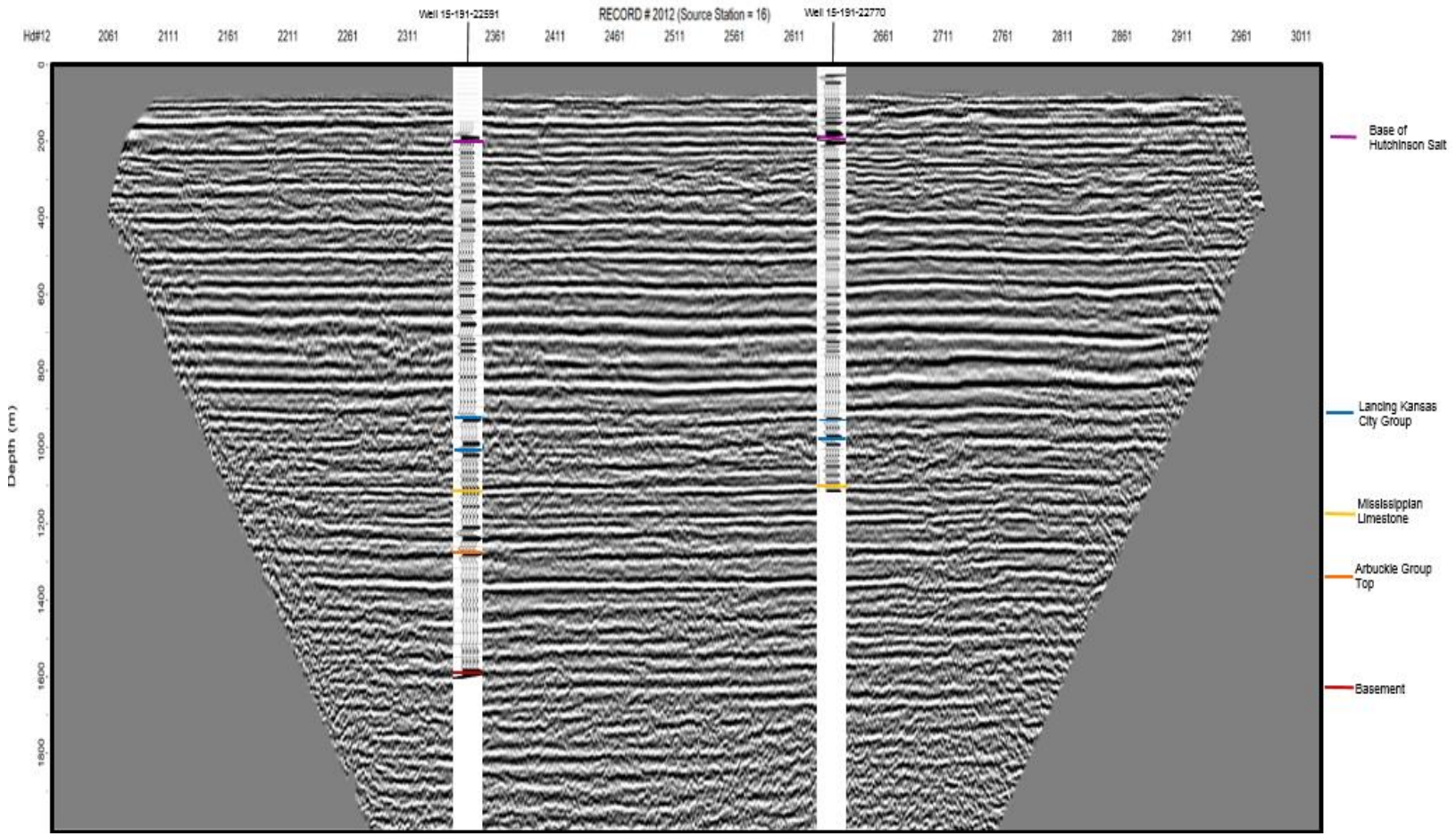

Figure 27b: Pre-migrated post JARR static correction. Synthetic seismic traces have been inserted at the appropriate locations along the seismic reflection line. Well 15-191-22591 (Survey, 2010) is represented on the left side and Well 15-191-22770 (Survey, 2015) is represented on the right hand side. The synthetic seismic traces were generated using a wavelet with a single frequency of 80 Hz. The synthetic seismic traces were generated using the proprietary KGS public synthetic trace generating software, in combination with the KGS Gemini software.

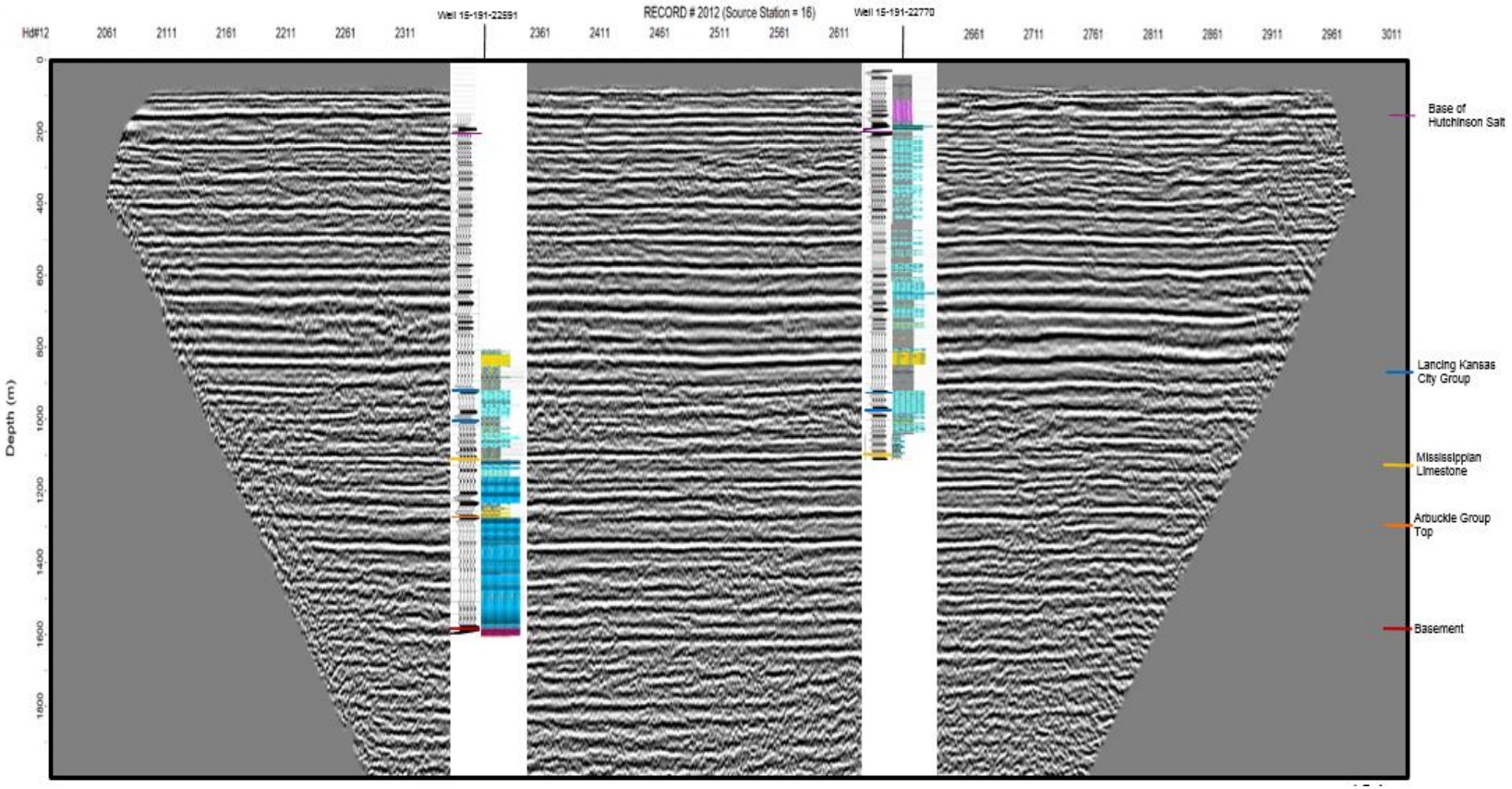

Figure 27c: Pre-migrated stacked section post JARR static corrections. Synthetic seismic traces have been inserted alongside lithologic logs derived from the wells specified in 26b. The lithologic logs are modified from Figure 2b and 2c to fit alongside the synthetic traces and the reflection data. The synthetic seismic traces were generated using a wavelet with a single frequency of 80 Hz. The synthetic seismic traces were generated using the proprietary KGS public synthetic trace generating software, in combination with the KGS Gemini software.

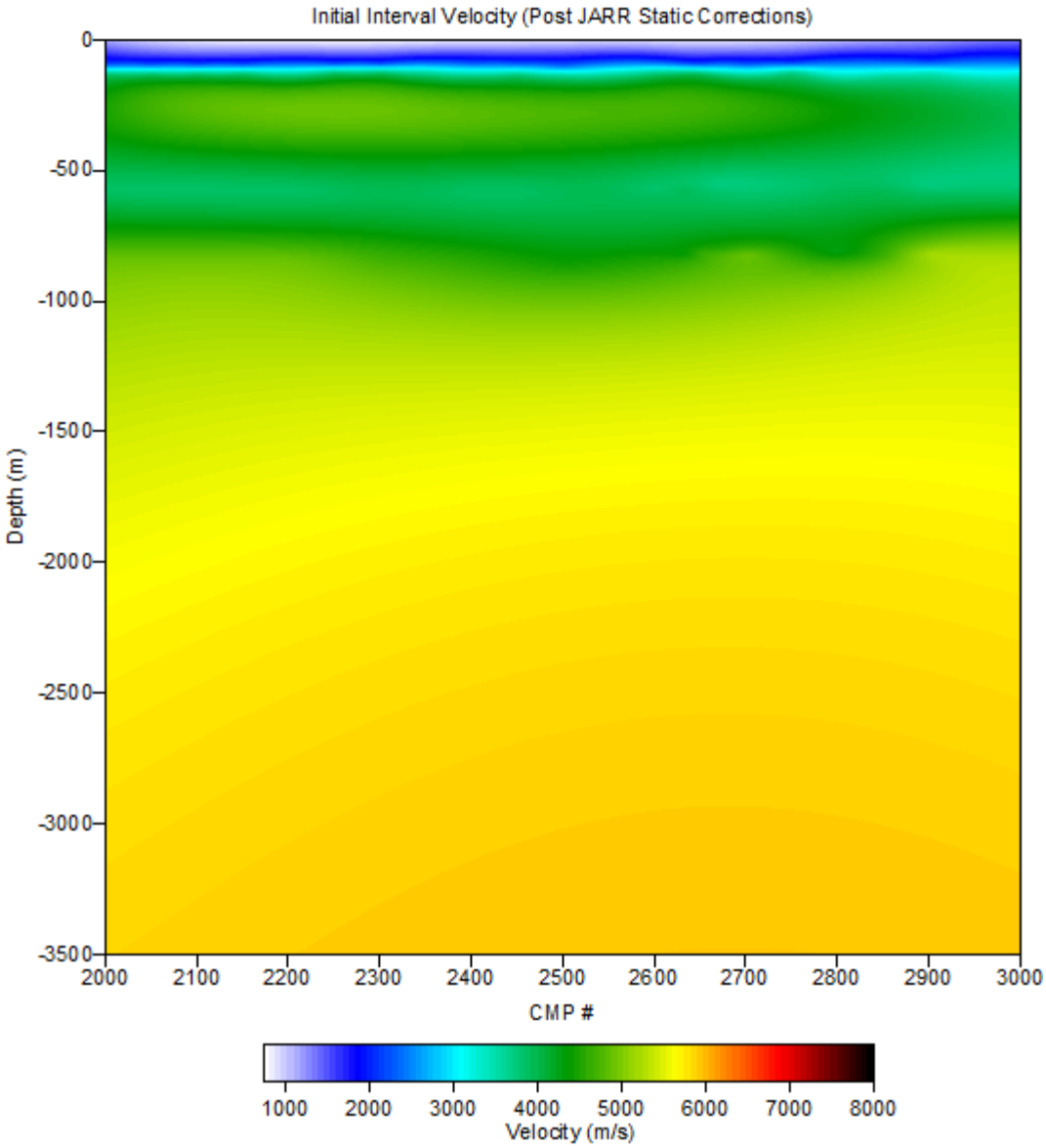

Figure 28a: Interval velocity map derived from statically corrected NMO analysis. The high interval velocity layer from ~125m - ~400m is indicative of the Hutchinson Salt member. The velocity inversion is expected due to the slower shale and limestone units beneath the Hutchinson Salt.

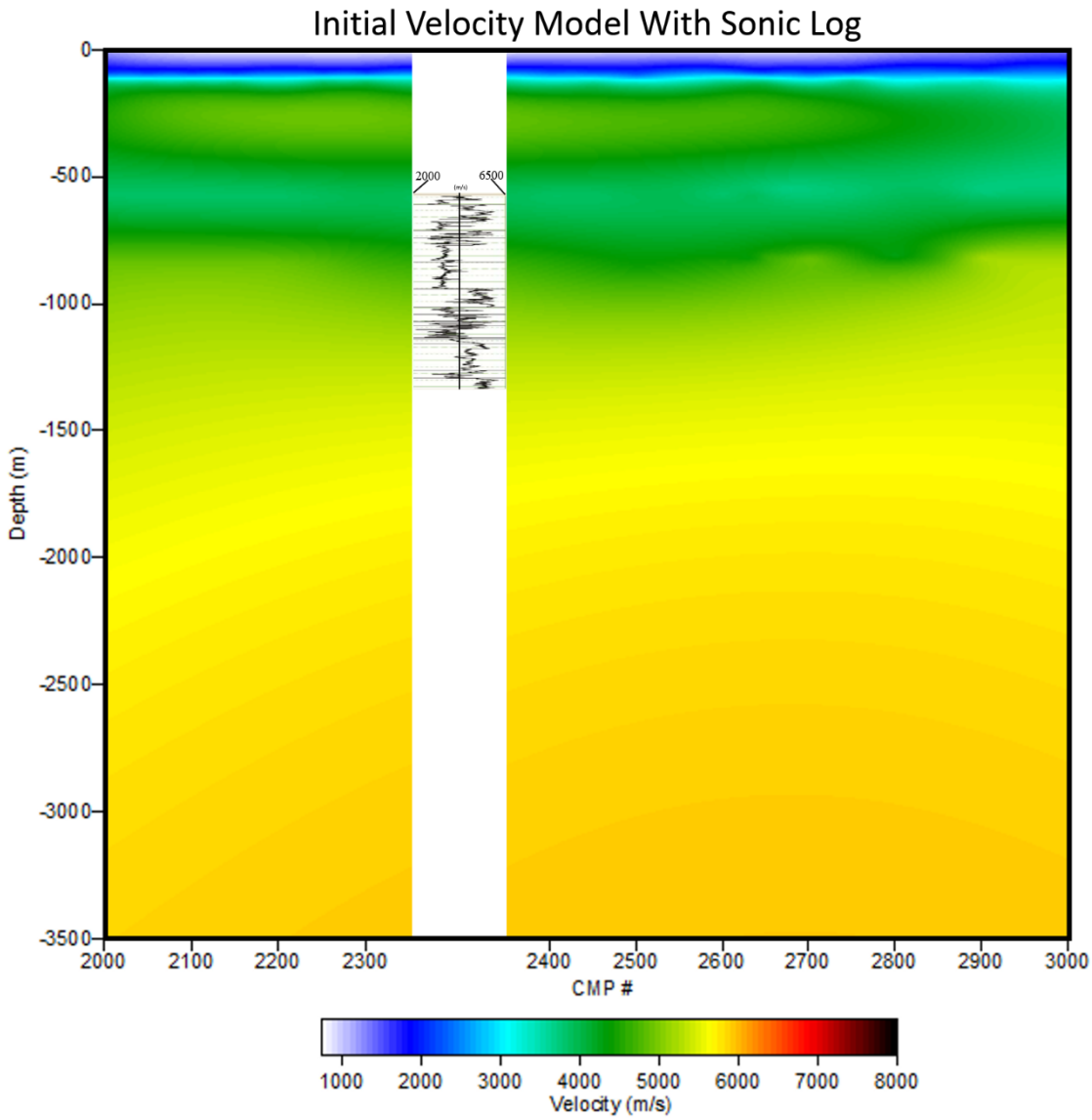

Figure 28b: Initial INMO velocity model post-JARR static corrections. A sonic log from the Wellington field has been inserted at its proper location along the seismic line. The well log is from Well 15-191-22591. The well log has been modified from (Sirazheiv, 2012).

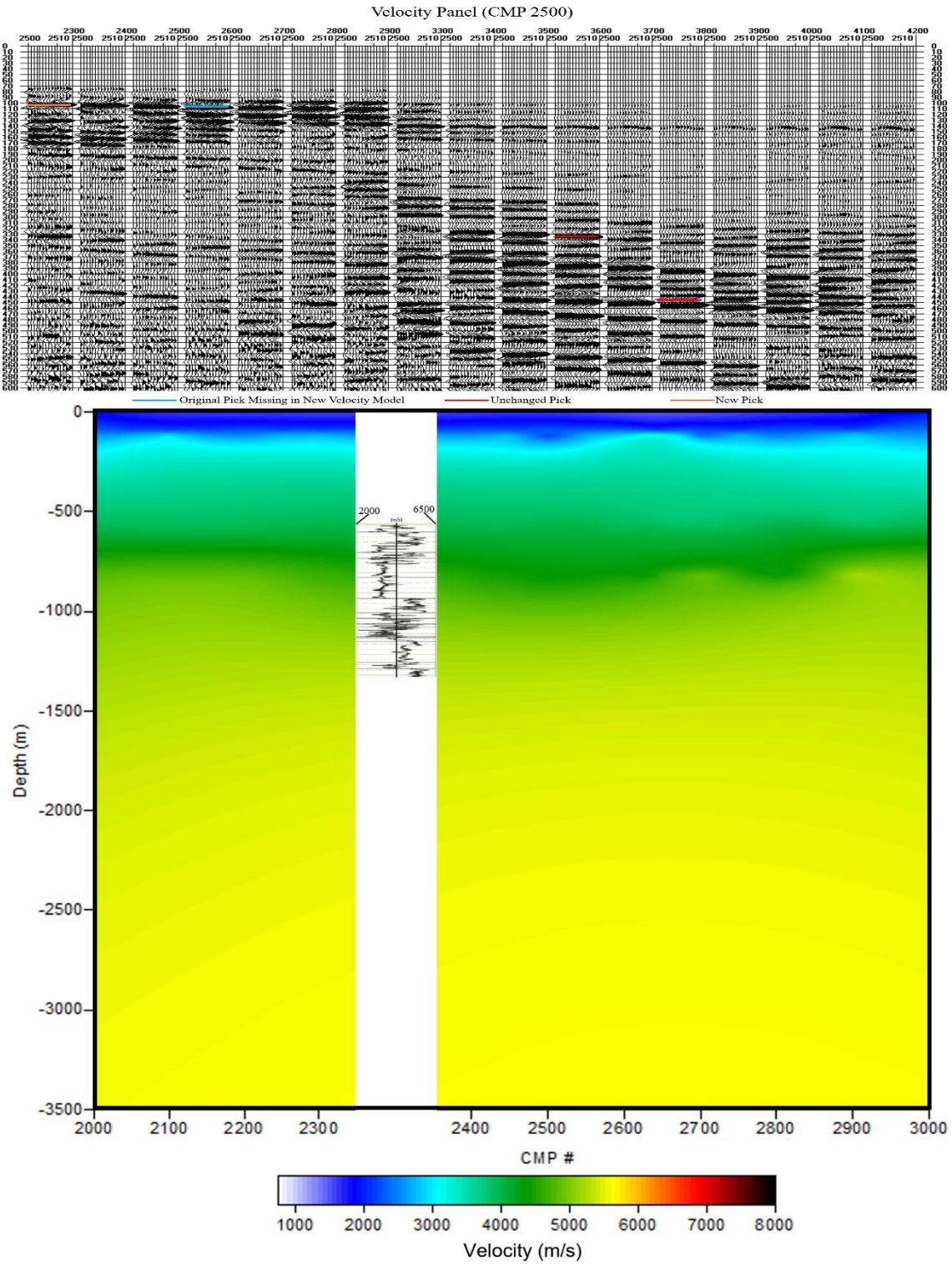

Figure 28c: Velocity panel 2500 indicates in orange the new velocity pick which generated the following INMO velocity function. The velocity panel shown above has a vertical scale in time. A sonic log from the Wellington field has been inserted at its proper location. The well log is from Well 15-191-22591. The well log has been modified from (Sirazheiv, 2012).

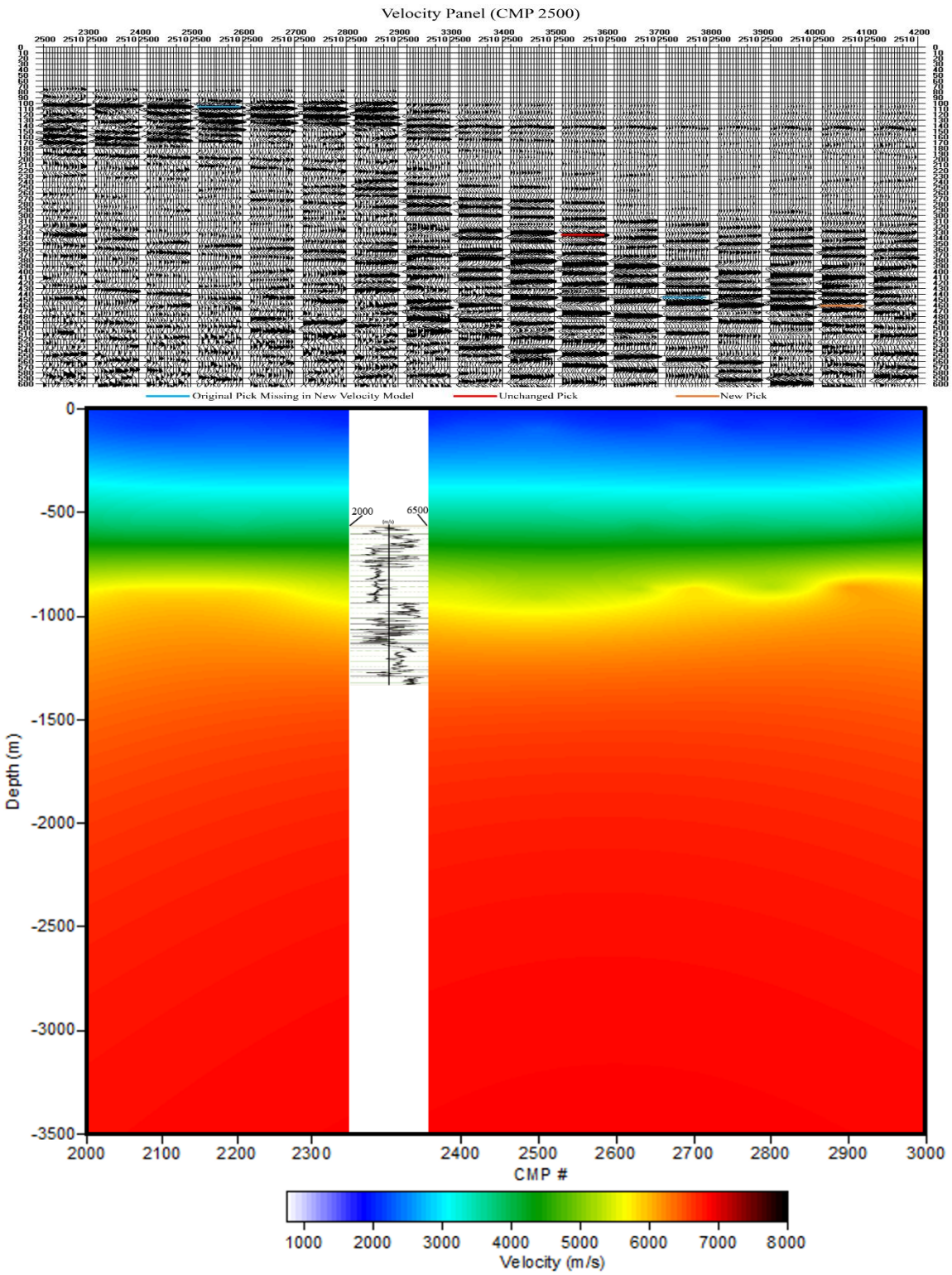

Figure 28d: Velocity panel 2500 indicates in orange the new velocity pick which generated the following INMO velocity function. The velocity panel shown above has a vertical scale in time. A sonic log from the Wellington field has been inserted at its proper location. The well log is from Well 15-191-22591. The well log has been modified from (Sirazheiv, 2012).

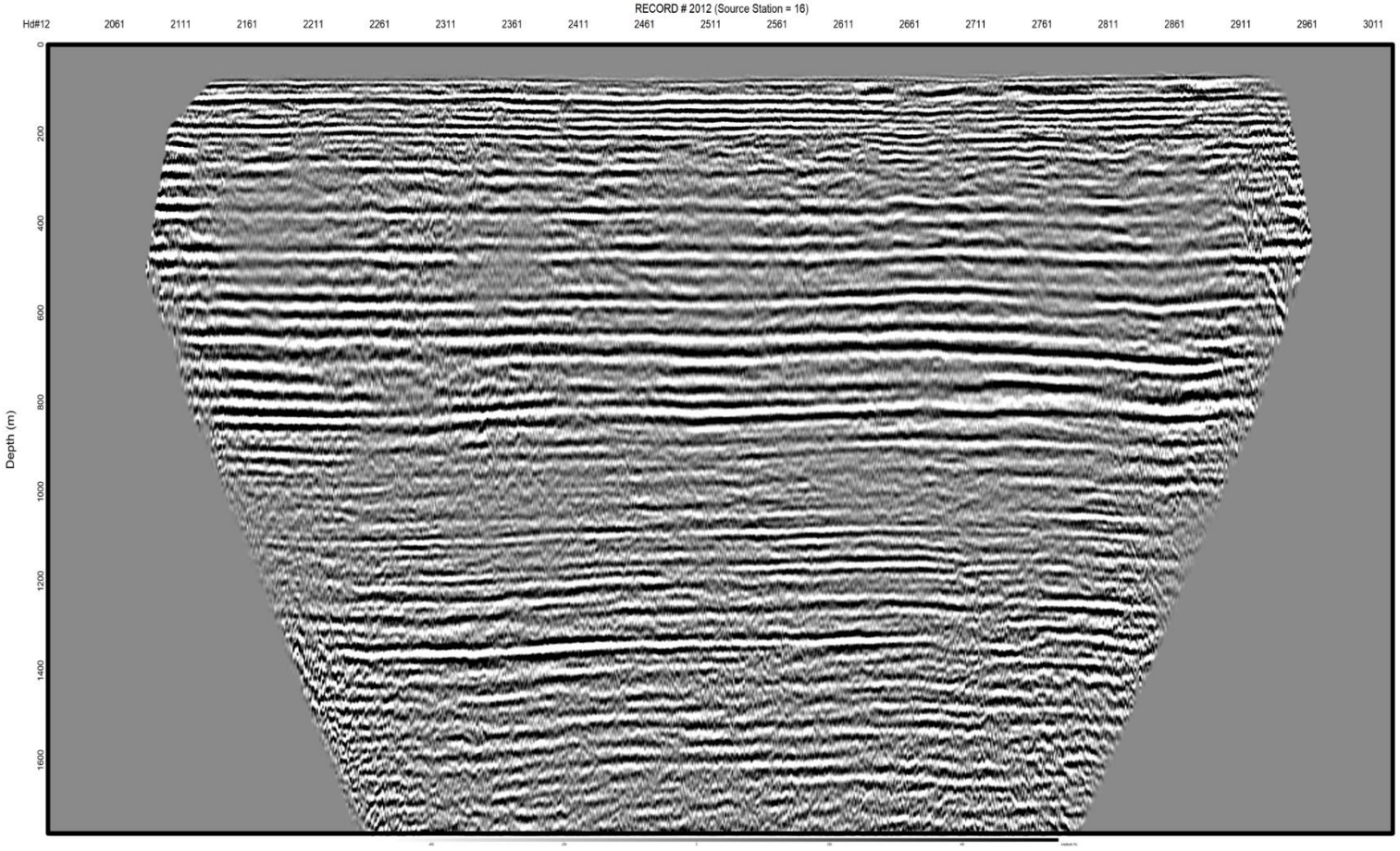

Figure 28e: Post-JARR static corrected section with Figure 28c velocities applied.

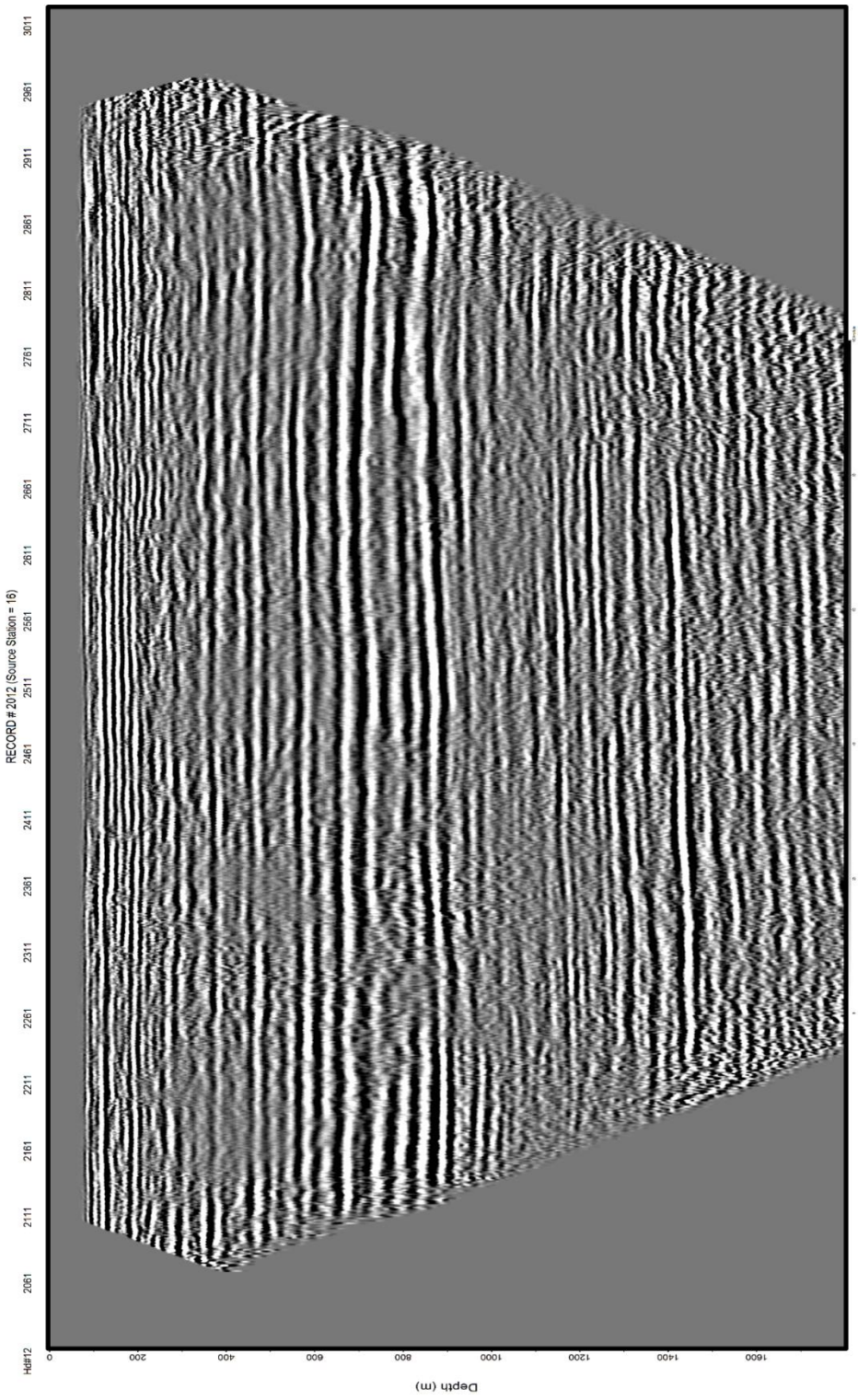

Figure 28f: Post-JARR static corrected section with Figure 28d velocities applied.

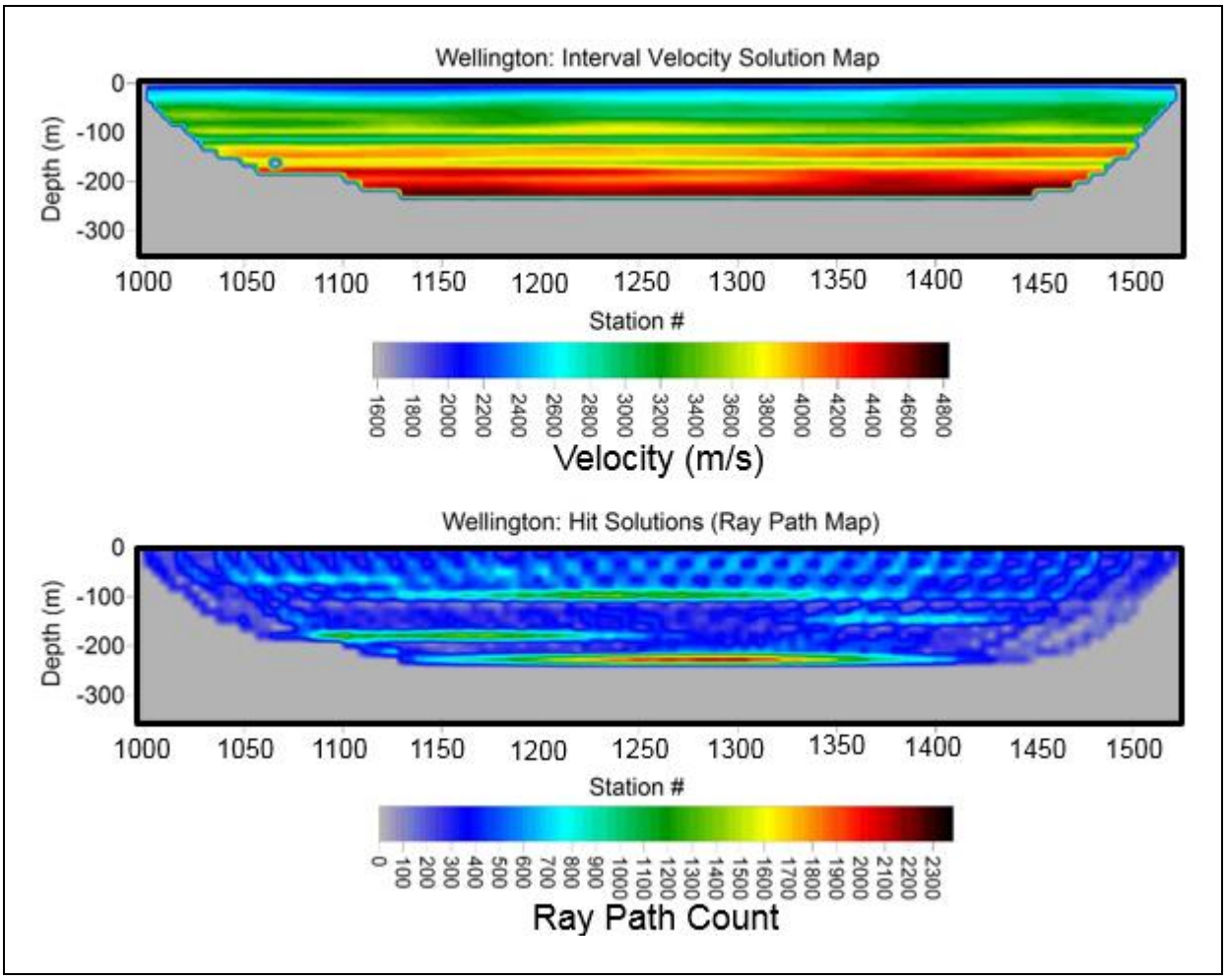

Figure 29: Interval velocity map derived from JARR method to be used in migration.

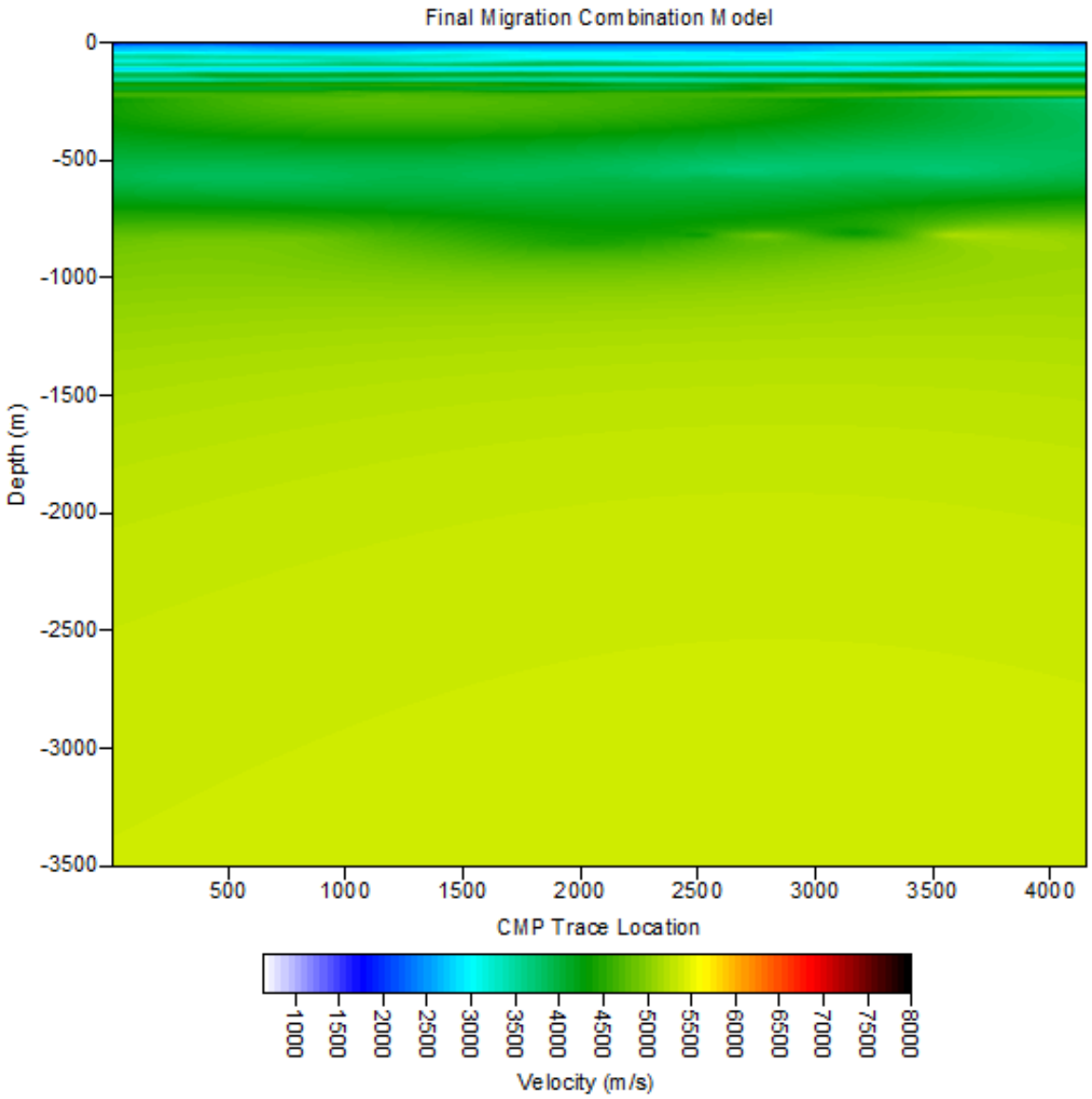

Figure 30: Combination model, near-surface velocity model derived from JARR method (Figure 29). The deep portion of the velocity model was derived from normal move-out corrections. This velocity model represents interval velocities.

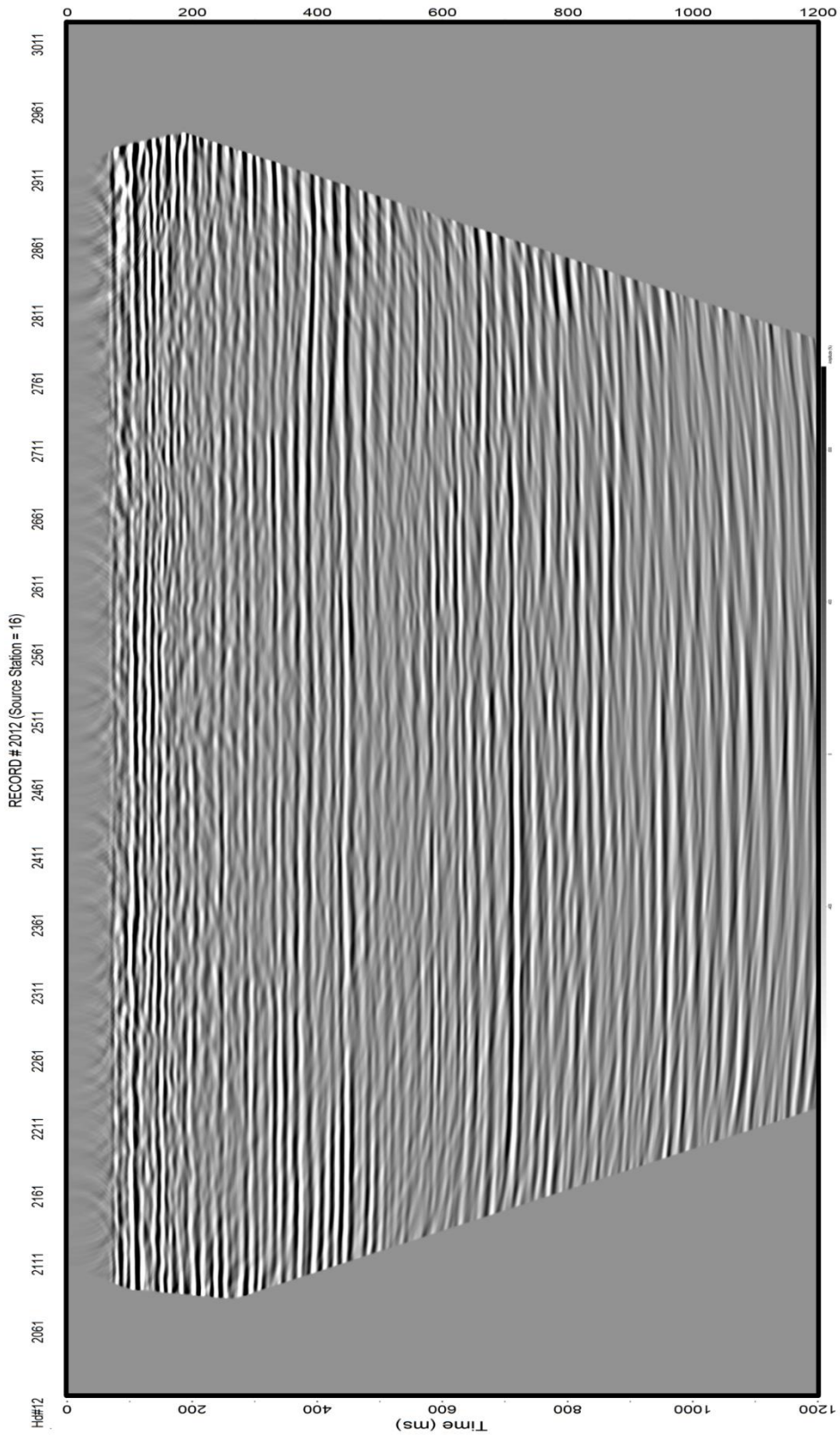

Figure 31: Post-Stack Stolt Migration applied to Wellington Kansas. This is a time section of the FK-Migration.

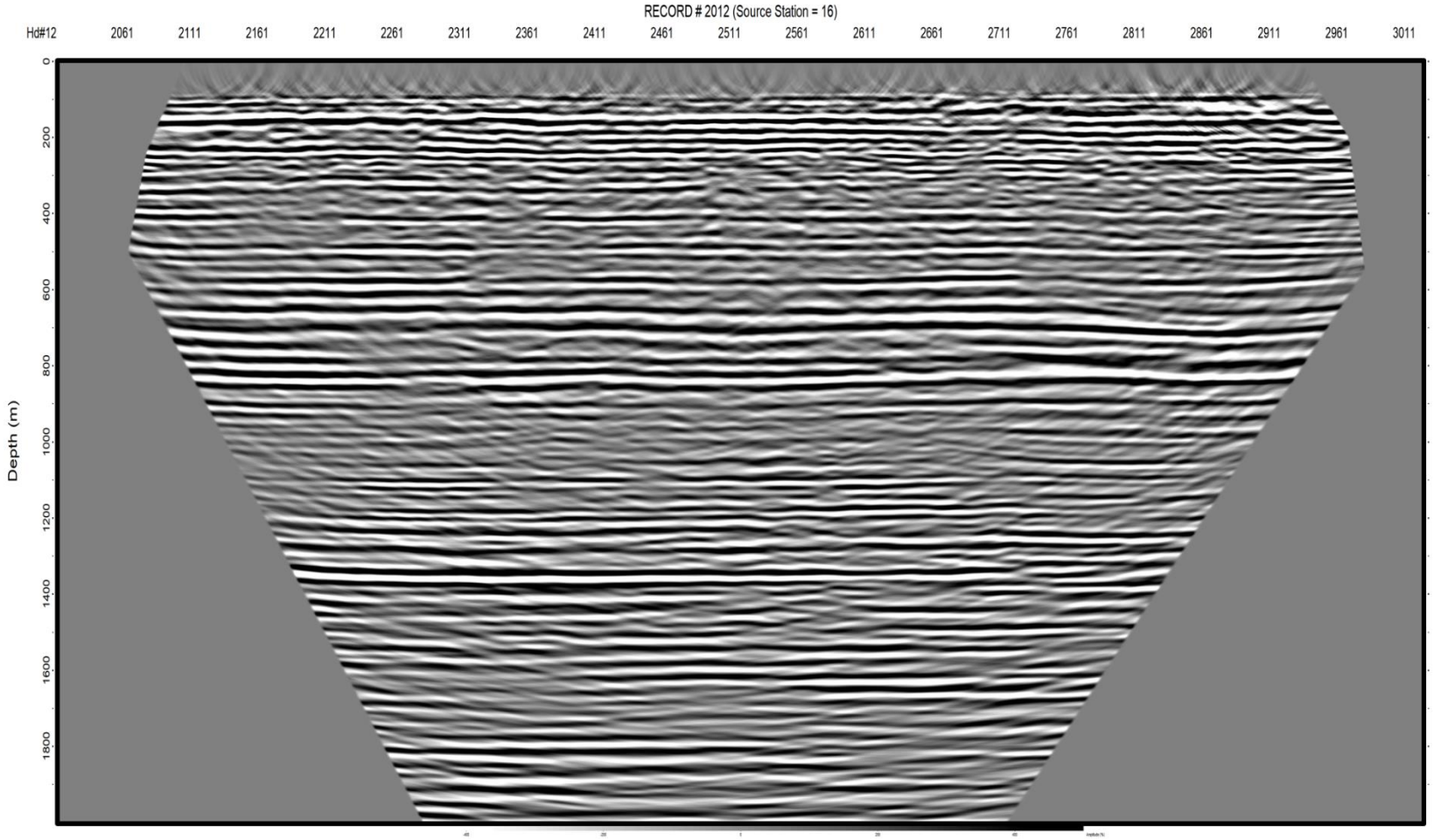

Figure 32: Post-Stack Stolt Migration applied to Wellington Kansas. This is a depth section of the FK-Migration.

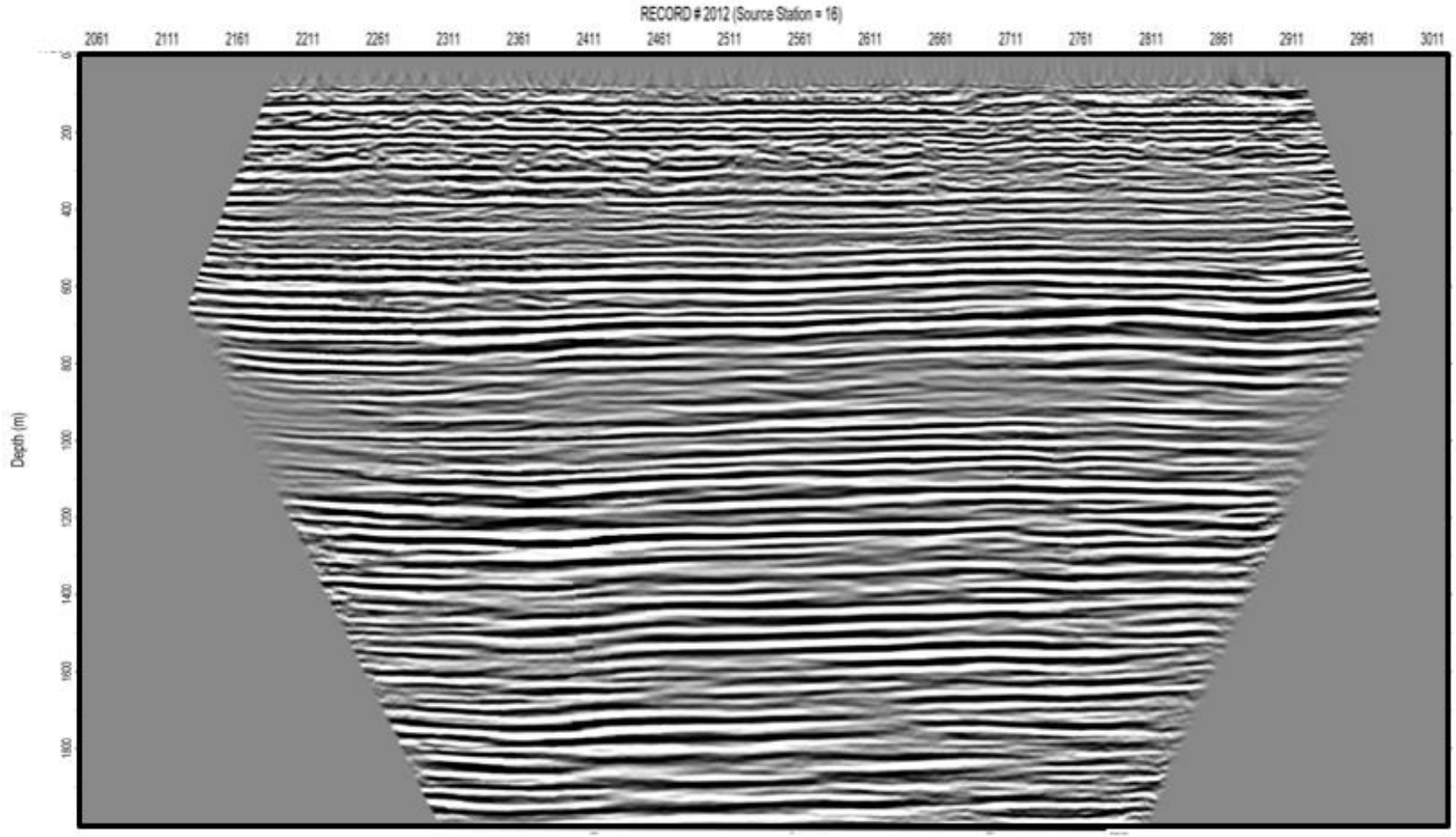

Figure 33: Post-Stack Kirchhoff Migration applied to of Wellington Kansas.

INMAN PROCESSING METHODS:

The Highway 61 Inman dataset was processed using near identical methods to the Wellington dataset. For brevity, the steps that were taken in the Inman dataset that have already been discussed and are virtually identical with regard to the Wellington dataset are provided in Table 2.

Processing Steps Table
SEG-Y conversion to KGS format
Cross-correlation with synthetic sweep
Geometry assignment from field notes
Vertical stacking of shot records (Figure 34)
Killing of noisy traces
…
Surgical Muting (Figure 38)
First Arrival Muting (Figure 39)

Table 2: Sequential steps taken for the Inman Dataset. The gap illustrates text detailing the unique steps.

A one decibel per second (dB/s) spherical divergence correction was applied to correct reflections for amplitude spreading due to three dimensional propagation of the wave-front (Newman, 1973). A spectral balance was applied to the data with corner frequencies, 25 – 50 – 200 – 250, to enhance the high frequency portion of the spectrum (Figure 35).

A low-cut filter with a zero frequency of 60 Hz and a one hundred percent frequency of 120 Hz optimally enhanced the signal to noise ratio of the reflections while filtering the surface waves and attenuating other noise in the dataset (Figure 35). Unlike Wellington, the focus of this

study was on the near-surface and the low frequencies were not necessary. To reduce linear surface wave noise an FK filter was used (Figure 36 and Figure 37).

One observation that is evident is the irregular nature of the reflections. From previous experience and published accounts with this phenomenon, it was diagnosed to be static problems (Wiggins et al., 1976; Taner and Koehler, 1981; Mayer, 2009). To address this static issue, the data was resorted into CMP gathers, velocity analysis was performed and a surface consistent statics table was calculated for the dataset (Figure 40a-d). A brute stack was then created to appraise the significance of the statics problem (Figure 41).

Trace-to-trace consistency of the reflection on the brute section are uncharacteristic and indicative of static problems in the dataset (Figure 42). The depth section created with the initial velocity model contained artifacts from incorrect velocities (Figure 43) that challenge proper NMO analysis. With static issues attributed to these artifacts, an initial smoothed velocity model was generated to use as the first pass model for JARR FAT (Figure 41). The goal of this JARR FAT analysis was to improve definition of the trace to trace statics and improve velocity function.

First arrivals were selected on the unfiltered data (Figure 44). A source file was created to tie the first arrival picks to the survey shot and receiver station geometry. Utilizing the JARR method introduced earlier, an INMO velocity model derived from standard velocity analysis was used as an initial a-priori model for the FAT. Testing of velocity solutions allowed selection of the most realistic, lowest RMS error solution (in milliseconds) (Figure 45). The parameters for the JARR method can be found in Table 3.

Static Corrections were calculated with a near-surface velocity model derived from the JARR FAT. A datum 32-meter datum was selected to calculate the proper static corrections. Unfortunately, much of the surface elevation was missing due to archiving issues. In place of on-

site elevation measurements, Google Earth was utilized to define very accurate elevation information over the survey. Inherently, there is more error in this method than direct GPS surveying. The image used was taken in 2015, and the survey was collected in 2005. Since, the JARR method must be provided with elevation information this was a necessary step. Fortunately, the elevation error is a single wavelength. The long-wavelength static corrected dataset (Figure 46), was re-processed consistent with the initial flow and a final time section and depth section were generated (Figure 47 and Figure 48, respectively). The static corrections were made based on a JARR method derived INMO velocity model with the parameters listed in Table 3.

After re-processing, first arrival times were selected and used for a second application of the JARR method. The improved velocity model derived from the velocity analysis run on the static corrected data was used as the initial a-priori reference model for a JARR run (Figure 49). The JARR images illuminated the widely varying velocity characteristics in the near surface (upper ~69 m (224 ft.)) (Figure 50). Producing the improved velocity functions was only possible with the static corrections derived from the JARR method. The parameters used for the migration velocity implementation of the JARR method can be found in Table 3.

Deep velocities derived from the interval NMO velocities were appended to the near surface tomography velocities derived from JARR. This produced an Inman combo-model with a total depth of ~1069 m (3,500 ft.) (Figure 51). Then, a post-stack Stolt (Figure 52) and Kirchhoff (Figure 53) migrations were applied to the dataset using the new combo-velocity model derived from the JARR method. Due to current file size limitations related to the software, the Kirchhoff migration could not be applied to the whole line as with the FK migration. For this reason, an area of interest was selected and the Kirchhoff migration was applied to this portion only (Figure 53).

Parameter	**JARR – Static Parameters**	**JARR – Migration Parameters**
Damping Value:	100	(First Pass) 50 (Second Pass) 50 (Third Pass) 50 (Fourth Pass) 50
Near – Offset Emphasis:	51 Times	(All Passes) 51 Times
Horizontal Smoothing:	3200	(First Pass) 2400 (Second Pass) 2400 (Third Pass) 2400 (Fourth Pass) 800
Smoothing Coefficient:	1	(First Pass) 1 (Second Pass) 1 (Third Pass) 2 (Fourth Pass) 2
Number of Inversion Iterations:	3	(First Pass) 6 (Second Pass) 4 (Third Pass) 3 (Fourth Pass) 3
"Leap-Frog" Iterations:	0	4
Initial RMS Error (ms):	18.8	94.0
Final RMS Error (ms);	7.2	3.16
Number of Tests:	8	38

Table 3: This table indicates all the values used for the JARR method for both statics and migration for the Inman, Kansas dataset. For the second pass, the solution from the first inversion is supplied as the a-priori reference model.

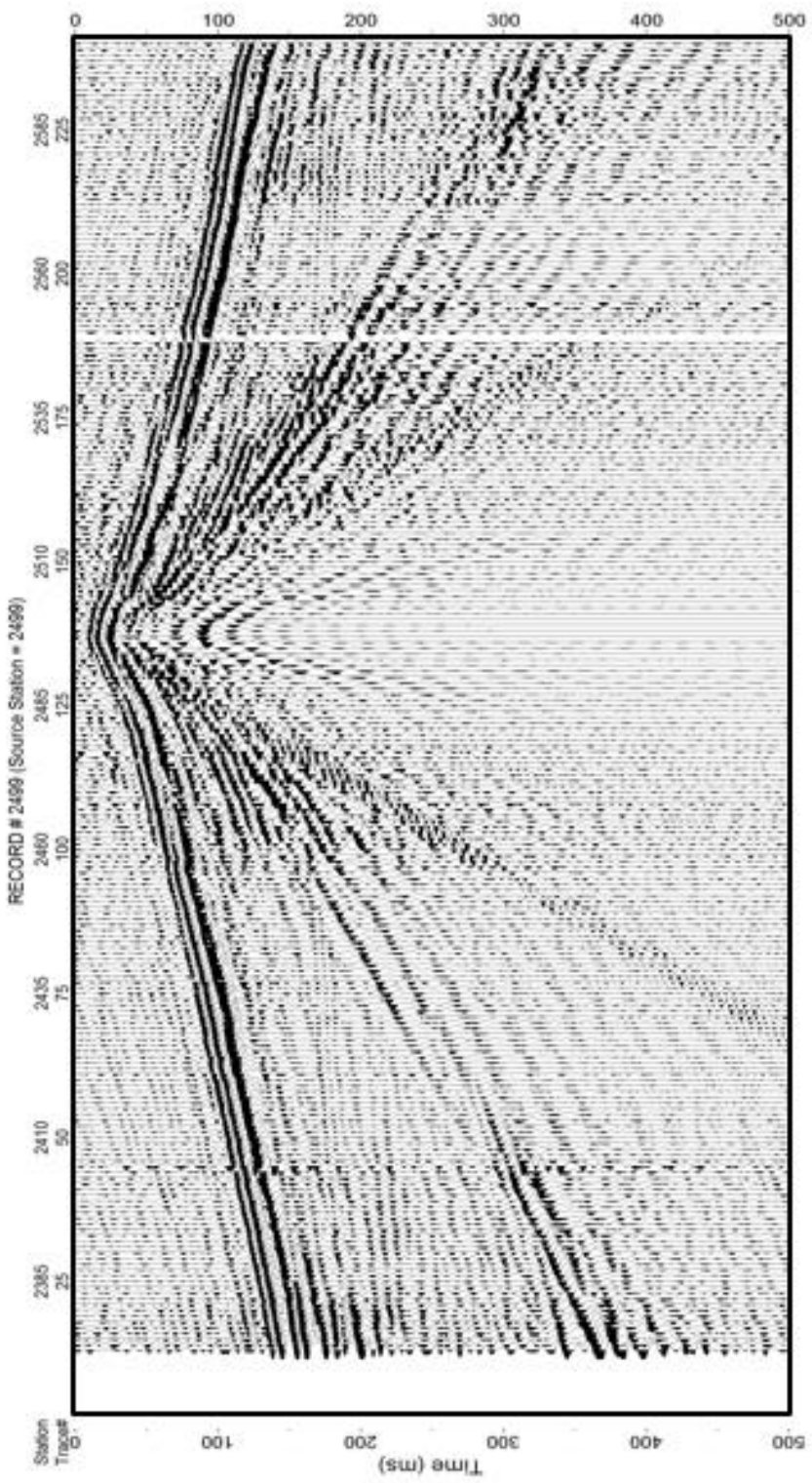

Figure 34: Representative shot record that has been vertically stacked. No other processing has been done.

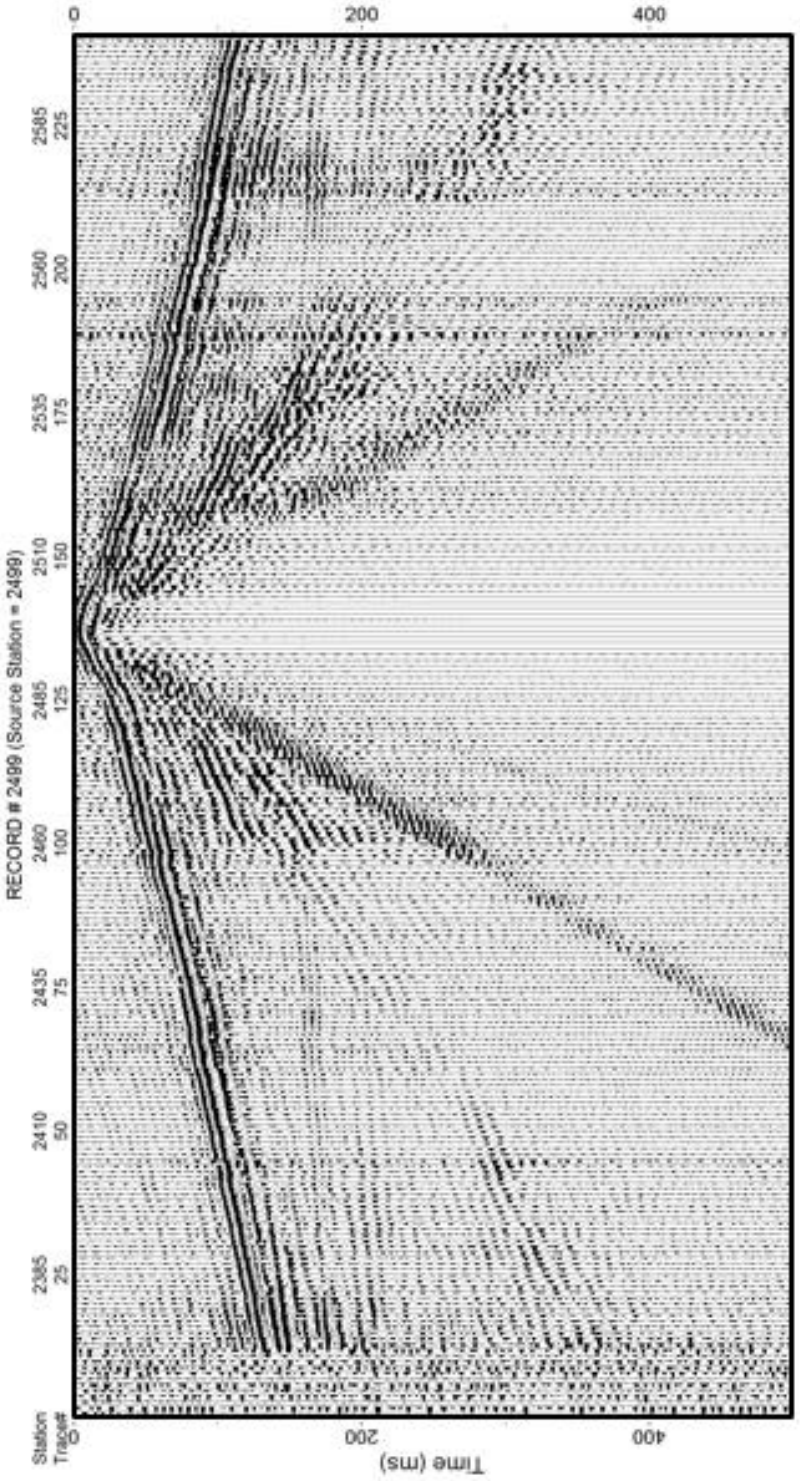

Figure 35: This is a representative shot gather after a spherical divergence, spectral balancing, and frequency filtering has been applied.

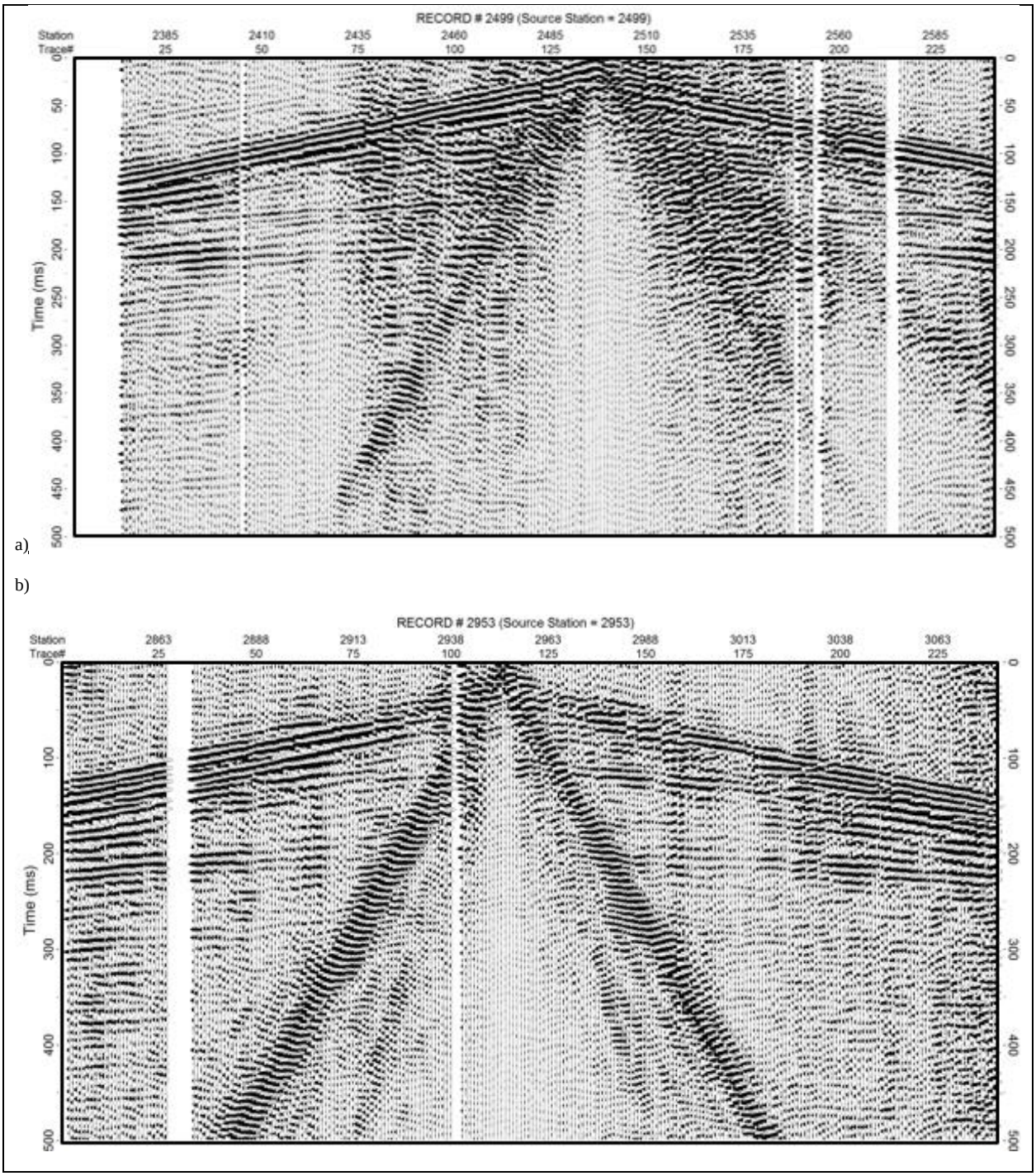

Figure 36: a) is a representative shot record from the first third of the line, where the FK filter applied generated artifacts near the shot location. b) is a representative shot record from the remaining two-thirds of the dataset which shows a clean FK filter applied, decimating surface-wave energy. The FK filter attenuated velocities between 550 and 2750 m/s.

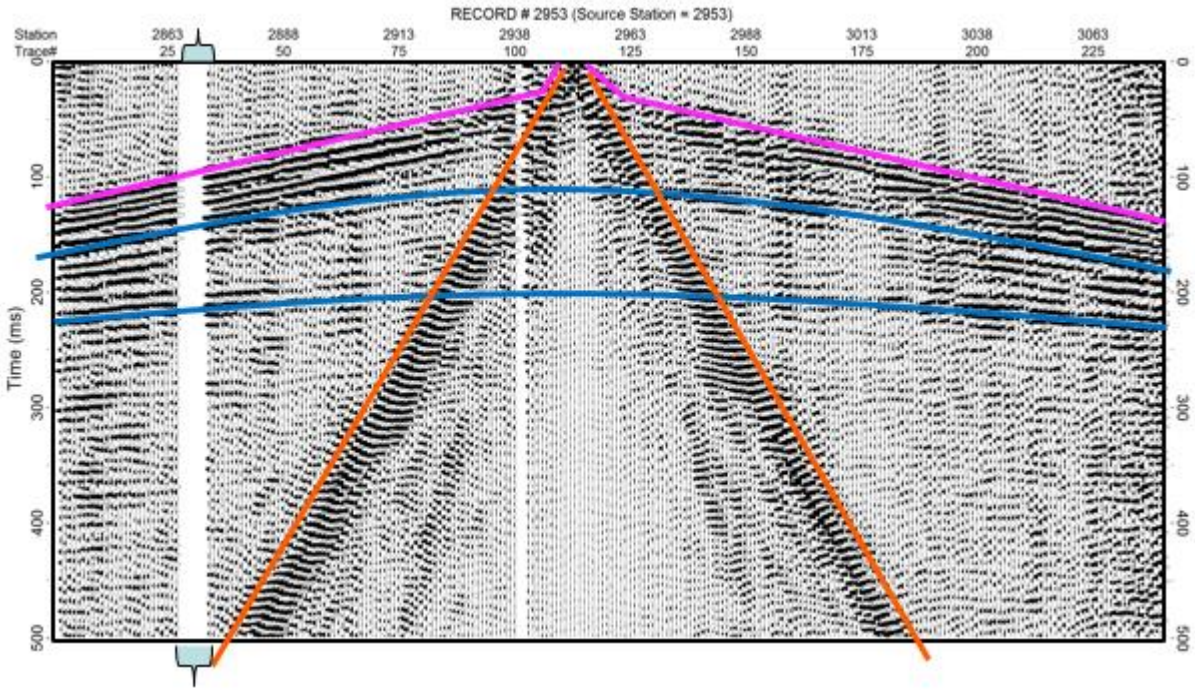

Figure 37: Representative interpreted FK-filtered shot record. The orange lines lie atop the air-coupled wave. The pink lines lie atop the first arrival refractions. The blue lines indicate reflections. The brackets indicate killed (muted) traces.

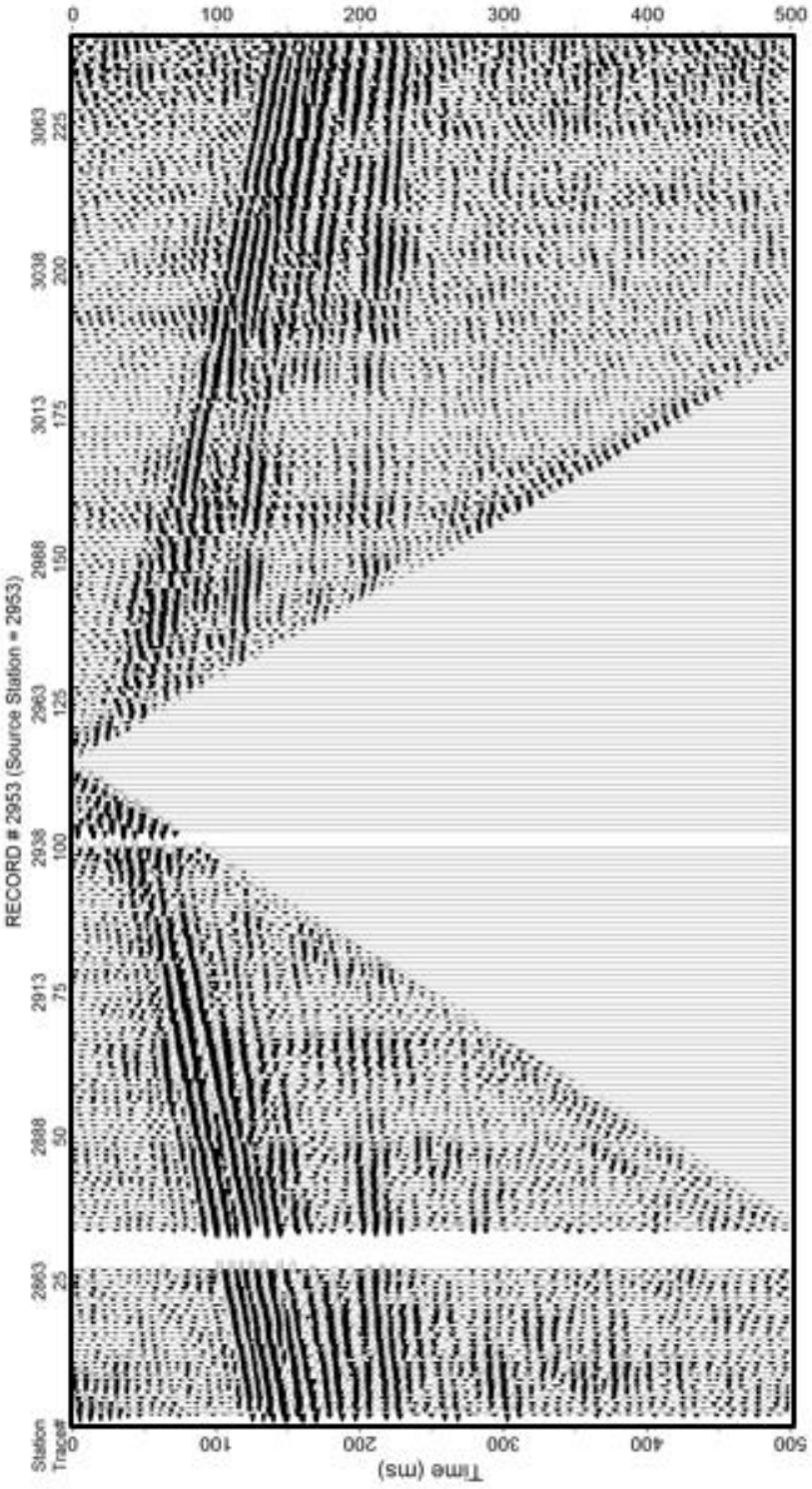

Figure 38: This is a shot record showing how the surgical cone mute was applied to remove remnant surface-wave energy along with the direct, and air-coupled wave.

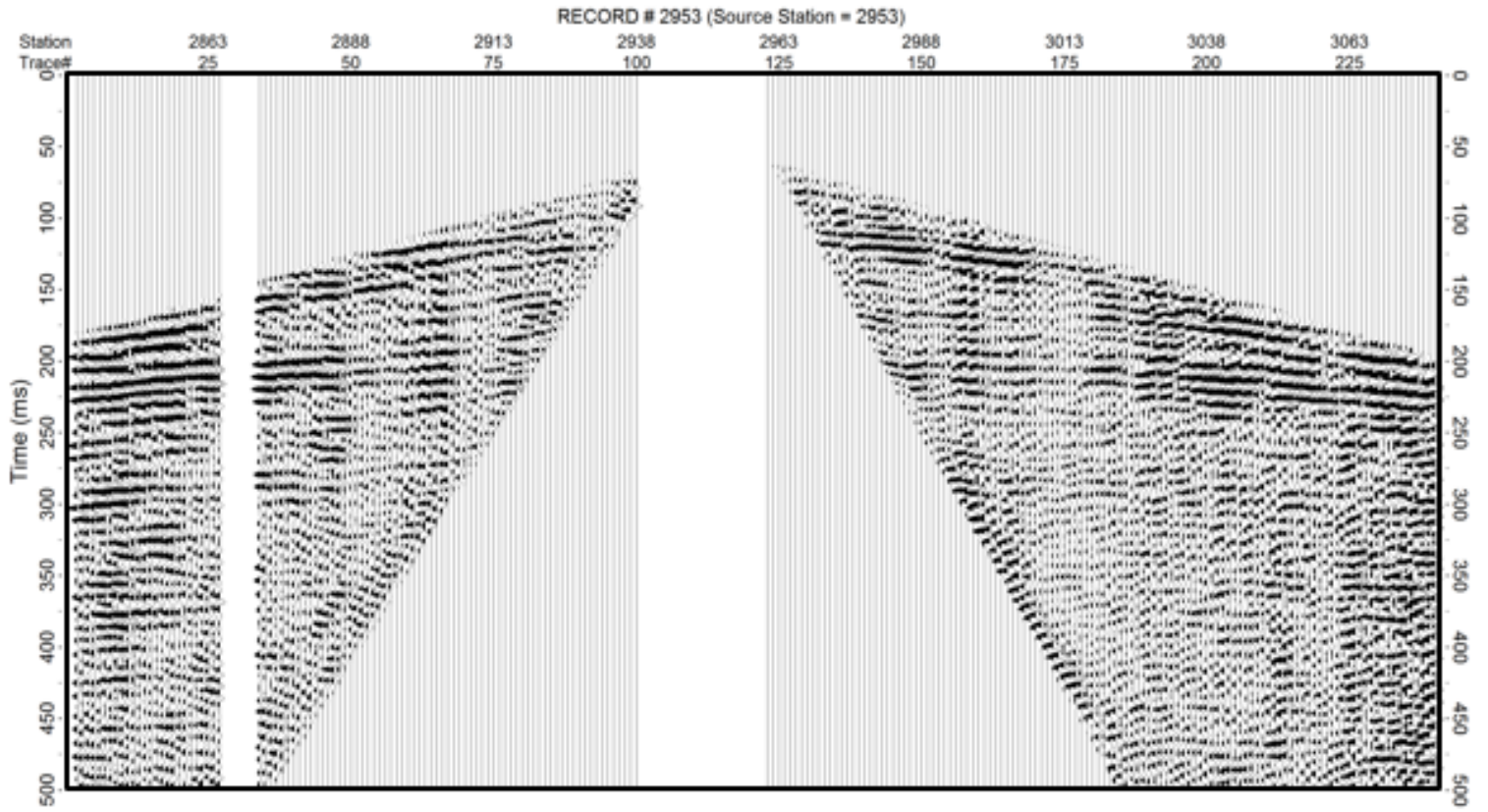

Figure 39: This is a shot record representing the first arrival mute which targeted the first arriving energy as well as refractions. These energies were removed due to their tendency to stack in coherently and appear as reflections.

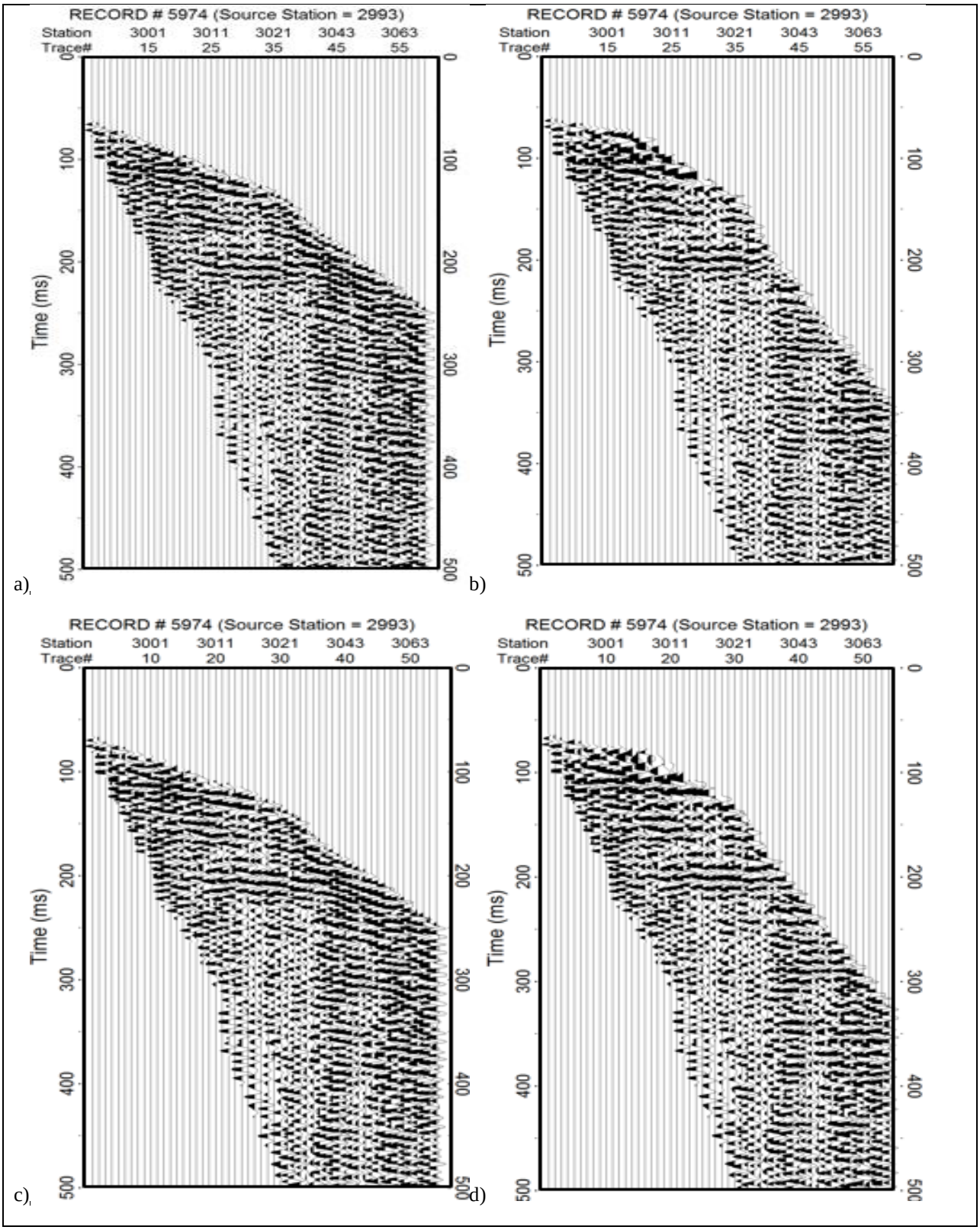

Figure 40: a) first pass CMP from Highway 61 b) NMO corrected first pass of Highway 61 c) CMP after three iterations of surface consistent statics has been applied. d) NMO corrected CMP.

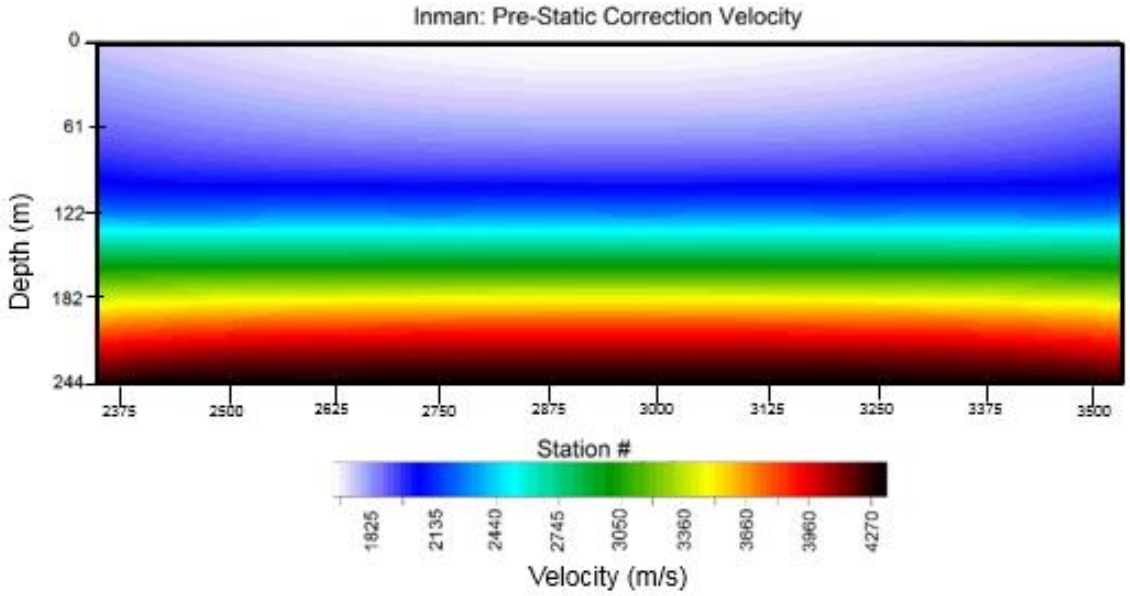

Figure 41: Initial interval velocity model derived from stacking velocities.

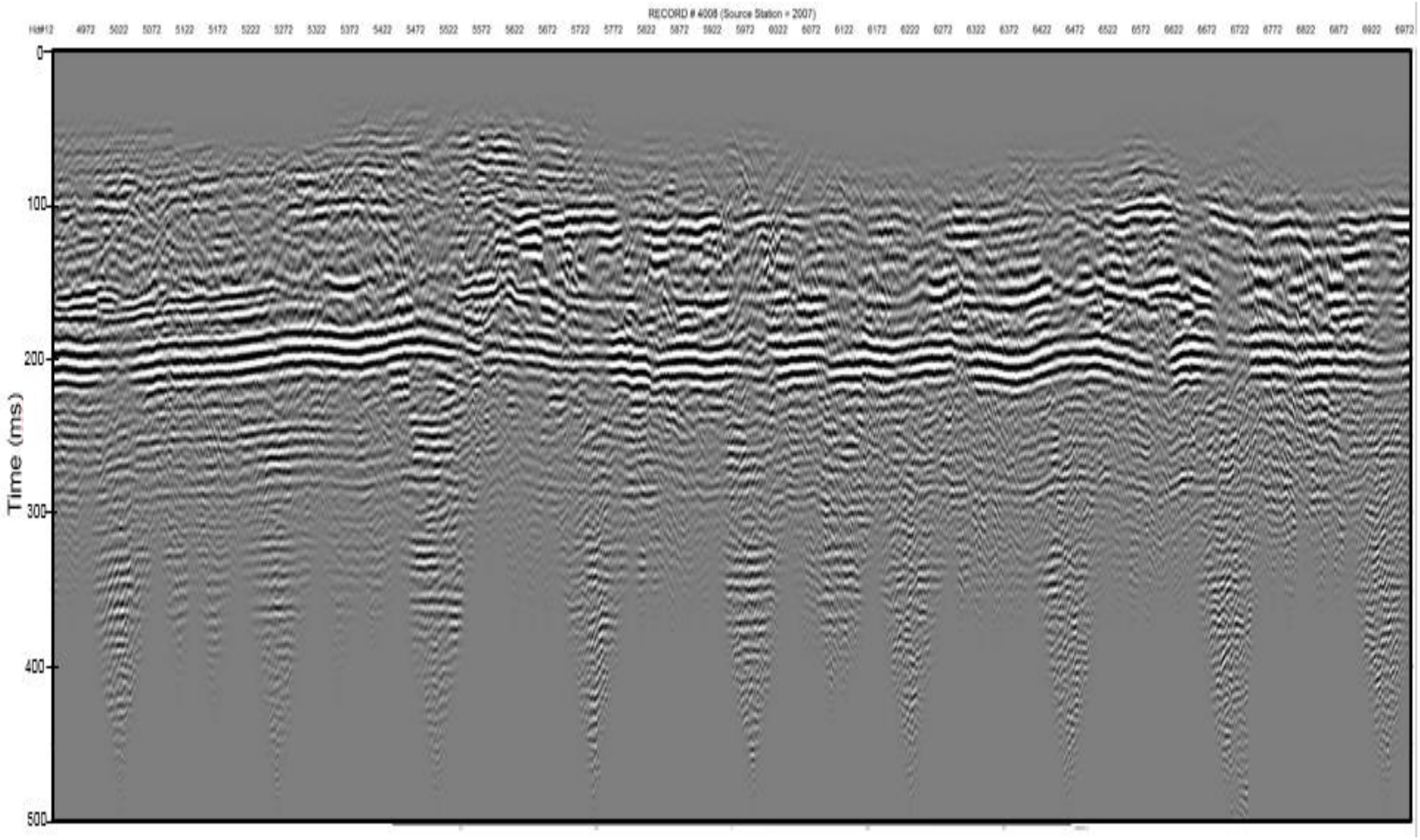

Figure 42: Inman, pre-JARR static correction, time section.

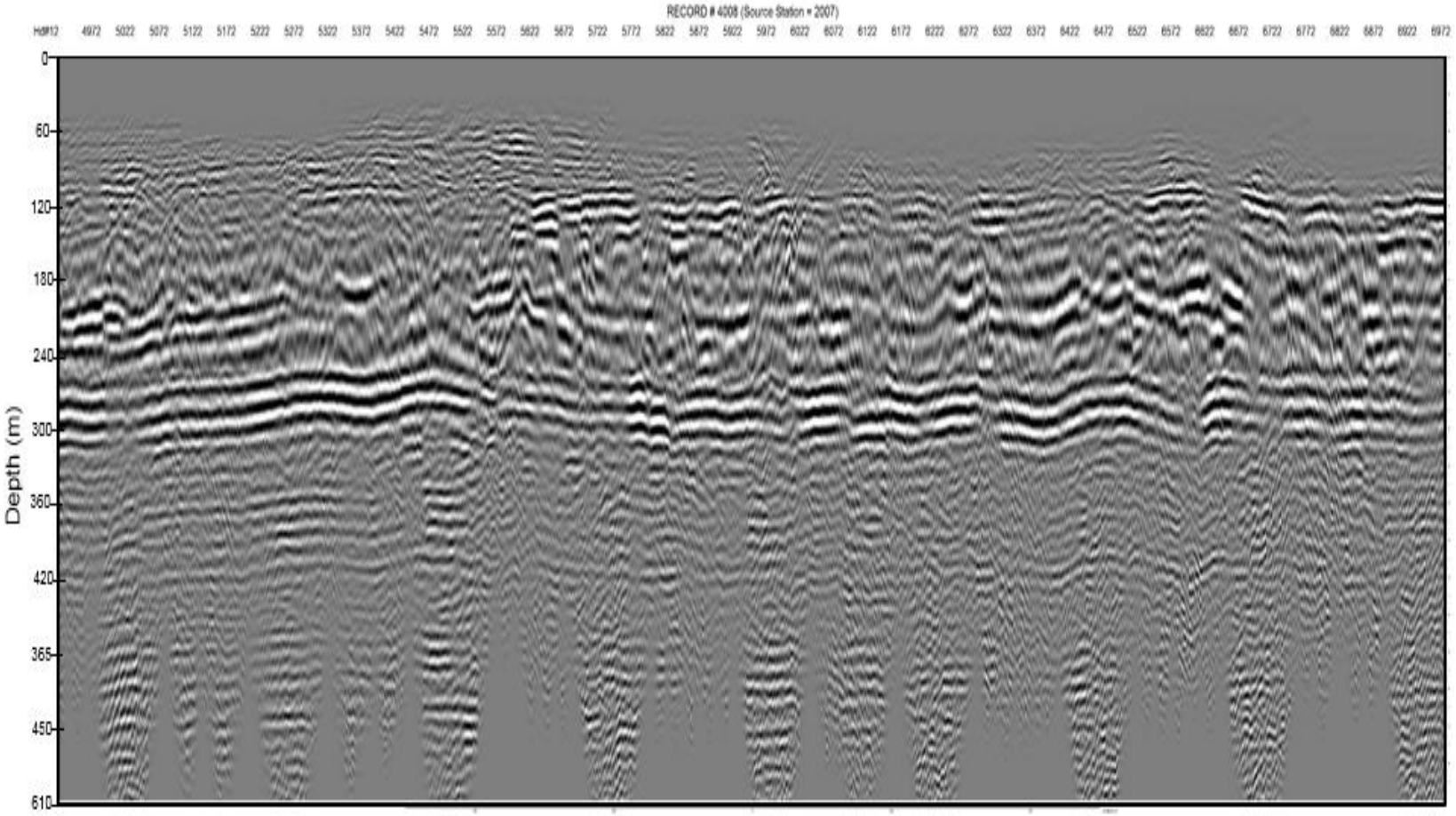

Figure 43: Inman, pre-JARR static correction, depth section.

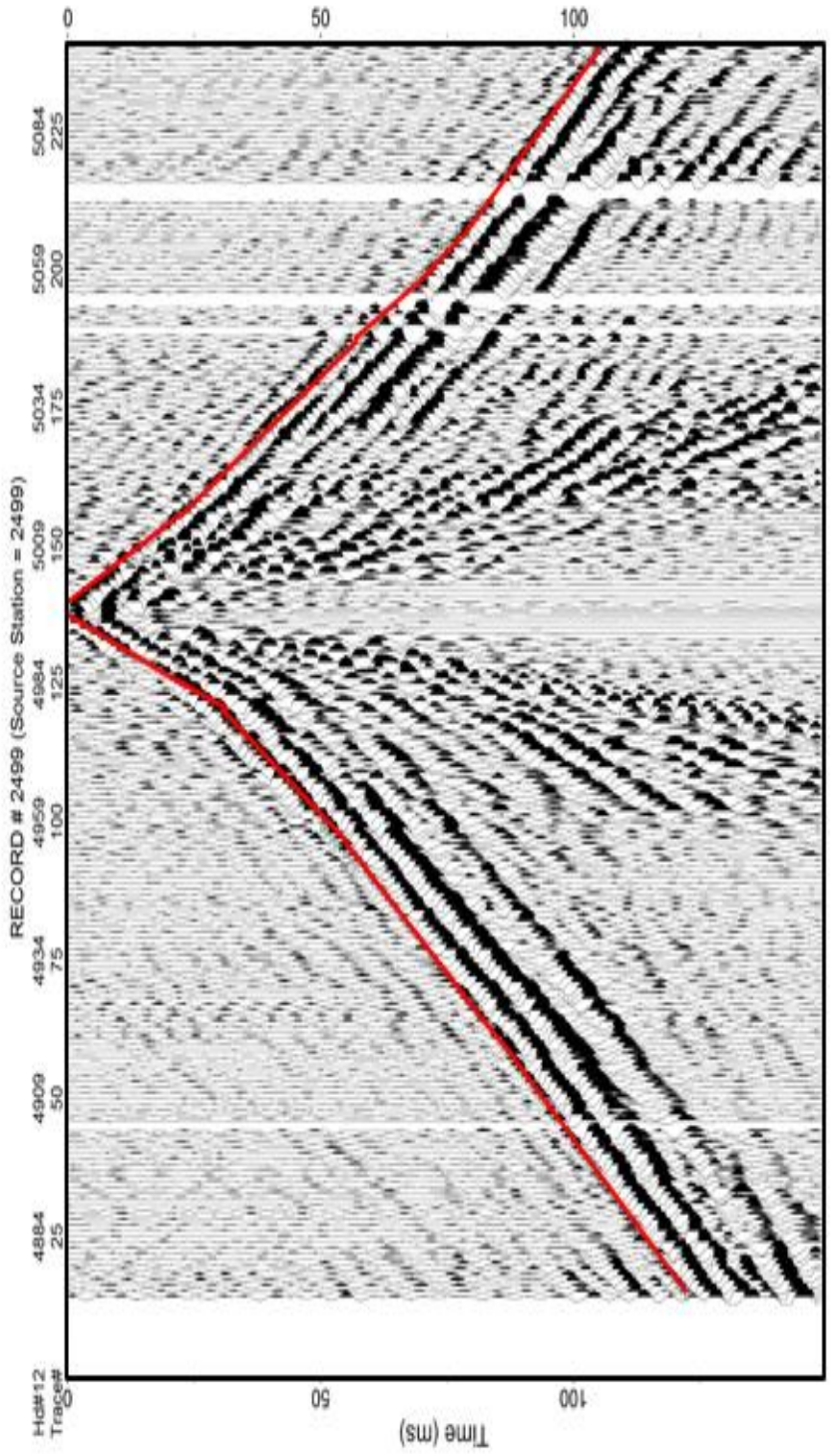

Figure 44: Representative shot record of first arrival picks. The first arrival picks are designated with red lines.

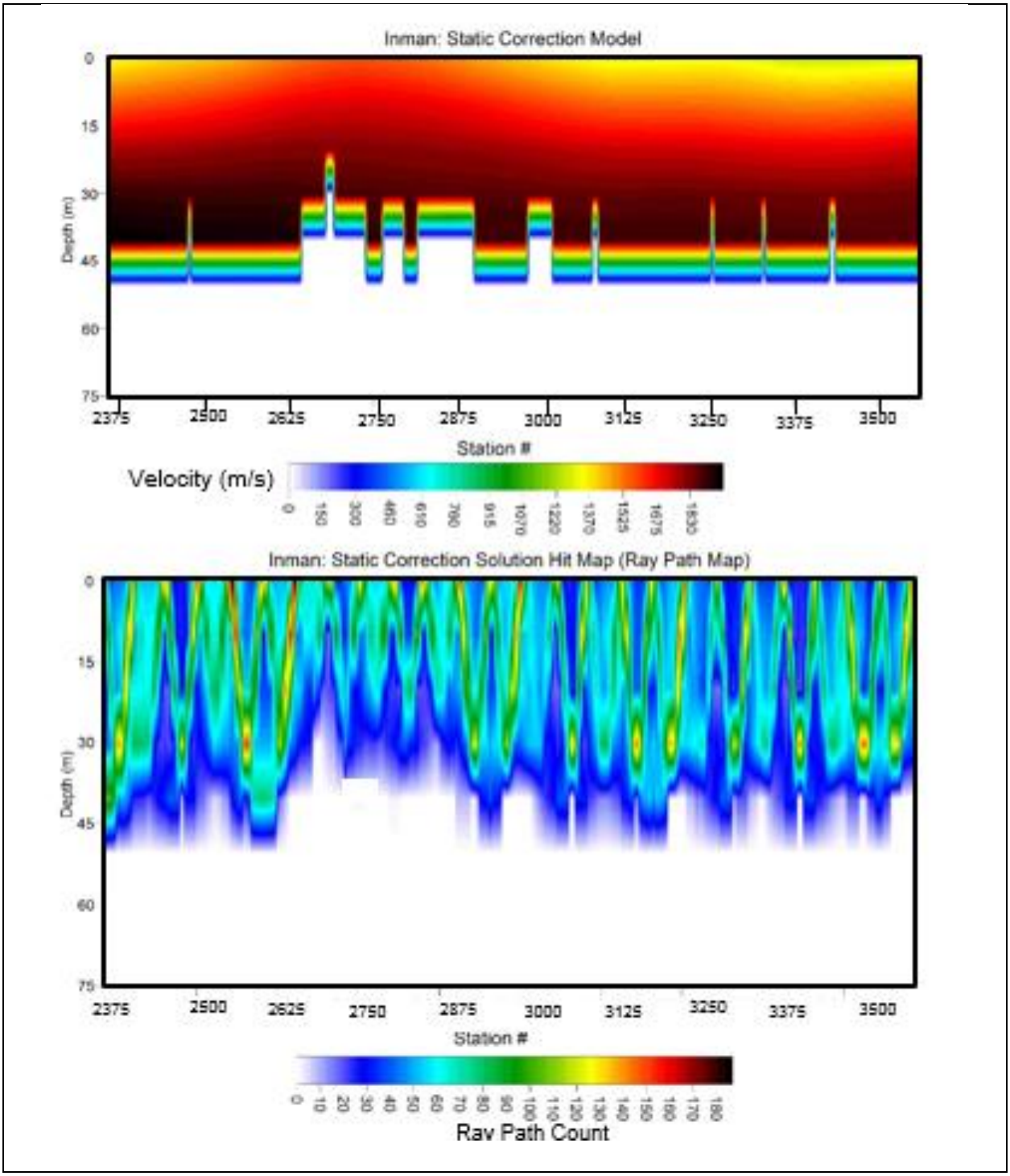

Figure 45: Final JARR FAT model where static corrections were derived, and the ray-path map from the FAT. A 32-meter datum was selected for the static corrections to be calculated.

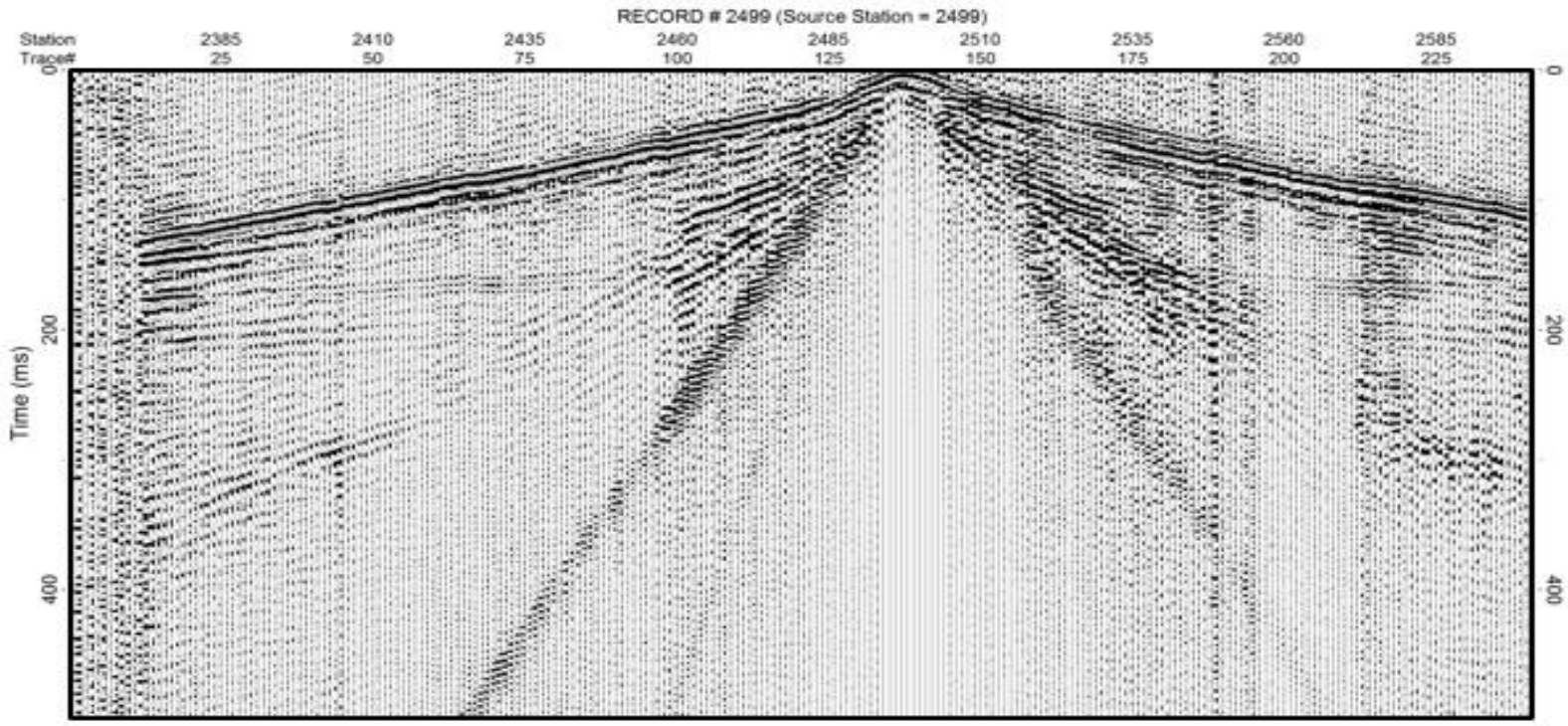

Figure 46: This is a representative shot gather after long wavelength static corrections were applied which were derived from the JARR FAT method.

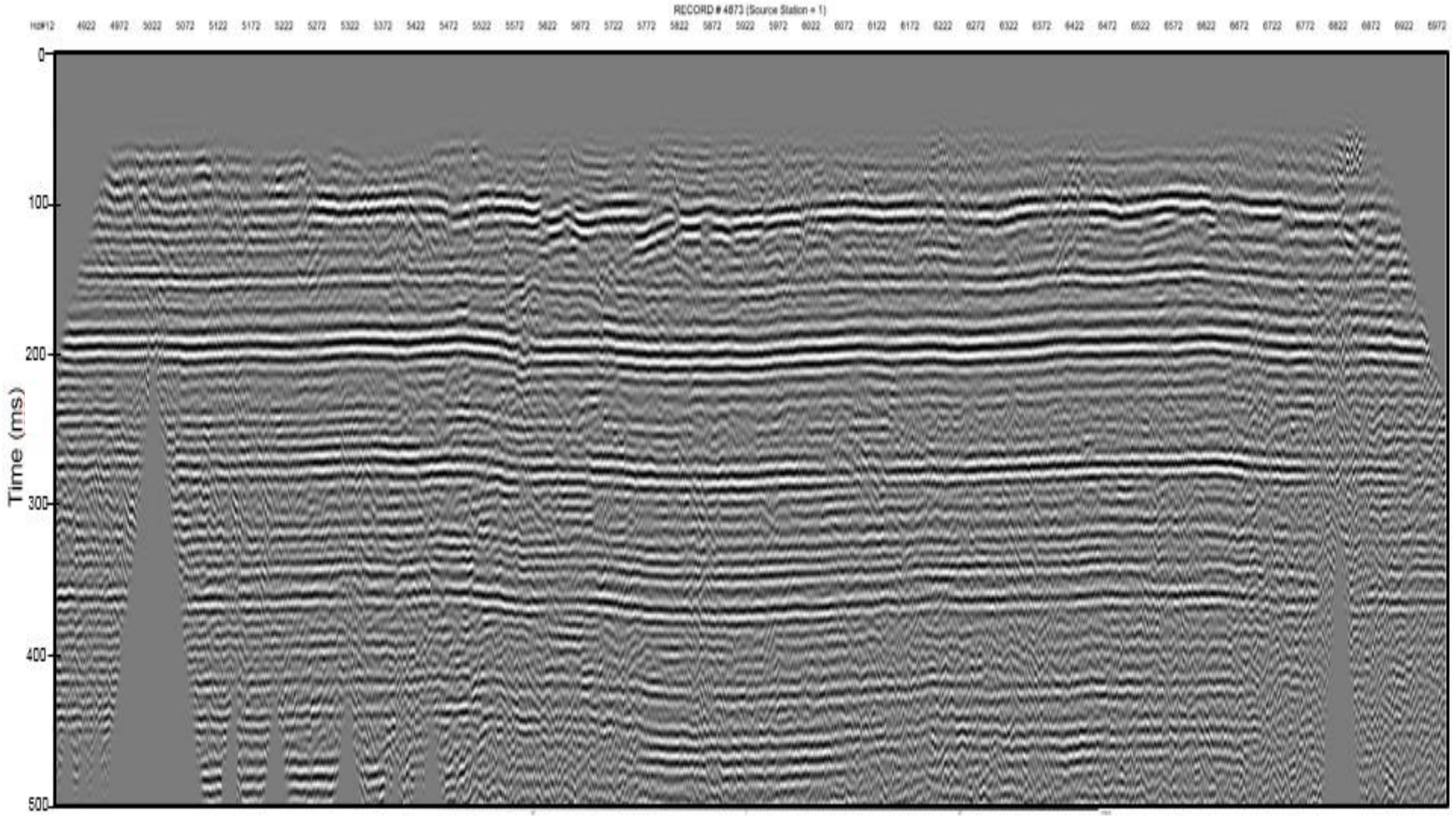

Figure 47: Inman, post-JARR static correction time section.

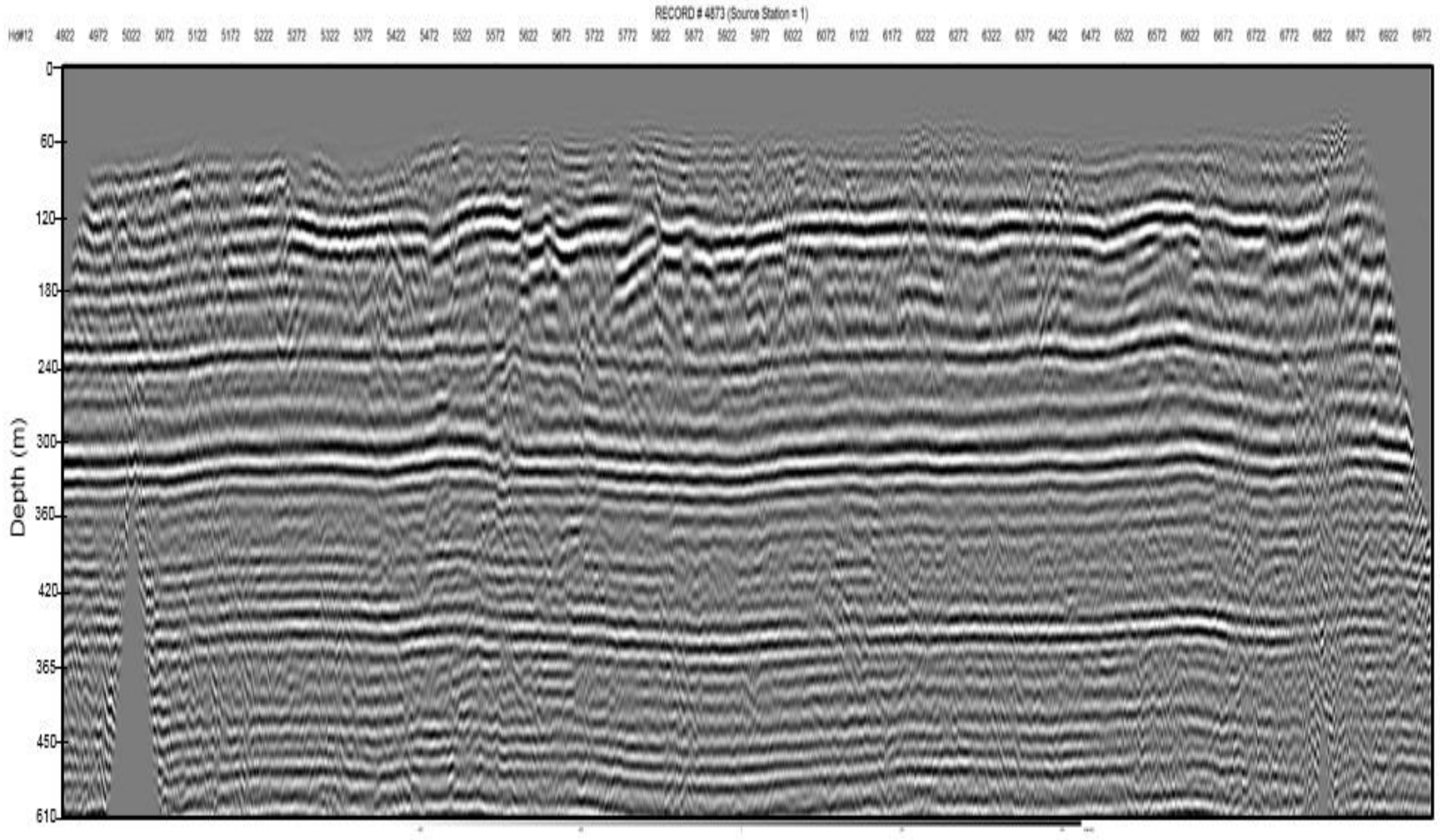

Figure 48: Inman, post-JARR static correction depth section.

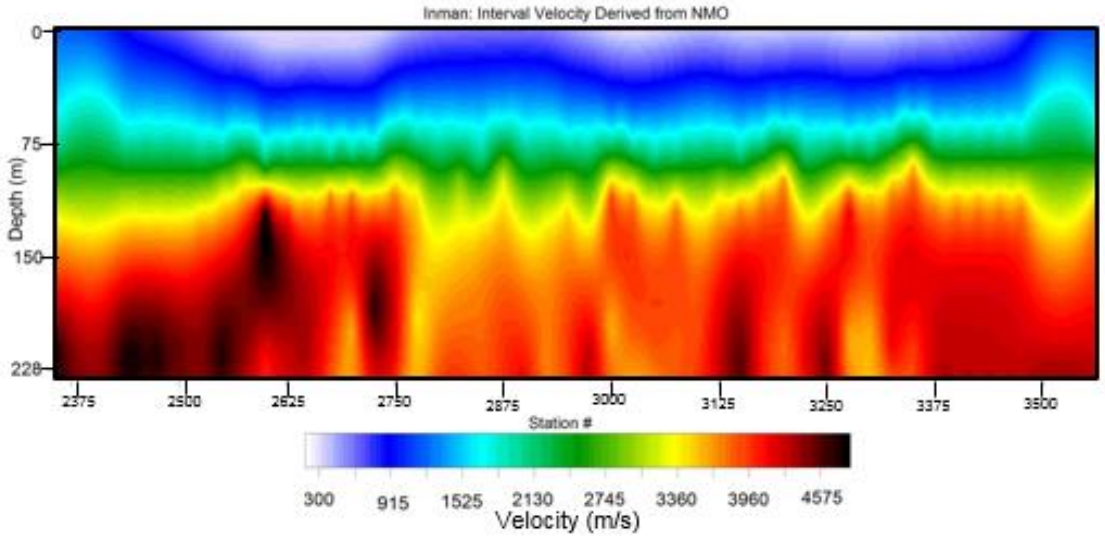

Figure 49: Initial velocity model derived from statically corrected NMO velocity analysis. Input velocity model for MVA using the JARR method.

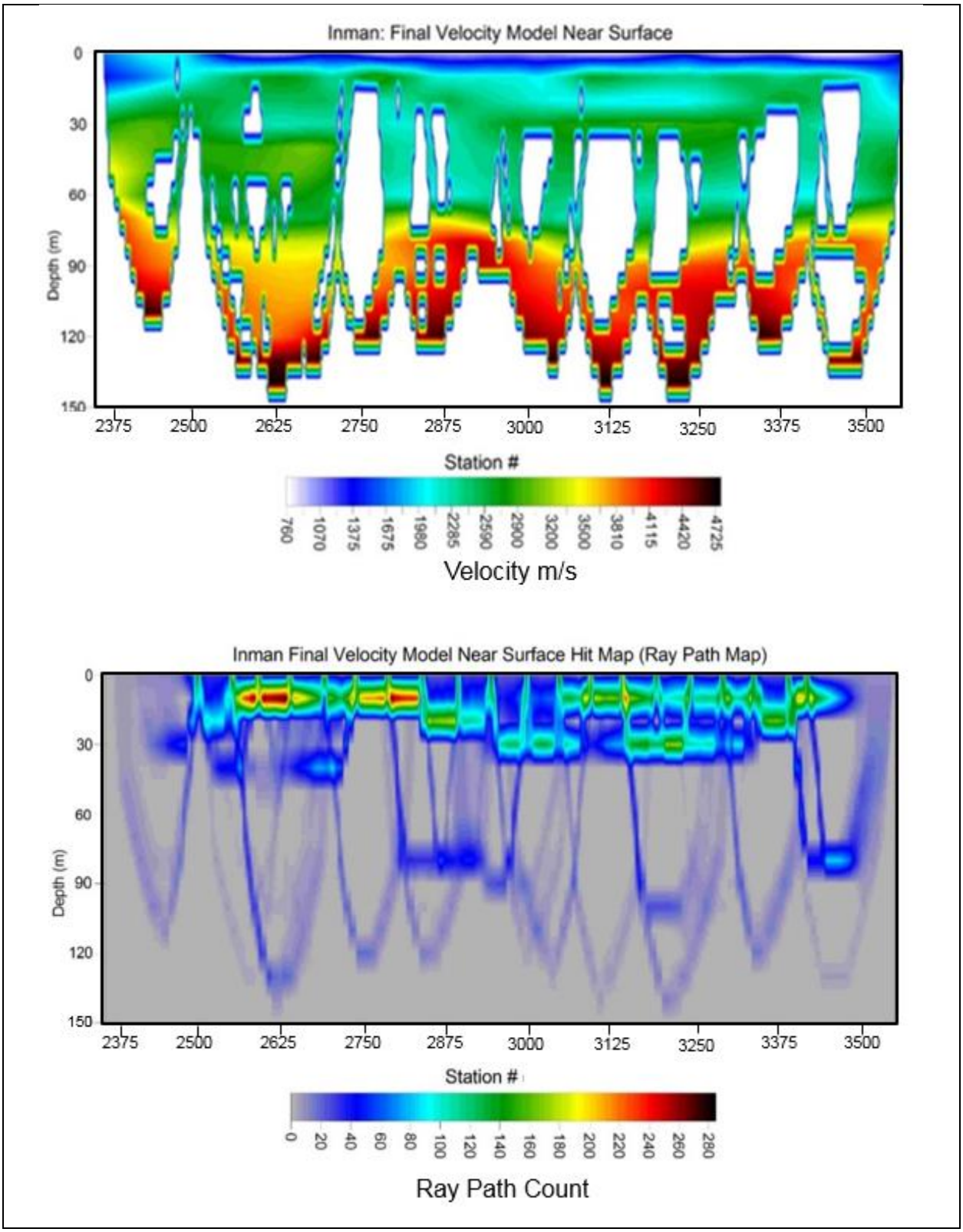

Figure 50: Velocity model of final result derived from the JARR FAT method and a ray-path map (hit map) showing the density and path of rays through the velocity model.

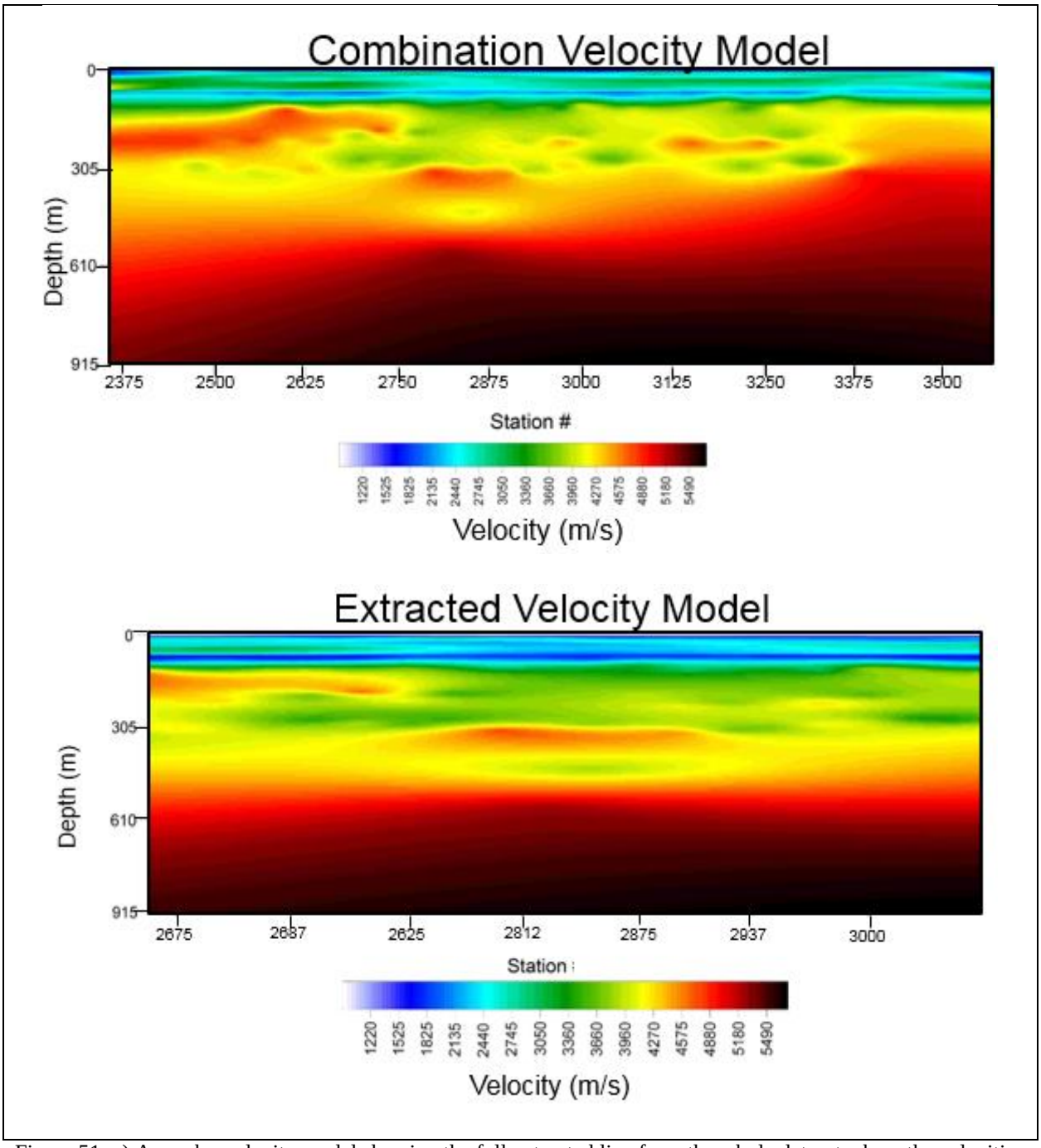

Figure 51: a) A combo-velocity model showing the full extracted line from the whole dataset where the velocities in the upper ~100 meters are represented by the JARR method and the deeper velocities are derived from the NMO corrections. b) is a further extracted velocity model such that the target area of interest is represented and the migration will produce files such that they are below the maximum file limit.

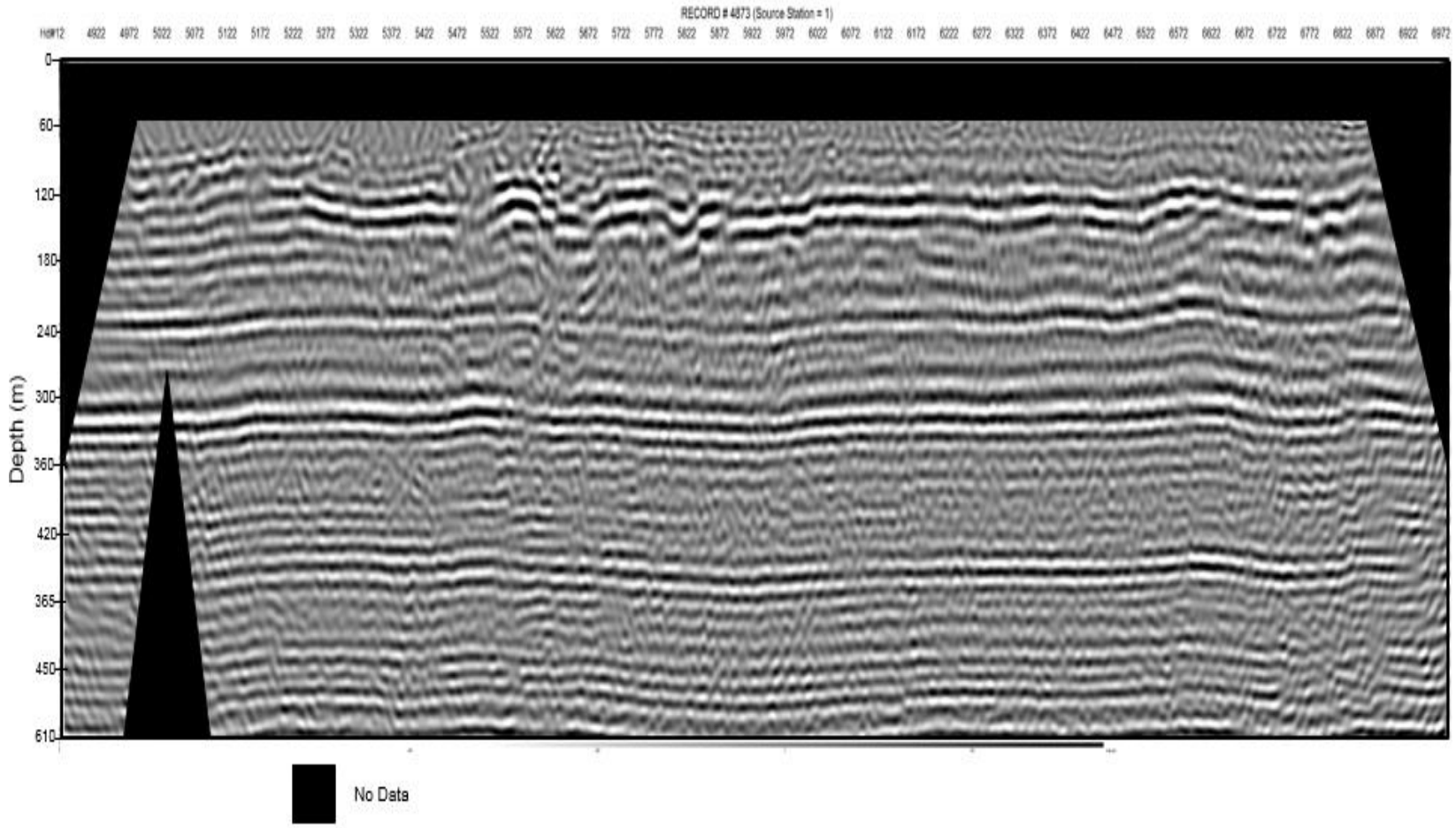

Figure 52: Inman Kansas, FK migration at true CDP spacing (4 feet).

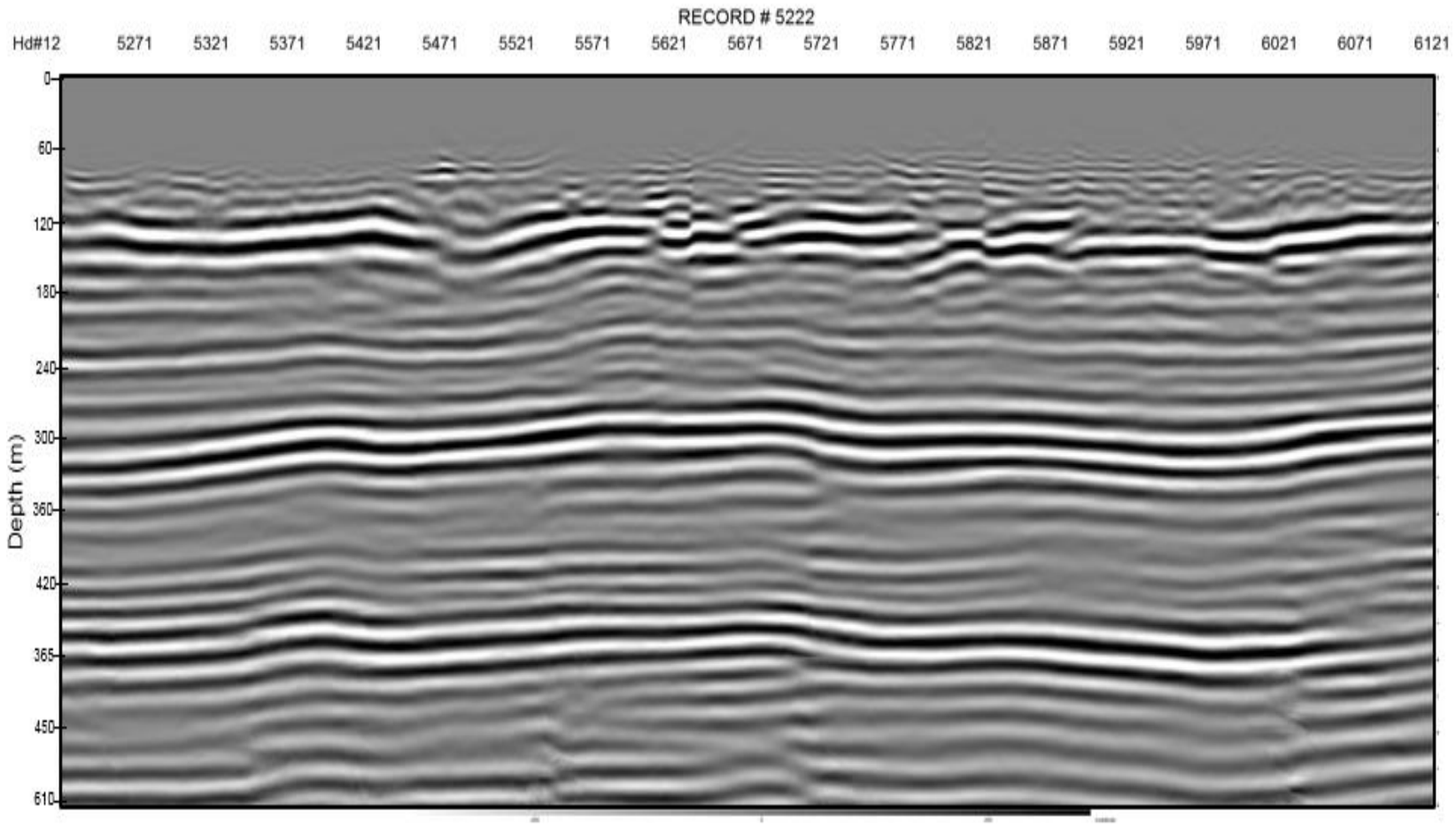

Figure 53: Kirchhoff migration of Inman extracted dataset.

RESULTS & INTERPRETATIONS:

WELLINGTON PETROLEUM FIELD, WELLINGTON KANSAS:

WELLINGTON STATIC CORRECTION:

The JARR FAT method was applied to the Wellington data to improve the image and correct for static variability. Comparing the effects of the improved static corrections as a result of the JARR method in the processing work flow conclusively demonstrates the effectiveness of the method. Reflection returns from the upper 600 meters with (Figure 55) and without (Figure 54) JARR demonstrate how improved velocity models for identical processing flow can alter the final seismic image.

The method was applied to correct for lateral variability due to velocity due to heterogeneity in the upper 250m of the data. Many reflections in the upper 200m appear flattened with an apparent increase in the lateral continuity of the reflections. Chattering of the reflections have been removed and there was greater amplitude uniformity. Furthermore, reflections (Figure 54) at approximately 400m and deeper are shifted down in depth by as much as 50m, again flattening and increasing lateral continuity. In addition to the aforementioned quality enhancements for the deeper statically corrected reflections (Figure 55), the amplitude uniformity has also increased in consistency across the section.

In conclusion, the JARR method has shown the ability to calculate and correct for near-surface static problems. The deeper reflections were less effected by the overall static issues associated with Wellington however, there was overall improvement in the coherency and reflection amplitude uniformity at depth after the data was corrected. These corrections greatly increased the overall quality of the near-surface. Without these corrections, true subsurface structures would have been obscured and the false reflection characteristics would have made the dataset un-interpretable in the near-surface.

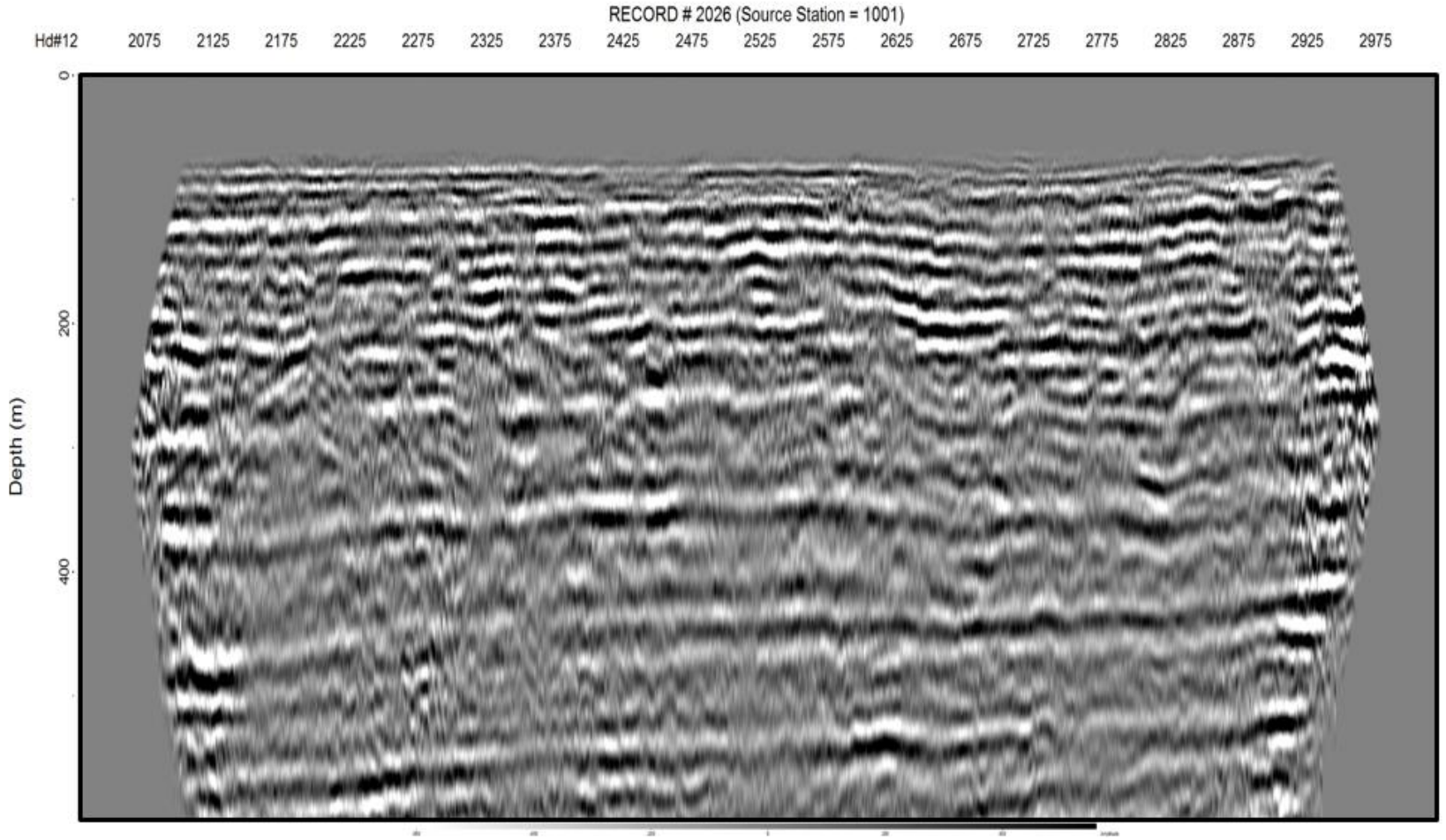

Figure 54: Pre-statically corrected Wellington stacked seismic data. This figure is an identical to Figure 22 however is zoomed in to the upper 600 meters.

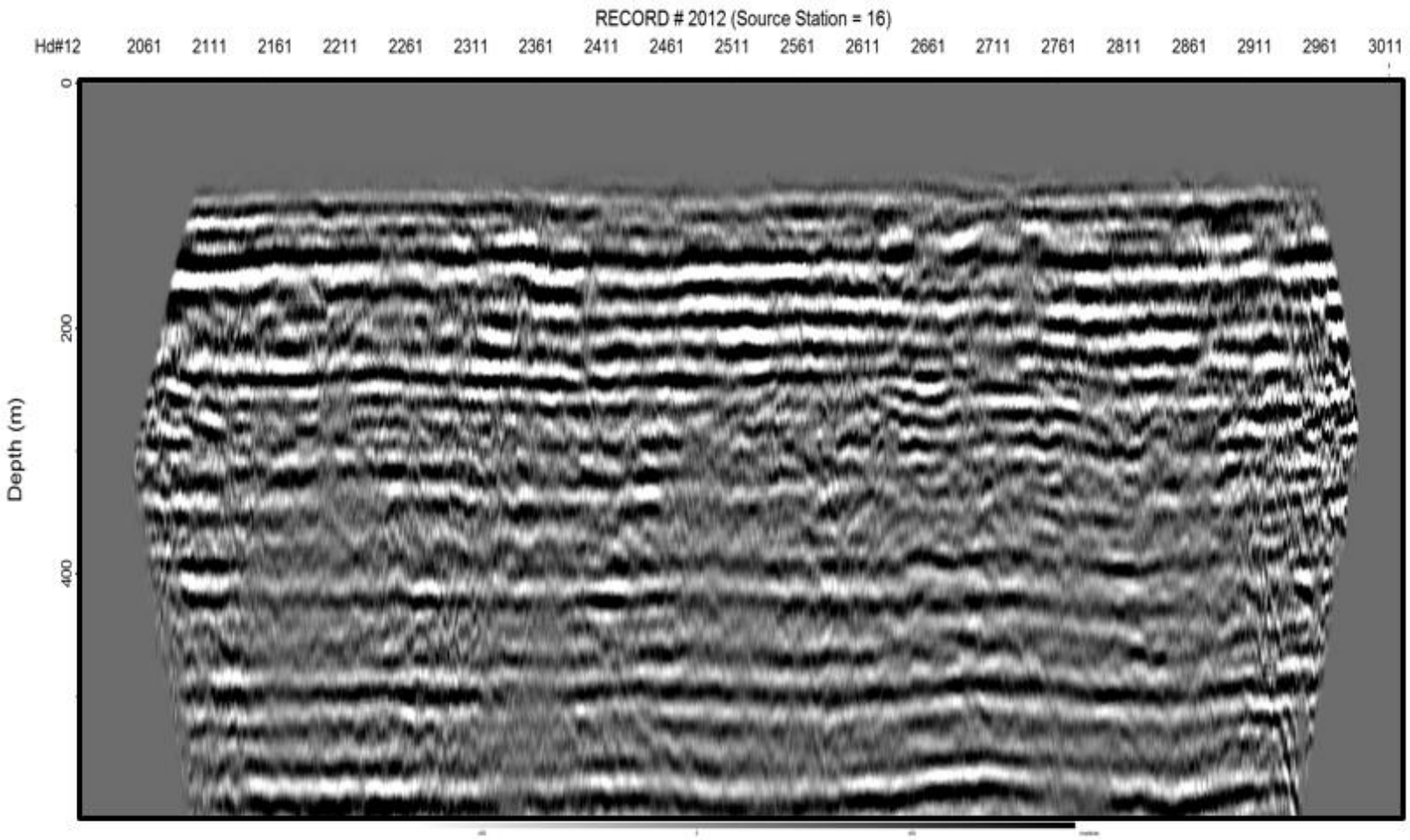

Figure 55: Post-statically corrected Wellington stacked seismic data.

WELLINGTON MIGRATION:

The Wellington Kansas seismic line was designed to image the deepest interval of the Paleozoic as well as the basement features ranging from 800m to over 1700m of depth in the area. The Lancing Kansas City (LKC) is interpreted near the top of the seismic section at approximately 900m depth. The next major reflection beneath the LKC event is interpreted as the Mississippian Limestone at approximately 1100m depth. The Mississippian Limestone has a characteristically weak reflection signature due to the gradational nature of the interface between it and the overlying unit (Fadolalkarem, 2015). The weak signature characteristic in conjunction with the depth correlation with well information strongly supports the interpretation that the yellow horizon is the Mississippian Limestone reflection. Beneath the Mississippian Limestone is the Arbuckle group at approximately 1350m based on time to depth conversions on seismic and lithologic logs from drilling. The exact time/depth of the contact is uncertain as a result of the disruption in reflection coherence between approximately CMP 2660 and CMP 2810. The deepest horizon the basement at approximately at 1575m depth (dark red line). These horizons were correlated to well (15-191-22591) (Table 4) (Survey, 2010), which is located at approximately station 1177 (CMP 2354). These horizons were also correlated to well (15-191-22770)(Survey, 2015), however this well barely penetrated the Mississippian (Figure 56).

Lithologic Unit	**Depth (Approximate Depths in Meters)**
Lancing Kansas City Base	927
Mississippian Limestone	1112
Arbuckle Group	1271
Basement	1573

Table 4: This data represents the interpreted lithology and their subsurface depth. Well (15-191-22591) (Survey, 2010).

The basement is inferred from the well information and by diffractions (Figure 56) emanating from the base of the interpreted unit. The agreement between both the diffractions and the known basement depth from well logs, reinforces the suggestion that this is the basement reflection. The degradation of reflection coherency, amplitude quality and frequency content increases rapidly at depths greater than approximately 1600m (Figure 26 in conjunction with Figure 56). This rapid degradation of data quality is attributed to lack of data and noise consistent with basement signature interfering with multiple reflections from higher up in the stacked section or reflection events caused by basement ringing. This is consistent with the attribution that the reflection event at 1575m is from the basement.

The depth accuracy of the reflections in the subsurface supports the suggestion that an improved velocity model was derived from the JARR method. Additionally, the accuracy of the velocity model derived in spite a-priori information (well log information, vertical seismic profile, check shot, etc.) illustrates the utility of the method for defining accurate velocity models for depth conversion. Furthermore, inaccuracies of the velocity model when compared to the sonic log can be attributed to the non-uniqueness of velocity analysis with no a-priori information. Additionally, it was shown that slight variations in reflection picking can drastically change the resulting velocity model to more closely resemble the sonic log. The original velocity model derived for the

Wellington dataset (Figure 20) was derived from first pass NMO analysis as described earlier. It indicates a relatively smooth increasing velocity with depth which follows conventional wisdom in many seismic situations. The improved velocity function derived from JARR analysis (Figure 28a) indicates a smooth increase in velocity to a pronounced velocity high at approximately 125m extending down to 400m depth where a velocity inversion occurs. The model then slowly increases in velocity to the bottom of the model. Initially, without explanation this could indicate an error. However, at the Wellington site, defined by Well 15-191-22770 there is a layer of Hutchinson Salt present. This salt layer extends from approximately 80m – 180m depth (Figure 2b). As stated earlier, the velocity increase seen on the velocity model (Figure 28a) appears at approximately the base of the Hutchinson Salt. The velocity at that depth reads to be approximately 4800-5000 m/s which matches the velocity of salt (Sheriff, 1976). Furthermore, the lithology present beneath the Hutchinson Salt Member are indicated by well log as interbedded limestone and shale. The velocities observed at this location are between 3200 – 3800 m/s which is in agreement of what is to be expected in terms of velocity at that particular depth (Sheriff, 1976). The agreement of expected velocities and lithologic units present at particular depths indicates that the JARR method static correction at a minimum allowed for more accurate picking of velocities through NMO velocity analysis.

Stolt migration, also known as an FK migration, was applied to the Wellington data (Figure 57). The changing frequency content is the most recognizable difference following the migration. The migration lowered the frequencies present, while the amplitude and lateral continuity appears to have increased in quality. Lateral continuity in the reflections between CMP 2660 and CMP 2910 has improved greatly. A specific example at that location would be the discontinuity that was infilled with reflections with a clear indication reflection offset between 1250m and 1450m

below the ground surface. This offset is interpreted to extend through the Arbuckle group is identified as a normal fault.

Each interpreted unit appears slightly flatter following the migration process. The base of the LKC and Mississippian Limestone appear more pronounced and laterally continuous. Reflection multiples/ringing below the basement also appears to have been corrected, and looks more prominent. However, these events also appear less linear and intersect one another more than the real reflections above them. Many of the basement diffractions have disappeared.

"Smiles", which can result from an inaccurate velocity model used during migration can be largely traced to the edge of the data. This indicates that these smiles are an artifact due to corrections at the boundary between no data and data rather than an inaccurate velocity model. Since these artifacts can be traced to a source (reason) they can be ignored. The migrated data appears to be artifact free with the exception of what was previously discussed.

A post-stack Kirchhoff depth migration was applied to the Wellington data using the same velocity model as the FK migration (Figure 58). Reflections have been flattened after the Kirchhoff migration with lateral continuity and amplitude consistency increased compared to un-migrated data. Like the FK migration, frequency content has decreased, a trait inherent to migration. However, the higher frequency content of the Kirchhoff migration does appear to be higher than that of the FK migration. The migration successfully enhanced reflection wavelet continuity between CMP 2660 and CMP 2910. The fault interpreted after FK migration (Figure 57) is still apparent on the Kirchhoff migration (Figure 58). Unlike with the FK migration, the Kirchhoff migration appears to have minimal edge effect or velocity dependent anomalies (e.g. smiles, frowns). The Kirchhoff migration does not appear to be as successful as the FK migration in its ability to resolve proper reflection location. There appears to be more structure after

Kirchhoff migration that does not seem consistent to what is seen in the pre-migrated image or the FK migrated image. This indicates that these structures (dipping units) are an artifact of the migration. Whether these artifacts are caused by the variability in the velocity function or the amount of noise present in the image, it appears that the Kirchhoff migration solution is not as accurate as the FK migrated image. Overall, the character of the Kirchhoff migration, and reflection wavelet enhancements between CMP 2660 and CMP 2910 indicate the Kirchhoff migration achieved relative success using velocity information derived from the JARR method.

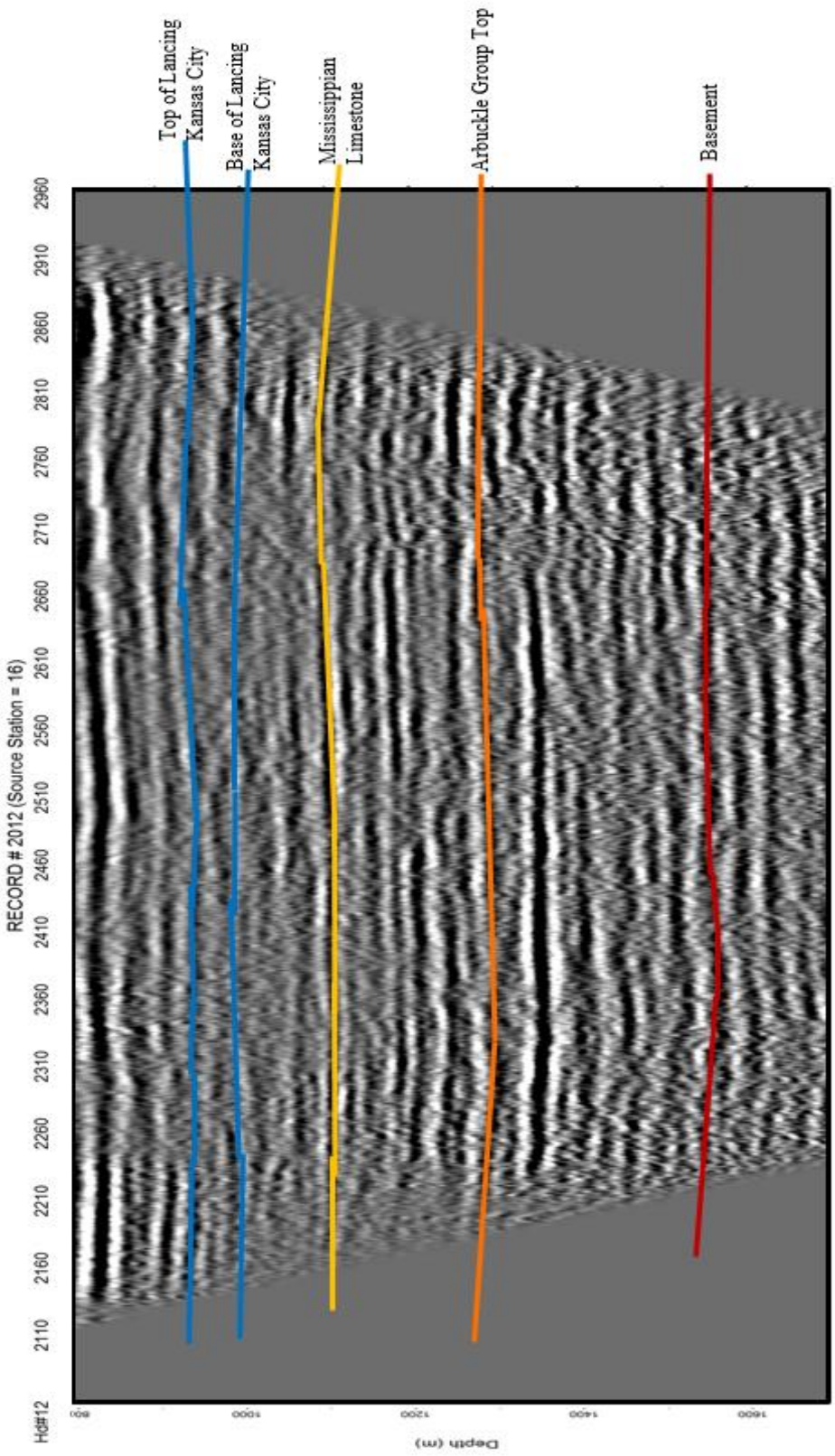

Figure 56: Interpreted un-migrated Wellington, Kansas deep section.

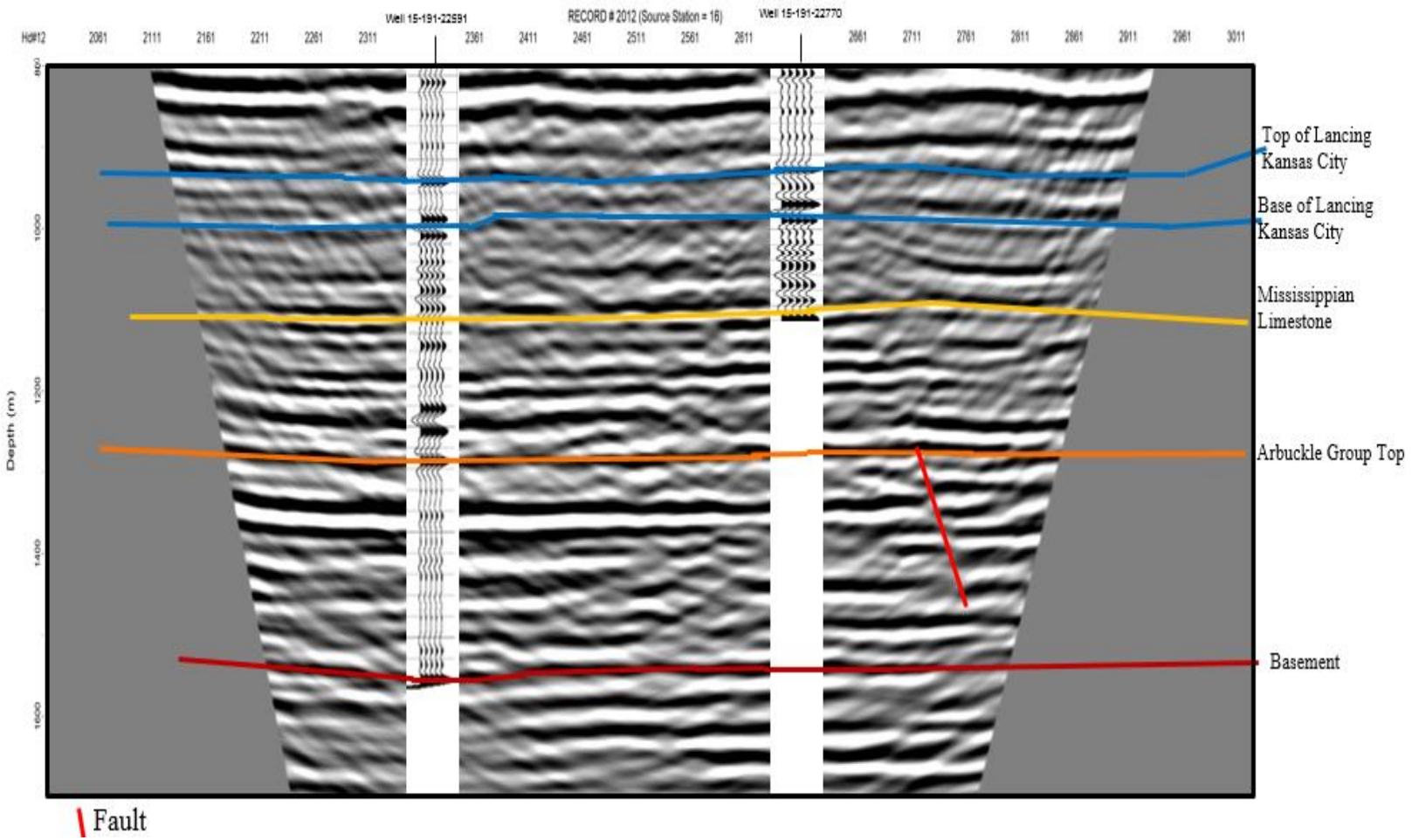

Figure 57: Interpreted Stolt Migrated Wellington deep section. The synthetic seismic traces were generated using the proprietary KGS public synthetic trace generating software.

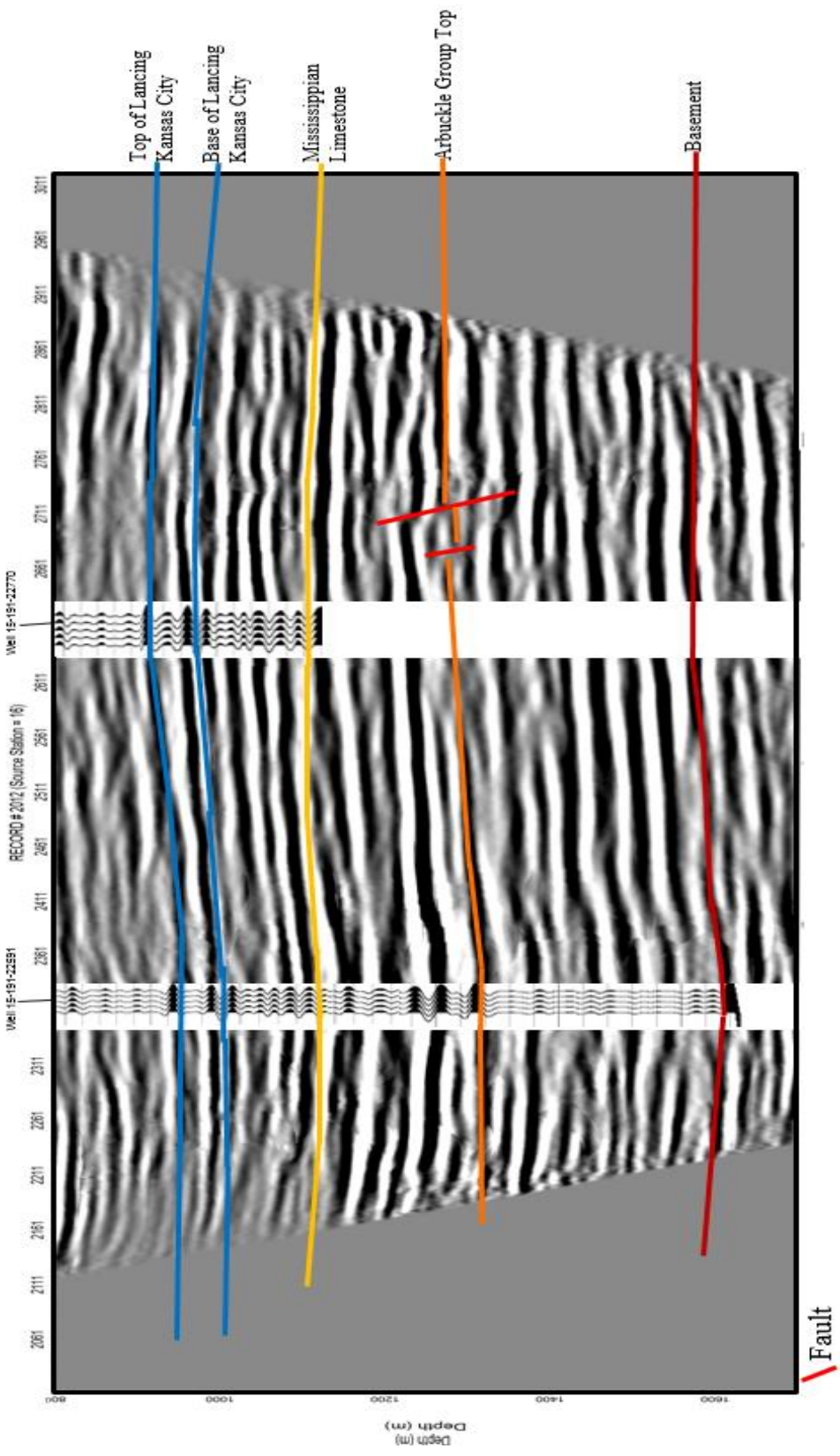

Figure 58: Un-interpreted Kirchhoff migration applied to the Wellington data. The synthetic seismic traces were generated using the proprietary KGS public synthetic trace generating software.

HIGHWAY 61, INMAN KANSAS:

INMAN STATIC CORRECTION:

Static corrections can be essential to enhancing the accuracy and usefulness of seismic images. The Inman dataset was used to evaluate the improved static corrections derived using the JARR method over conventional methods. CMP stacked data from Inman without statics suffered from data drop-out below 300ms due to aggressive muting necessary to avoid energy that could not be removed through filtering (Figure 59). With appropriate static corrections derived from JARR, muting was minimal and deeper reflections are now evident (Figure 60). Minimal muting was possible due to more consistent energy allowing for more extensive filtering and suppression.

A common problem with pre-static or non-static corrected data are inaccurate stacking velocities which can lead to poor depth conversions (Figure 61). A notable anomaly between 120 and 240m are due to poor velocity depth conversions. After appropriate static corrections depth converted seismic sections are noticeably devoid of the anomaly between 120 and 240m with structures beginning to emerge (Figure 62).

Comparing the pre-static JARR static corrected data (Figure 59, Figure 61) with the JARR statically corrected data (Figure 60, Figure 62), it is clear that reflection continuity, frequency content, and amplitude uniformity are substantially enhanced in the corrected data. The Inman dataset especially benefited from the JARR methods derivation of static corrections. Without the static corrections, a major near-surface structure would have been completely obscured and interpretations of reflection depth would have been inaccurate. After the statics were applied the overall quality of the reflections in amplitude uniformity, continuity and location accuracy are greatly improved. Furthermore, a prominent subsurface structure consistent with dissolution was properly restored along with flattening and proper reflection location. In conclusion, the JARR

methods derived static corrections were necessary for enhancing the Inman dataset to the quality required for proper interpretation.

INMAN MIGRATION:

The Highway 61 seismic line was designed to image dissolution features in the subsurface and especially features that might develop into sinkholes, and as such record data with limited depth capabilities. The maximum reflector depth that has a clearly observable reflection on the data is roughly 1,000 meters. Only the upper 600 meters are included in the imaging depth due to the objective of the study (Figure 63). The shallowest major reflection visible is the base of the Upper Wellington Formation (UWF) and is interpreted with a purple line. The Hutchinson Salt Member is highlighted in orange where there is no apparent dissolution, and in light blue where it is interpreted that there is some salt dissolution. This interpretation is based on an evident decrease in the lateral coherency of units within and immediately outside the salt.

Within the sequence below the salt is the top of the Chase Group (in orange) and a flat uniform horizon reflection (in yellow), that matches the Nolans Limestone. Faults are interpreted to bound the dissolution zone offsetting the base of the UWF. From CMP 5740 to CMP 5800, the UWF appears at around 180 meters depth to possess unique characteristics that can either result from slumping or be the result of a diffraction scattering from an interpreted fault that bounds the northern side of the interpreted dissolution feature. The Chase group appears to also be offset by faults around CMP 5600 and 5700 which is consistent with previous work imaging these units to the east of Hutchinson, Kansas (Judy, 2015), and the local stratigraphic column (Anderson et al., 1998). The structural interpretations are unique to this work, but based off of the study conducted by Judy (2015).

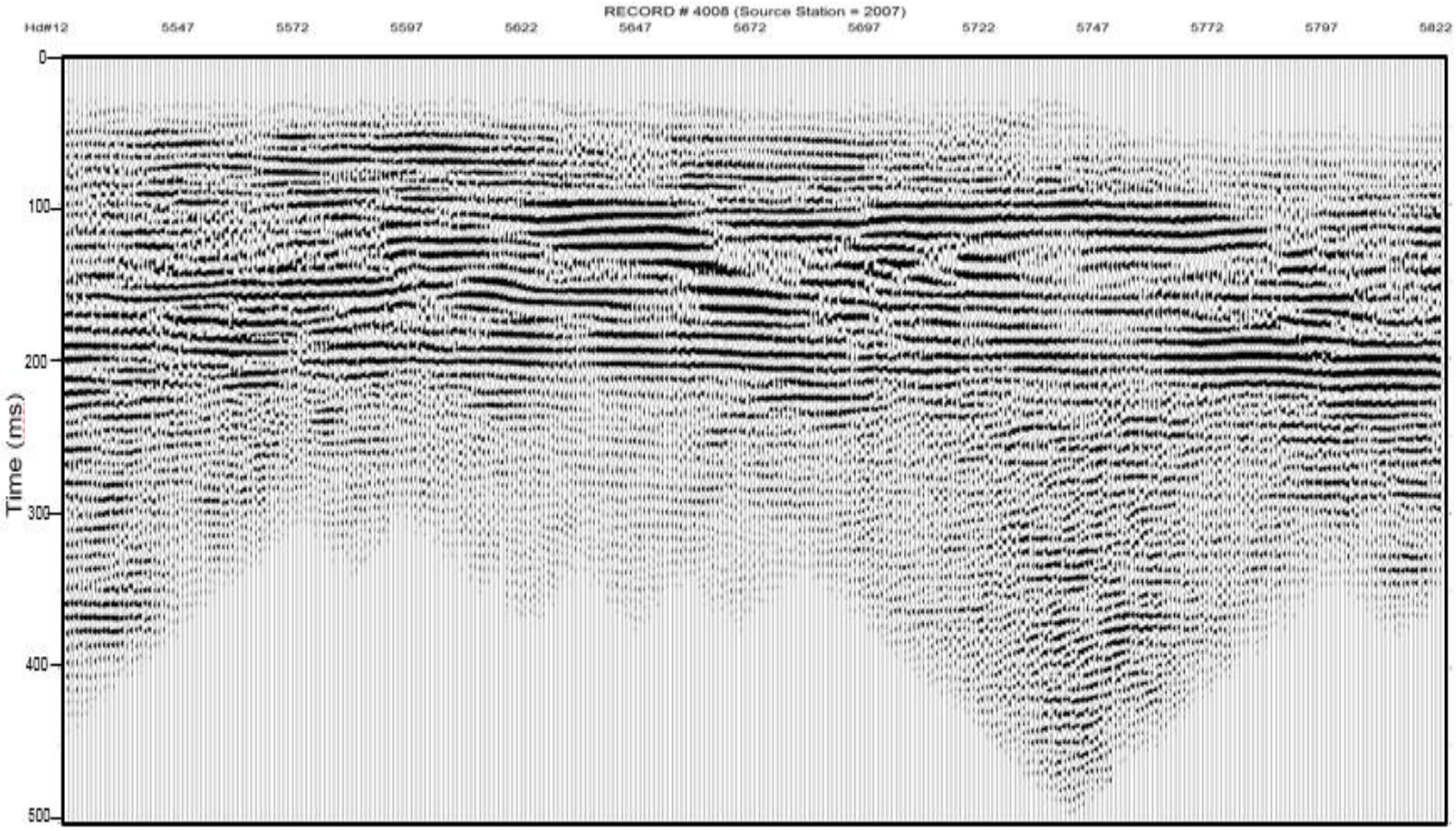

Figure 59: Highway 61, Inman Kansas seismic time section over the area of interest. This is pre-statically corrected data, with the improved statically corrected NMO velocities applied.

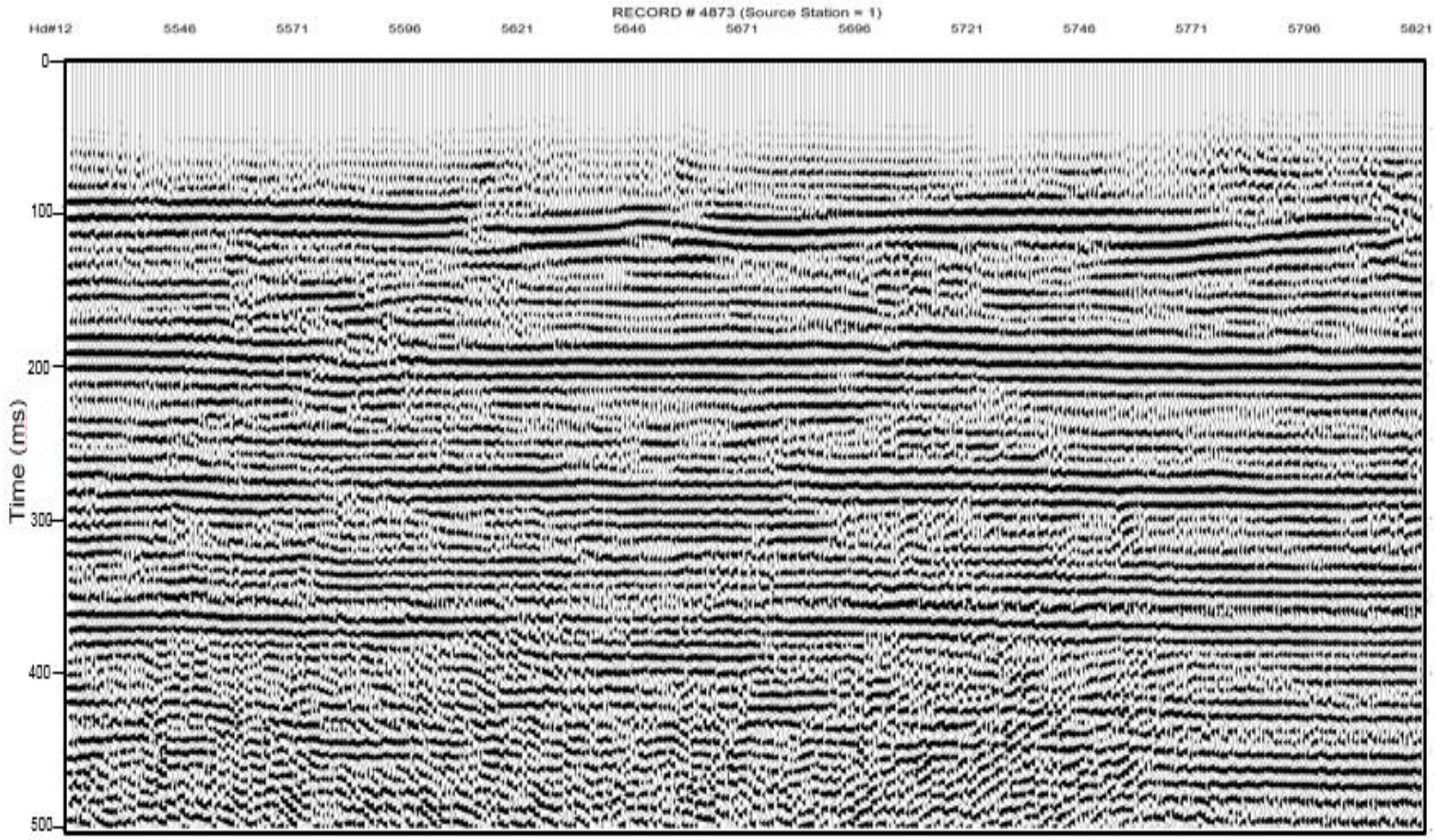

Figure 60: Highway 61, Inman Kansas seismic time section over the area of interest. This is statically corrected data.

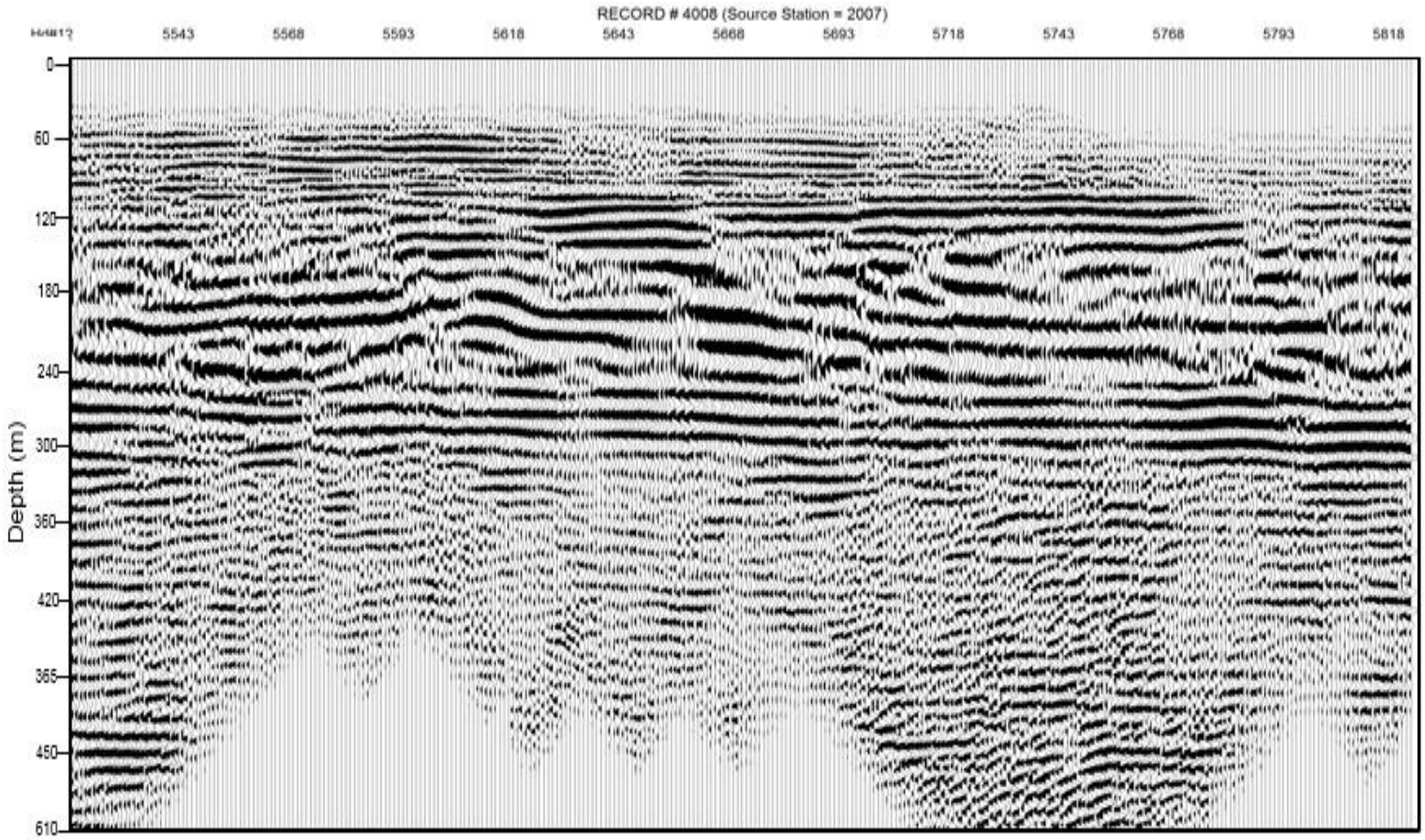

Figure 61: Highway 61, Inman Kansas seismic depth section over the area of interest. This is pre-statically corrected data, with the improved statically corrected NMO velocities applied.

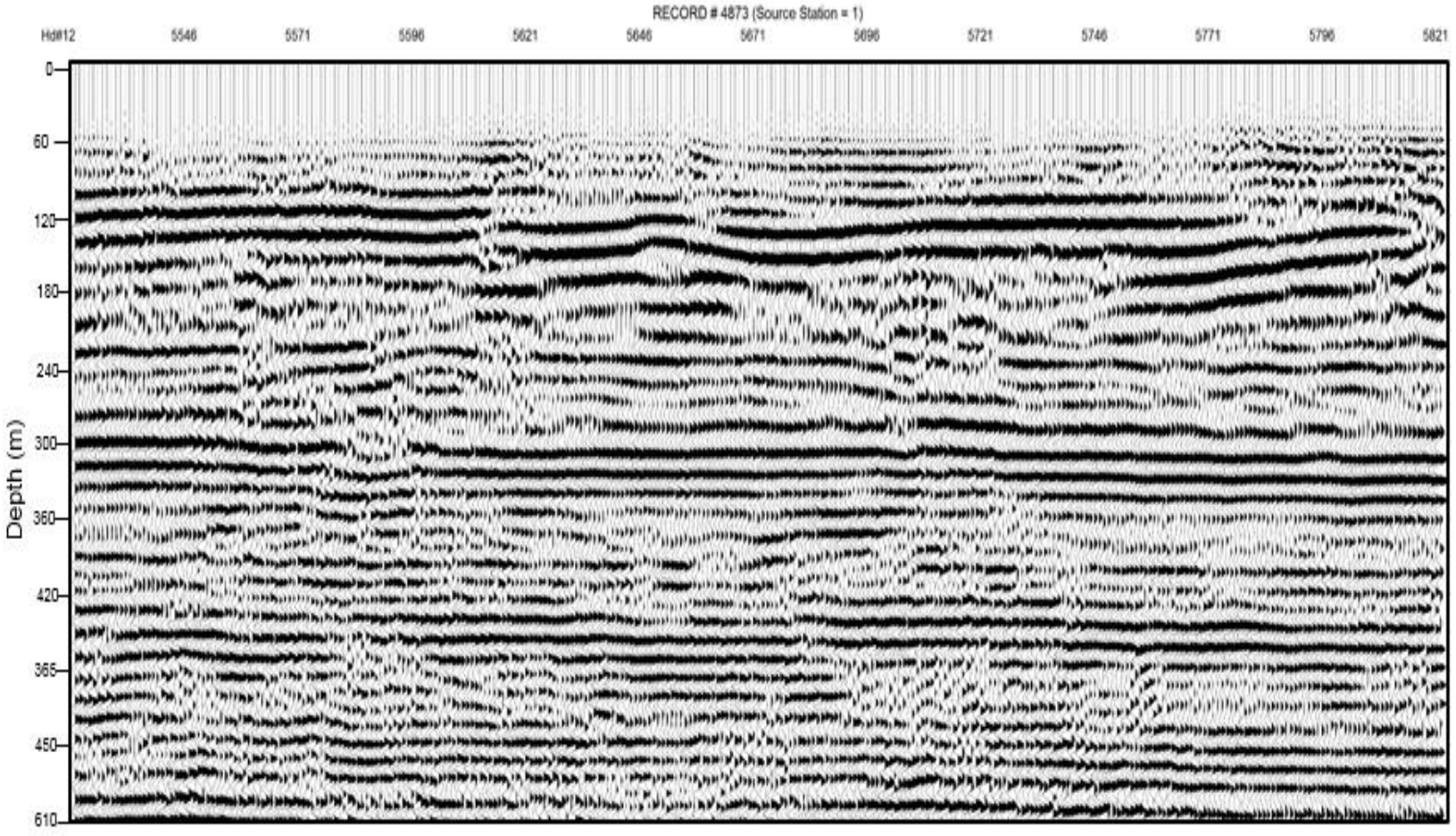

Figure 62: Highway 61, Inman Kansas seismic depth section over the area of interest. This is statically corrected data.

The Stolt migration appears to have migrated the Inman data with little to no artifacts (smiles and frowns) that have commonly plagued near surface migration (Figure 64). There are artifacts in the upper 75 meters that are strictly due to a lack of data evident on the un-migrated image. Although the continuity of reflections is comparable between the migrated and un-migrated data, there is an obvious decrease of high frequency content. The offsets in reflections that were interpreted in the UWF reflections on the un-migrated section remain a distinct feature on the migrated dataset.

The Kirchhoff migration (Figure 65) contained reflections offsets in the UWF and are in fact more defined than the FK migration or the un-migrated images. This observation increases confidence in the interpretation of these faults between CMP 5600 and 5700. The diffraction that was interpreted on the un-migrated section at CMP 5740 – 4800 at a depth of 180 meters was corrected in the FK migration, and has been partially collapsed in the Kirchhoff migrated section. A clean break in the UWF reflection at CMP 5790 appears to indicate the diffraction a fault that was previously obscured by misplaced reflecting points. Unlike with the FK migration, the high frequency content in these data have been almost completely eliminated by the Kirchhoff migration. The Kirchhoff migration appears to do a tremendous job restoring deeper reflection continuity when compared to the FK migration as well as the un-migrated data.

As with the Wellington dataset, it appears that the FK migration was more successful in restoring the subsurface more accurately when compared to the Kirchhoff migration. However, the degree of which the migrated images are different is not as drastic as what is presented in the Wellington dataset.

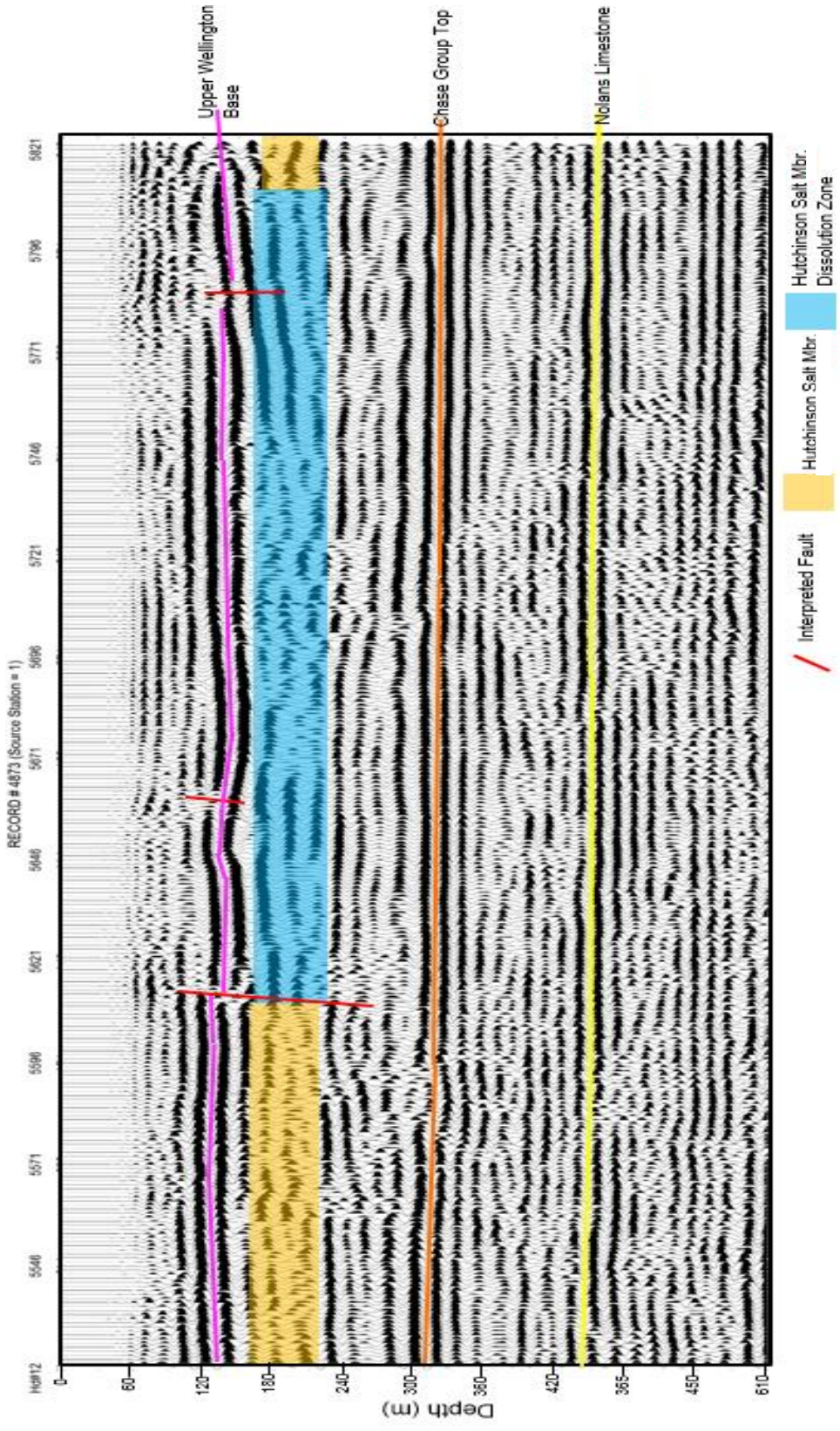

Figure 63: Interpreted pre-migrated stack Highway 61 subset.

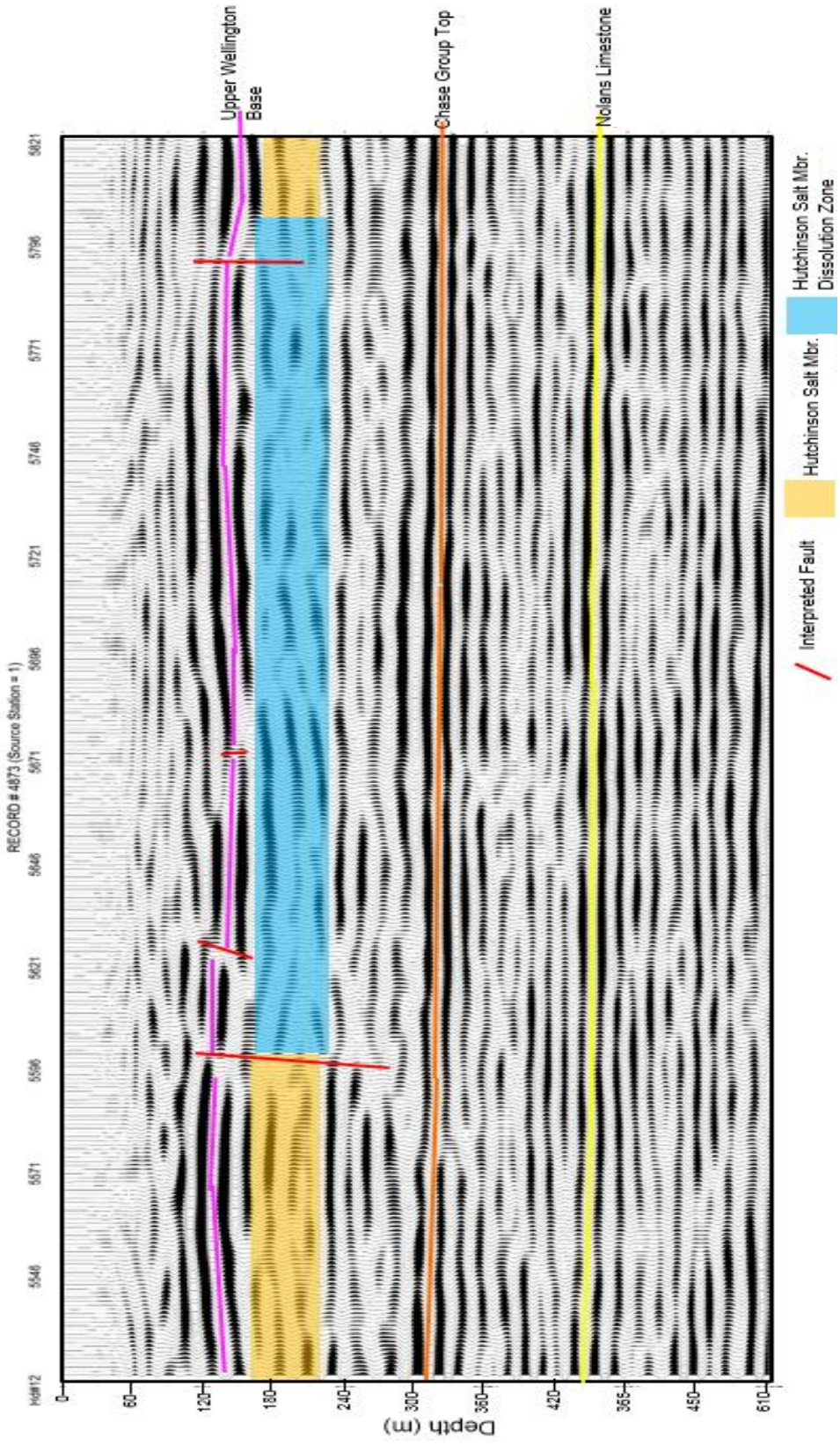

Figure 64: Interpreted Stolt migration applied to the Highway 61 subset.

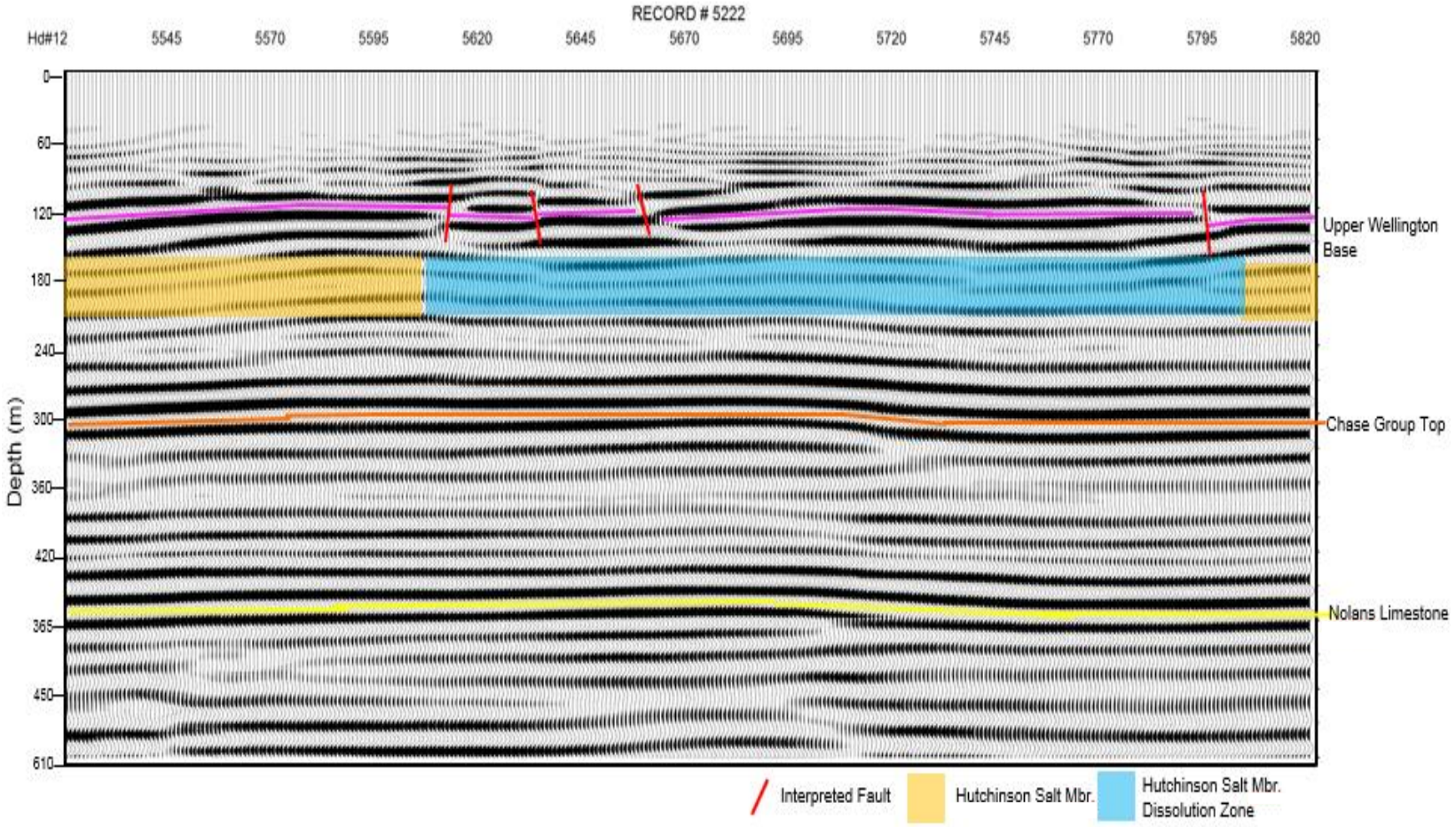

Figure 65: Interpreted Kirchhoff migrated Highway 61 subset.

DISCUSSION & CONCLUSION:

This research introduced the JARR method as an approach for calculating near-surface velocity functions and was evaluated using data from two distinct locations in Kansas in two unique applications. The application was designed to provide static corrections derived from improved velocity functions for data with long-wavelength issues. The second application of the JARR method was intended to calculate a more accurate velocity function for the near surface improving the effectiveness of migration. Although the JARR method was designed to address these two applications, this research demonstrated the robust ability of the JARR method to invert for an accurate near-surface velocity function using accurate reflection velocities and refraction velocities (first arrival refractions).

In general, the JARR method has demonstrated that it is capable of delineating fine scale lateral and vertical velocity function resolution when utilized in conjunction with FAT. Furthermore, the JARR method was shown to work on two distinct datasets with two unique imaging goals. The demonstration of the JARR method on these two unique datasets illustrates the versatility of the methods capabilities.

With regard to the specific geophysical processing, two methods were used to illuminate the effectiveness of the JARR methods ability to calculate accurate velocity functions. The first processing method that was tested using the JARR methods ability to define accurate velocity functions was static corrections. After static corrections were applied the reflections were flattened and more in agreement with the structural nature of geology associated with Kansas, rather than the trace-to-trace variability and laterally discontinuous reflections that dominated the pre-corrected datasets in the near-surface. With regard to the Inman dataset the emergence of a dissolution feature is evident in the post-corrected data, which is obscured in the pre-corrected data. Static corrections needed to be accurately applied to the Inman dataset to properly and fully

interpret the section. The effectiveness of the static corrections indicates the underlying calculations derived by the JARR method produced an accurate velocity model of the subsurface in both datasets. After comparing these pre- and post- corrected data, it is apparent that the JARR method was capable of calculating accurate near-surface velocity functions to be utilized in static corrections.

This novel approach was shown as a way to calculate near-surface migration velocities in a quantitative manner, something previously only an option for exploration depth data. This unique damped JARR solution provided accurate near-surface velocities. Reflections were corrected without artifacts that stem from over and under correction due to poor velocity control. This method has also demonstrated improvement with both exploration depth and near-surface data, and it can be utilized across a variety of data types with confidence to solve various complex subsurface structures and geometries. Although both migration algorithms were compatible with the JARR method, the FK migration appeared to handle the velocity variation and noise level in the Wellington dataset better. The synthetic seismic traces as well as the lithology derived from well information tended to correlate better with the FK migrated data when compared to the Kirchhoff migrated data. In terms of the Inman dataset, each migration appears to be an equally likely solution. This is especially true with lack of well control or ability to ground truth.

However, this method is not without limitations. Data that lacks significant source-receiver offset would suffer. This method hinges on the ability for the first arrivals/refractions to sample a relatively decent depth into the subsurface. If the data lacks significant offset, this method would have little to no relevance.

This research has shown that through the use of the JARR method improved near-surface velocity information can be obtained for inclusion in statics and migration approaches. Based on

the results garnered from the datasets tested in this work, the JARR method is capable of determining velocities in the near-surface with significantly accurate vertical and horizontal resolution. This vertical and horizontal resolution is precisely the result of the damped a-priori model providing a real-world constraint on the inversion. The increased vertical and horizontal resolution can be seen when comparing the non-JARR method velocity function and the velocity functions once derived. The Wellington migration velocity function best illustrates the JARR methods ability to invert for complex vertical resolution velocity functions while the Inman migration velocity function illustrates the methods ability to calculate lateral resolutions accurately. Without determining the initial model from NMO velocity analysis, it would not have been possible to calculate and obtain such useful velocity information.

This research has shown two processes that utilize of the JARR FAT method and how the inclusion of JARR FAT improves accuracy of results targeting near- surface issues. Data examples from two uniquely different depth regimes reinforces and illustrates the robustness of the JARR method to not only provide accurate static corrections, but also provide accurate migration velocities for both shallow and deep data by providing accurate near-surface velocity functions. This unique method helps provide solutions that give confidence to reflection images from a wide variety of situations.

REFERENCES:

Al-Saleh, S. M., and, Jiao, J., 2012, Migration velocity analysis using traveltime wavefield tomography. Geophysics, **77**, no. 5,U73-U85. doi: 10.1190/geo2011-0440.1.

Alaei, B., 2006, An integrated procedure for migration velocity analysis in complex structures of thrust belts. Journal of Applied Geophysics, **59**, no. 2,89-105. doi: http://dx.doi.org/10.1016/j.jappgeo.2005.08.004.

Anderson, N. L., Martinez, A., Hopkins, J. F., and, Carr, T. R., 1998, Salt dissolution and surface subsidence in central Kansas; a seismic investigation of the anthropogenic and natural origins models. Geophysics, **63**, no. 2,366-378. doi: 10.1190/1.1444336.

Baker, G. S., Steeples, D. W., and, Drake, M., 1998, Muting the noise cone in near-surface reflection data: An example from southeastern Kansas. GEOPHYSICS, **63**, no. 4,1332-1338. doi: doi:10.1190/1.1444434.

Berkhout, A. J., 1981, Wave field extrapolation techniques in seismic migration, a tutorial. GEOPHYSICS, **46**, no. 12,1638-1656. doi: 10.1190/1.1441172.

Black, R., Steeples, D. W., and, Miller, R. D., 1993, Migration of shallow reflection data. SEG Technical Program Expanded Abstracts 1993,520-522. doi: 10.1190/1.1822538.

Brittle, K. F., Lines, L. R., and, Dey, A. K., 2001, Vibroseis deconvolution: a comparison of cross-correlation and frequency-domain sweep deconvolution. Geophysical Prospecting, **49**, no. 6,675-686. doi: 10.1046/j.1365-2478.2001.00291.x.

Chun, J. H., and, Jacewitz, C. A., 1981, Fundamentals of frequency domain migration. GEOPHYSICS, **46**, no. 5,717-733. doi: 10.1190/1.1441211.

Claerbout, J. F., 1971, TOWARD A UNIFIED THEORY OF REFLECTOR MAPPING. GEOPHYSICS, **36**, no. 3,467-481. doi: 10.1190/1.1440185.

Claerbout, J. F., and, Doherty, S. M., 1972, DOWNWARD CONTINUATION OF MOVEOUT- CORRECTED SEISMOGRAMS. GEOPHYSICS, **37**, no. 5,741-768. doi: 10.1190/1.1440298.

Clapp, R. G., Biondi, B., and, Claerbout, J. F., 2004, Incorporating geologic information into reflection tomography. GEOPHYSICS, **69**, no. 2,533-546. doi: doi:10.1190/1.1707073.

Coruh, C., and, Costain, J. K., 1983, Noise attenuation by Vibroseis whitening (VSW) processing. Geophysics, **48**, no. 5,12.

Dix, C. H., 1955, SEISMIC VELOCITIES FROM SURFACE MEASUREMENTS. GEOPHYSICS, **20**, no. 1,68-86. doi: 10.1190/1.1438126.

Earth, G., 6-19-2015, 38 11'59.11" N and 97 47'56.03"W. Inman Kansas Reflection Line.

Fadolalkarem, Y. 2015, Pre-stack Seismic Attribute Analysis of the Mississippian Chert and the Arbuckle Group at the Wellington Field, South-central Kansas, University of Kansas.

Google Earth. September 1, 2015., 37 18'46.94" N and 97 26'33.06" W. Wellington Seismic Reflection Line.

Goupillaud, P. L., 1976, SIGNAL DESIGN IN THE "VIBROSEIS"® TECHNIQUE. GEOPHYSICS, **41**, no. 6,1291-1304. doi: 10.1190/1.1440680.
Guangnan, H., Bing, Z., Hongxi, L., Hua, Z., and, Zelin, L., 2014, 2D seismic reflection tomography in strongly anisotropic media. Journal of Geophysics and Engineering, **11**, no. 6,065012.
Ivanov, J., Miller, R., and, Xia, J. 1998, High frequency random noise attenuation on shallow seismic reflection data by migration filtering, SEG Technical Program Expanded Abstracts 1998. 870-873.
Ivanov, J., Miller, R. D., Xia, J., and, Dunbar, J. B. 2007, Applications of the JARS method to study levee sites in southern Texas and southern New Mexico, SEG Technical Program Expanded Abstracts 2007. 1725-1729.
Ivanov, J., Miller, R. D., Xia , J., Dunbar, J. B., and, Peterie, S. L. 2010, Refraction nonuniqueness studies at levee sites using the refraction-tomography and JARS methods; in in R. D. Miller, J. D. Bradford and K. Holliger, eds., Advances in Near-Surface Seismology and Ground-Penetrating Radar: Society of Exploration Geophysicists. 327-338.
Ivanov, J., Miller, R. D., Xia, J., Steeples, D., and, Park, C. B., 2006, Joint analysis of refractions with surface waves: An inverse solution to the refraction-traveltime problem. GEOPHYSICS, **71**, no. 6,R131-R138. doi: 10.1190/1.2360226.
Ivanov, J., Schwenk, J. T., Peterie, S. L., and, Xia, J., 2013, The joint analysis of refractions with surface waves (JARS) method for finding solutions to the inverse refraction problem. The Leading Edge, **32**, no. 6,692-697. doi: 10.1190/tle32060692.1.
Kansas Geological Survey. 2015, Wellington--Oil and Gas Production. Kansas Geological Survey: Energy - Oil and Gas Fields: Kansas Geological Survey.
Kelly, T. E., and, Merriam, D. F., 1964, Structural Development of the Sedgwick Basin, South-Central Kansas. Kansas Academy of Science, **67**, no. 1,15.
Kruger, J. M. 1996, On-line gravity and magnetic maps of Kansas. Kansas Geological Survey: Open-file Report no. 96-51.
Lambrecht, J. L., Miller, R. D., and, Rademacker, T. R., 2004, Advantages and disadvantages of pre-correlation, pre-vertical stack processing on near-surface, high-resolution Vibroseis data. Seg Expanded Abstract,4.
Lillie, R. J. 1999, Whole Earth Geophysics An introductory Textbook for Geologists & Geophysicists, in Robert A. McConnin, ed.: Prentice-Hall Inc. A Pearson Education Company. 58 - 90.
Marsden, D., 1993, Static corrections—a review, Part II. The Leading Edge, **12**, no. 2,115-120. doi: 10.1190/1.1436936.
Mayer, L. M. 2009, Increasing reflection coherency through improved static corrections: An iterative tomographic approach, University of Kansas.
Merriam, D. F. 1963, The Geologic History of Kansas. Vol. Bulletin 162: State of Kansas. Original edition, December 1963. Reprint, 1998.
Miller, K. C., Harder, S. H., Adams, D. C., and, Terry O'Donnell, J., 1998, Integrating high- resolution refraction data into near- surface seismic reflection data

processing and interpretation. GEOPHYSICS, **63**, no. 4,1339-1347. doi: doi:10.1190/1.1444435.
Min, D.-J., and, Shin, C., 2006, Refraction tomography using a waveform-inversion back-propagation technique. Geophysics, **71**, no. 3,R21-R30. doi: 10.1190/1.2194522.
Nemeth, T. 1995, Velocity estimation using tomographic migration velocity analysis, SEG Technical Program Expanded Abstracts 1995. 1058-1061.
Newman, P., 1973, DIVERGENCE EFFECTS IN A LAYERED EARTH. GEOPHYSICS, **38**, no. 3,481-488. doi: doi:10.1190/1.1440353.
Park, C. B., Miller, R. D., and, Xia, J., 1998, Imaging dispersion curves of surface waves on multi-channel record 68th Annual International Meeting, SEG, Expanded Abstracts, no. 1,1377-1380.
Ristow, D., and, Jurczyk, D., 1975, Vibroseis deconvolution. Geophysical Prospecting, **23**, no. 2,363-379.
Schneider, W. A., 1978, INTEGRAL FORMULATION FOR MIGRATION IN TWO AND THREE DIMENSIONS. GEOPHYSICS, **43**, no. 1,49-76. doi: 10.1190/1.1440828.
Sheriff, R. E., 1976, Inferring Stratigraphy from Seismic Data. The American Society of Peetroleum Geologists Bulletin, **60**, no. 4,528-542.
Sheriff, R. E. 2002, Encyclopedic Dictionary of Applied Geophysics. Edited by Eugene F. Scherrer. 4th Edition ed: Society of Exploration Geophysicists.
Sirazheiv, A. 2012, Seismic attribute analysis of the mississippian chert at the wellington field, south-central kansas, University of Kansas.
Steeples, D. W., and, Miller, R. D. 1988, Seismic Reflection Methods Applied to Engineering, Environmental, and Ground- Water Problems, Symposium on the Application of Geophysics to Engineering and Environmental Problems 1988. 409-461.
Stefani, J. P. 1993, Possibilities and limitations of turning ray tomography: A synthetics study, SEG Technical Program Expanded Abstracts 1993. 610-612.
Stolt, R. H., 1978, MIGRATION BY FOURIER TRANSFORM. GEOPHYSICS, **43**, no. 1,23-48. doi: 10.1190/1.1440826.
Stork, C., 1992, Reflection tomography in the postmigrated domain. GEOPHYSICS, **57**, no. 5,680-692. doi: doi:10.1190/1.1443282.
Stork, C., and, Clayton, R. W., 1991, Linear aspects of tomographic velocity analysis. GEOPHYSICS, **56**, no. 4,483-495. doi: doi:10.1190/1.1443065.
Survey, K. G. 2010, Specific Well--15-191-22591. Kansas Geological Survey Oil and Gas: Kansas Geological Survey.
Survey, K. G. 2015, Specific Well--15-191-22770. Kansas Geological Survey Oil and Gas Wells: Kansas Geological Survey.
Taner, M. T., and, Koehler, F., 1981, Surface consistent corrections. GEOPHYSICS, **46**, no. 1,17-22. doi: 10.1190/1.1441133.
Taner, M. T., Postma, R. W., Lu, L., and, Baysal, E. Depth-Migration Velocity Analysis.

Walters, K. L. 2017, Geology and ground-water resources of Sumner County, Kansas [Map]. Kansas Geological Survey, Cartographic Services, 6-30-2008 1961 [cited 6-10-2017 2017]. Available from http://www.kgs.ku.edu/General/Geology/County/rs/sumner.html.

Wiggins, R. A., Larner, K. L., and, Wisecup, R. D., 1976, RESIDUAL STATICS ANALYSIS AS A GENERAL LINEAR INVERSE PROBLEM. GEOPHYSICS, **41**, no. 5,922-938. doi: 10.1190/1.1440672.

Williams, C. C., and, Lohman, S. W. 1949, Geology and Ground-Water Resources of a Part of South-Central Kansas with special reference to the Witchita municipal water supply. Kansas Geological Survey: Kansas Geological Survey. http://www.kgs.ku.edu/Publications/Bulletins/79/index.html (accessed 9-15-2016).

Xia, J. H., Miller, R. D., and, Park, C. B., 1999, Estimation of near-surface shear-wave velocity by inversion of Rayleigh waves. Geophysics, **64**, no. 3,691-700.

Yilmaz, O. 2001, Seismic Data Analysis Processing, Inversion, and Interpretation of Seismic Data. Edited by Michael R. Cooper. 2 vols, Investigation in Geophysics: Society of Exploration Geophysicists.

Yilmaz, Ö. a., and, Claerbout, J. F., 1980, Prestack partial migration. GEOPHYSICS, **45**, no. 12,1753-1779. doi: 10.1190/1.1441064.

Zhu, J., Lines, L., and, Gray, S., 1998, Smiles and frowns in migration/velocity analysis. GEOPHYSICS, **63**, no. 4,1200-1209. doi: doi:10.1190/1.1444420.

Zhu, X., Sixta, D. P., and, Angstman, B. G., 1992, Tomostatics: Turning- ray tomography + static corrections. The Leading Edge, **11**, no. 12,15-23. doi: doi:10.1190/1.1436864.